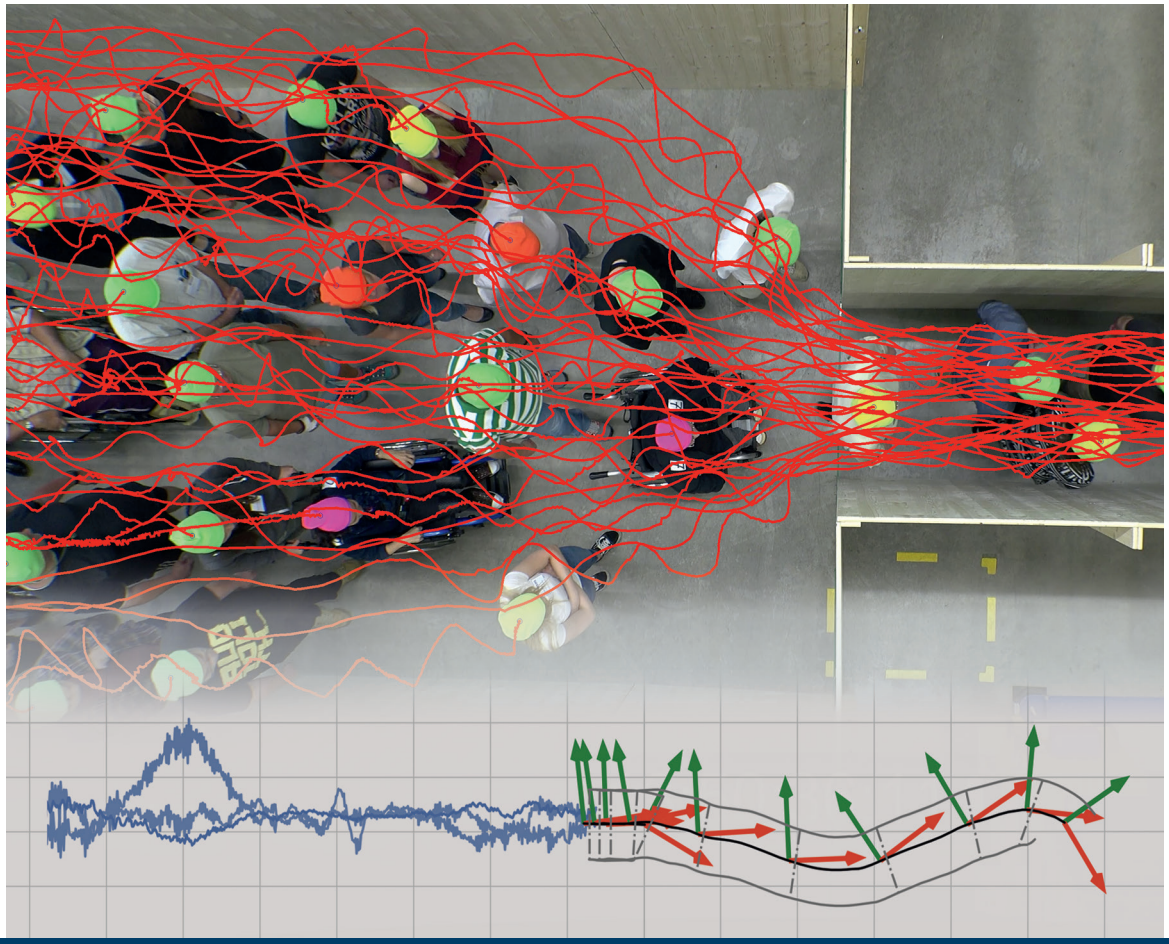

Utilizing Inertial Sensors as an Extension of a Camera Tracking System for Gathering Movement Data in Dense Crowds

Jette Schumann

IAS Series
Band / Volume 50
ISBN 978-3-95806-624-3

Mitglied der Helmholtz-Gemeinschaft

JÜLICH
Forschungszentrum

BERGISCHE
UNIVERSITÄT
WUPPERTAL

Utilizing Inertial Sensors as an Extension of a Camera Tracking System for Gathering Movement Data in Dense Crowds

Fakultät für Architektur und Bauingenieurwesen

Dissertation zur Erlangung eines Doktorgrades
(Dr.-Ing.)

vorgelegt von

Jette Schumann
aus Ueckermünde

Wuppertal 2021

The PhD thesis can be quoted as follows:

urn:nbn:de:hbz:468-20220706-085440-3
[http://nbn-resolving.de/urn/resolver.pl?urn=urn%3Anbn%3Ade%3Ahbz%3A468-20220706-085440-3]

DOI: 10.25926/4ja7-fm32
[https://doi.org/10.25926/4ja7-fm32]

Forschungszentrum Jülich GmbH
Institute for Advanced Simulation (IAS)
Civil Safety Research (IAS-7)

Utilizing Inertial Sensors as an Extension of a Camera Tracking System for Gathering Movement Data in Dense Crowds

Jette Schumann

Schriften des Forschungszentrums Jülich
IAS Series Band / Volume 50

ISSN 1868-8489 ISBN 978-3-95806-624-3

Bibliografische Information der Deutschen Nationalbibliothek.
Die Deutsche Nationalbibliothek verzeichnet diese Publikation in der Deutschen Nationalbibliografie; detaillierte Bibliografische Daten sind im Internet über http://dnb.d-nb.de abrufbar.

Herausgeber und Vertrieb:	Forschungszentrum Jülich GmbH Zentralbibliothek, Verlag 52425 Jülich Tel.: +49 2461 61-5368 Fax: +49 2461 61-6103 zb-publikation@fz-juelich.de www.fz-juelich.de/zb
Umschlaggestaltung:	Grafische Medien, Forschungszentrum Jülich GmbH
Druck:	Grafische Medien, Forschungszentrum Jülich GmbH
Copyright:	Forschungszentrum Jülich 2022

Schriften des Forschungszentrums Jülich
IAS Series, Band / Volume 50

D 468 (Diss. Wuppertal, Univ., 2021)

ISSN 1868-8489
ISBN 978-3-95806-624-3

Vollständig frei verfügbar über das Publikationsportal des Forschungszentrums Jülich (JuSER) unter www.fz-juelich.de/zb/openaccess.

This is an Open Access publication distributed under the terms of the Creative Commons Attribution License 4.0, which permits unrestricted use, distribution, and reproduction in any medium, provided the original work is properly cited.

Acknowledgements

This work summarizes my research during the last six years at the Research Center Jülich and the Charles Darwin University in Darwin, Australia. It was great to be a part of interdisciplinary research projects, to conduct and participate in experiments, and to search for explanations for observed phenomena. However, this journey would not have been possible without the support of my supervisors, colleagues, fantastic friends, and family.

First, I would like to thank my doctoral supervisor, Prof. Armin Seyfried, for his constructive discussions, his honest words, and guidance. Besides, I want to thank Jun. - Prof. Antoine Tordeux who put trust in my work and showed a sincere interest in my research.

Furthermore, I would like to thank Dr. Maik Boltes who has been an excellent supervisor. He has kept me on track, cheered me up in difficult times, and taught me that it is okay to run into limits when doing research. Working with him has always been a pleasure and I am thankful for his caring and humorous nature.

I highly appreciate the scholarship granted by the German Academic Exchange Service (DAAD) which made a six-month visit to the Charles Darwin University possible. During that stay, Dr. James Lee has been a fantastic supervisor and made my stay abroad fruitful on a professional but also personal level (seriously).

I would like to thank my colleagues Arne Graf, Alexander Belt, Gregor Jäger, Marc Fehling, and Juliane Adrian who have accompanied me on this journey. I am grateful for their not only professional but friendly relationship and their moral support. I especially want to thank Anne Küsters and Paul (-aul-aul) Geoerg who became true friends. I am very grateful for their support, advice, and motivating words. Besides, I would like to thank all my colleagues of the IAS-7, because they made my time in Jülich very worthwhile.

My journey was challenging, sometimes nerve-wracking, and would have been much more difficult without my friends and family. Special thanks go to Kerstin and Philipp Glock, Kathrin and Artur Derichs, and Caroline Krumrück. I am grateful to have them in my life and thank them for maintaining my social life in research-intensive times. A big thank you also goes to my lovely Degi who pushed me to the finishing line.

Last, I would like to thank my parents, Heike and Frank Schumann, and my sister Nele. Despite the local distance, they have always been a constant source of support. My parents raised me to be an ambitious person and made me always feel that they were very proud of me.

I dedicate this thesis to my grandparents Christa and Albrecht Lippoldt who, also no longer with us, have followed my research, conference visits, and my time in Darwin with great interest.

Abstract

The understanding of pedestrians' movement is crucial for the safe design of public facilities and venues, especially in crowded situations. However, some observed processes and influencing factors in crowds cannot be described in detail yet. Laboratory pedestrian experiments offer the possibility to specifically vary these factors in order to investigate their influence on the movement of the crowd. Typically, camera systems are used for data capturing in pedestrian experiments but show difficulties in very crowded scenarios as occlusions may occur.

Therefore, a hybrid tracking system was designed with the aim of improved and extended data capturing in laboratory pedestrian experiments. For this purpose, an existing overhead camera system was extended by a system of inertial measurement units worn by the participants. The main focus here was on trajectory reconstruction for wheelchair users and capturing the rotation of the participants' upper bodies in dense crowds. To this end, several methods for processing inertial and camera data have been implemented in order to derive the position and rotational data of the participants. Furthermore, methods for fusion of both data have been developed to provide a uniform database and also to improve the accuracy of the tracking methods.

The hybrid tracking system was used in several studies to capture different movement processes. As a result, a software framework was developed for the automatic processing, validation, and analysis of the captured data. The applied position tracking approaches have been found to be sufficient for particular data sets only indicating the need for further methods restricting the drift. Methods for calculating the rotation of the upper body showed promising results and contribute to an extended deep analysis of crowd dynamics in future experiments.

Kurzfassung

Für eine sichere Gestaltung von Gebäuden und Veranstaltungsorten ist das Verständnis der Bewegung von Fußgängern von entscheidender Bedeutung. Die Dynamik von Menschenmengen wird von vielen Faktoren beeinflusst, deren Zusammenhänge noch nicht vollständig beschrieben werden können. Kontrollierte Fußgängerstudien bieten die Möglichkeit, einzelne Faktoren gezielt zu variieren und zu untersuchen. Bei derartigen Experimenten werden oft Kamerasysteme zur Datenerfassung eingesetzt. Diese Technik weist in Szenarien mit hohen Dichten Grenzen auf, da es zu Verdeckung der zu erfassenden Bewegungen kommen kann.

Mit dem Ziel einer verbesserten und erweiterten Datenerfassung in Laborstudien mit Fußgängern wurde ein hybrides Tracking-System entwickelt. Ein Kamerasystem wurde um inertiale Sensoren erweitert, um Trajektorien von Rollstuhlfahrern und die Rotation des Oberkörpers in dichten Menschenmengen zu erfassen. Verschiedene Methoden zur Verarbeitung von Inertial- und Kameradaten wurden implementiert, um Positions- und Rotationsdaten der Probanden herzuleiten. Es wurden Methoden zur Fusion beider Datensätze entwickelt, um eine einheitliche Datenbasis zu schaffen und die Genauigkeit der Tracking-Methoden zu verbessern.

Das hybride Tracking-System wurde in mehreren Studien eingesetzt, in welchen verschiedenartige Bewegungsabläufe erfasst wurden. Für die automatische Verarbeitung, Validierung und Analyse der erfassten Daten wurde ein Software-Framework entwickelt. Die Methoden zur Positionsrekonstruktion haben sich für ausgewählte Datensätze als ausreichend erwiesen. Eine Weiterentwicklung der Methoden ist notwendig, um Abweichungen weiter einzuschränken und übergreifend gute Ergebnisse erzielen zu können. Die Methoden zur Berechnung der Rotation des Oberkörpers zeigten vielversprechende Ergebnisse und tragen in zukünftigen Experimenten zu einer tiefgreifenden Analyse der Dynamik von Menschenmengen bei.

Contents

1 Introduction **1**

1.1 Motivation . . . 1

1.2 State of the Art . . . 3

1.2.1 Data Capturing in Pedestrian Experiments . . . 3

1.2.2 Tracking with Inertial Measurement Units . . . 5

1.3 Objectives, Approach and Limitations . . . 9

1.4 Thesis Outline . . . 13

2 Data Capture **15**

2.1 Hybrid Tracking System . . . 15

2.1.1 Camera System . . . 15

2.1.2 IMU System . . . 17

2.2 Conducted Studies . . . 19

2.2.1 Movement Studies with Heterogeneous Crowds . . . 20

2.2.2 Validation with a 3D Camera Tracking System . . . 22

3 Methodology **27**

3.1 Overview . . . 27

3.1.1 Frames of Reference . . . 27

3.1.2 Data Flow and Processing . . . 28

3.2 Tracking with Inertial Sensors . . . 31

3.2.1 Data Preprocessing . . . 31

3.2.2 Orientation Tracking . . . 32

3.2.2.1 Orientation Representation . . . 32

3.2.2.2 Madgwick's Orientation Filter . . . 33

3.2.3 Distance Tracking . . . 36

3.2.3.1 Application of Double Integration . . . 36

3.2.3.2 Application of a Kalman Filter . . . 37

3.3 Fusion of IMU and Camera Data 39
3.3.1 Synchronization and Calibration 39
3.3.2 Utilizing Camera Data while Tracking 43
3.3.2.1 Processing Camera Data 43
3.3.2.2 Correction 44
3.3.2.3 Adaptive Correction 45

4 Framework **47**
4.1 Code Structure 47
4.2 Data Flow and Processing 51

5 Analysis and Results **55**
5.1 Distance Tracking 55
5.1.1 IMU Data Example 55
5.1.2 Validation of Heading Accuracy 58
5.1.3 Double Integration 59
5.1.4 MAUKF 64
5.1.5 Effects of the Correction Methods 65
5.1.6 Comparison of the Different Approaches 67
5.2 Heading Tracking 68
5.2.1 Method for Validation 69
5.2.2 Rotation of Wheelchair 70
5.2.3 Rotation of Upper Body 75

6 Application **81**
6.1 Study Setup 81
6.2 Twist Angle 84
6.2.1 Definition and Calculation 84
6.2.2 Error Analysis 86
6.3 Analysis and Results 88
6.3.1 Rotation in the Bottleneck 89
6.3.2 Rotation and Motivation 97
6.3.3 Rotation and Density 99
6.3.4 Rotation and Flow 101
6.4 Future Experiments 102
6.4.1 Suggested Improvements 102
6.4.2 Further Analysis 103

7 Closing Remarks **105**
7.1 Conclusions 105
7.2 Outlook 108

Appendix A List of Commerical IMU Systems **111**

Appendix B Framework Usage and Extension **113**
B.1 Preparatory Work and Requirements 113
B.2 Configuration Files 114
B.3 Using the Classes 116

Appendix C Supplementary Material for SiME Studies **119**
C.1 Documentation of Analyzed Data Sets 119
C.2 Raw IMU Data 120

Appendix D Supplementary Material for Optitrack Studies **121**
D.1 Calculated Angles 121
D.2 Error in Heading 126

Appendix E Supplementary Material for Studies on Twist Angle **129**
E.1 Synchronization 129
E.2 Classification of IMU Data Sets 129

Appendix F Publications **139**

References **141**

Nomenclature

Abbreviations and Acronyms

2D	Two-Dimensional
3D	Three-Dimensional
DOF	Degrees of Freedom
GPS	Global Positioning System
GT	Ground Truth
ID	Identifier
IMU	Inertial Measurement Unit
INS	Inertial Navigation System
IPS	Indoor Positioning System
KF	Kalman Filter
LIDAR	Light Detection and Ranging
MARG	Magnetic, Angular Rate and Gravity
MAUKF	Measurement Augmented Kalman Filter
MEMS	Micro Electro-Mechanical System
PDR	Pedestrian Dead Reckoning
RFID	Radio-Frequency Identification
SHS	Step-and-Heading System

SiME	Safety for all People (German acronym for "Sicherheit für Menschen mit körperlicher, geistiger oder altersbedingter Beeinträchtigung")	
SLAM	Simultaneous Localization and Mapping	
UWB	Ultra-Wideband	
WLAN	Wireless Local Area Network	
ZUPT	Zero Velocity Update	

Latin Symbols

$\boldsymbol{a}$	Vector of acceleration	$\mathrm{m\,s^{-2}}$
$\boldsymbol{b}$	Vector of earth's magnetic field	G
$\boldsymbol{g}$	Vector of gravity	$\mathrm{m\,s^{-2}}$
$\boldsymbol{m}$	Vector of magnetometer's measurements	G
$\boldsymbol{s}$	Vector of position	m
$\boldsymbol{v}$	Vector of velocity	$\mathrm{m\,s^{-1}}$
$\boldsymbol{w}$	Vector of angular velocity	$^{\circ}\,\mathrm{s^{-1}}$
$\boldsymbol{x}$	State vector used in Kalman Filter	
$\boldsymbol{y}$	Measurement vector used in Kalman Filter	
C	Camera reference frame	
I	Local IMU reference frame	
i	Time step	
k	Iteration step	
n	Number of iterations	
q	Quaternion	
W	Global world reference frame	
fr	Frame rate	$\mathrm{s^{-1}}$

Greek Symbols

α	Heading angle	$^\circ$
μ	Step size for the gradient descent algorithm	
σ	Standard deviation	

Subscripts and Superscripts

${}^{A}_{B}(.)$	Quaternion specific notation for the orientation of frame B relative to A
${}^{C}(.)$	Quantity given in camera frame
${}^{I}(.)$	Quantity given in IMU frame
${}^{W}(.)$	Quantity given in world frame
$(.)_{\text{camera}}$	Quantity based on camera data
$(.)_{\text{diff}}$	Quantity related to difference between values
$(.)_{\text{imu}}$	Quantity based on IMU data
$(.)_{x}$	X-component of a quantity
$(.)_{y}$	Y-component of a quantity
$(.)_{z}$	Z-component of a quantity
$(.)_{\text{linear}}$	Acceleration-specific notation indicating that influence of gravity has been removed
$(.)_{\text{pusher}}$	Quantity related to the pushing person

Mathematical Symbols

$0_{m\times n}$	Zero matrix with dimensions m and n	
Δt	Sampling period	s
∇	Nabla operator	
$\otimes$	Quaternion product	
I_m	Identity matrix with dimension m	
$\boldsymbol{q}^*$	Conjugated quaternion	

List of Figures

1.1 Crowd at a music festival. 2
1.2 Overview of the outline. 13

2.1 Processing steps of camera data. 17
2.2 IMU system. 19
2.3 Sample images of the SiME studies. 20
2.4 Wheelchair equipped with IMUs. 21
2.5 Attachment of IMUs and Optitrack markers. 23
2.6 Technical configuration of camera system. 24
2.7 Setup of Optitrack experiments. 25

3.1 Reference frames for applied tracking method. 29
3.2 Overview of the tracking algorithm. 30
3.3 Acceleration data for heel drop. 40
3.4 Assignment of frames and samples. 42
3.5 Qualitative example of the adaptive correction. 46

4.1 Overview of main classes. 48
4.2 Distance tracker classes. 50
4.3 Basic data flow and operations in the framework. 53

5.1 Camera and IMU data of a wheelchair user. 57
5.2 Heading validation for a wheelchair user. 59
5.3 IMU tracking data for double integration. 60
5.4 Results for double integration. 62
5.5 Results for double integration with data of another sensor. 63
5.6 Results for MAUKF. 64
5.7 Example of improvement by MAUKF. 66
5.8 Effects of correction methods on the trajectories. 67
5.9 Sketch of validation method. 69

5.10 Optitrack and IMU orientation for a wheelchair. 71
5.11 Example of calculated heading of the wheelchair. 72
5.12 Error in heading calculation for wheelchair scenario. 73
5.13 Heading tracking of the upper body while standing. 76
5.14 Error in heading calculation for rotation while standing. 77
5.15 Example of calculated heading for a walking person. 78
5.16 Error in heading calculation for a walking person. 79
5.17 Example of calculated heading for walking with strong rotation. . . . 80

6.1 Overview of studies on twist angle. 83
6.2 Visualization of the twist angle. 84
6.3 Twist angle while walking. 87
6.4 Examples of asymmetric shoulder movement. 88
6.5 Twist angles in entrance phase. 90
6.6 Twist angle data for one person passing the bottleneck. 91
6.7 Corresponding sample images for one person passing the bottleneck. . 92
6.8 Partitioning of the bottleneck into regions of interest. 93
6.9 Relation of twist angles and entrance region for low motivation. . . . 94
6.10 Relation of twist angles and entrance region for high motivation. . . . 95
6.11 Scenarios of participants approaching the bottleneck at the same time. 96
6.12 Relation of bottleneck width and twist angle. 97
6.13 Different rotation scenarios depending on the bottleneck width. . . . 98
6.14 Relation of individual density and twist angle in the bottleneck. . . . 100
6.15 Relation of flow and twist angle. 102

C.1 Example of raw IMU data. 120

D.1 Angles for a wheelchair moved with arms. 122
D.2 Angles for a wheelchair moved with feet. 123
D.3 Angles for trunk rotation while walking. 124
D.4 Angles for trunk rotation while standing. 125
D.5 Error in heading for a wheelchair moved with feet. 126
D.6 Error in heading calculation for crowd walking. 127

E.1 Example of good IMU data. 131
E.2 Examples of acceptable IMU data. 132
E.3 Example of unusable IMU data with gyroscope offset. 133
E.4 Examples of unusable IMU data with failed convergence. 134

List of Tables

5.1 Overview of distance tracking quality. 68
5.2 Overview of heading tracking quality for a wheelchair. 74
5.3 Overview of heading tracking quality for rotation of the upper body. . 80

C.1 Overview of validated SiME data sets. 119

E.1 Classification of sensor data for run with $N = 25$. 135
E.2 Classification of sensor data for run with $N = 8$. 136
E.3 List of considered sensors for run with $N = 25$. 137
E.4 List of considered sensors for run with $N = 8$. 137

Chapter 1

Introduction

1.1 Motivation

When attending concerts, shopping in malls, or traveling through train stations - we often find ourselves in large crowds. Being part of a crowd can lead to situations that may be perceived as uncomfortable by people experiencing the situation. Furthermore, this could create dangerous situations. Especially if there is not enough space for the people to move self-determined. Although the movement of crowds affects our daily lives, there are still gaps in understanding this complex process. Therefore, research in the area of pedestrian dynamics is needed.

As a profound understanding of crowd dynamics is crucial for a safe design of public buildings and spaces, many research activities regarding pedestrian movement have been undertaken in recent decades. An important pillar of this research are pedestrian experiments which provide movement data of crowds as a basis for analyses [1]. Collecting data such as trajectories of the heads allow a detailed analysis of the participants' movement [2] and its results are used for the development of models. These models are applied in simulations which are an important tool for detecting and assessing safety risks when designing facilities or event planning.

Many studies have been conducted investigating the movement of crowds for different scenarios [1, 3–5]. Self-organizing phenomena in crowds (such as the formation of lanes) have been observed and the effects of various factors on the movement of the crowd have been investigated. However, there are still major discrepancies in the collected data and findings [1, 5–7]. Furthermore, many factors that are influencing the movement of a crowd were not examined in detail yet due to their large variety. This underlines the need for further experiments to create a comprehensive and coherent database of movement data.

Laboratory crowd experiments are a very useful empirical method for collecting new movement data [4]. When observing real-life scenarios (field studies) with large crowds such as a typical festival (see Fig. 1.1), it is difficult to analyze the processes in detail. Many variables and their effects that have lead to the observed situation are unknown but are important for a deep understanding of the movement such as the exact number of people, the available individual space, the age distribution, or motivation. In contrast to this, laboratory studies allow to focus on determined influencing factors (such as the density or spatial layout of boundaries) and to vary those specifically. In this way, the gathering of detailed movement data under chosen conditions is possible.

Figure 1.1: Parookaville festival in Germany visited by 210 000 people in 2019. Sufficient space in front of the stages and a high capacity of the paths leading to and from these are crucial for the participants' safety, especially in emergencies.

For laboratory studies, various tracking systems have been developed to record the movement of the crowd. Camera systems are quite popular and provide trajectory information with high temporal and spatial resolution. Furthermore, with the help of markers it is also possible to gather additional individual information such as the height and age of the participants. Knowing the exact trajectories of participants' heads and the spatial layout of the scenario boundaries, important quantifiers of crowd movement can be calculated such as the velocity, density, and flow and their relation represented by Fundamental diagrams [8]. Nevertheless, in addition to the position data, capturing further information is desired. Typically, the more is known about the participants, the more complex the analysis becomes. However, the approximation

of reality improves when considering many factors influencing the crowd movement. Valuable additional information would be, for example, knowing where participants looked, their posture, how they perceived the situation, if they felt stressed, or how they interacted with each other. A capturing system that provides as much of that data as possible is desirable. However, due to missing or limited technical possibilities, data capturing systems have their restrictions.

This thesis contributes to the field of data capturing in laboratory pedestrian experiments by utilizing inertial sensors in addition to a camera tracking system. With inertial sensors that are worn by the participants, individual relative movement data can be recorded and processed to rotational and positional information. Providing position data based on inertial sensors can compensate for the weakness of the camera system operating incorrectly or a lack of data due to occlusions. Besides, the information of the rotation of body parts represents novel movement data that are difficult to extract from video recordings and offers new possibilities for the analysis of crowd movement. This work focuses on the rotation of the upper body since this is accompanied by a change of individual space and therefore density which is important when analyzing crowd properties.

1.2 State of the Art

In the following, a brief overview of data capturing and localization systems used by different research groups is given. Since the hybrid tracking system investigated and developed in this work consists of a camera system and inertial sensors, these two techniques are the main focus.

1.2.1 Data Capturing in Pedestrian Experiments

Computer vision methods are widely used for capturing especially spatio-temporal properties such as location and identity [9]. In this field, various capturing techniques utilizing cameras and image processing methods have been used that provide movement data with different levels of detail. A low level of detail is given when the optical flow is calculated based on video recordings which can help to detect critical motion patterns and abnormal activities [10–12]. In [13] a depth camera was used for the detection and tracking of pedestrians. Additionally, methods for estimating the velocity and density without detecting single pedestrians are presented in [14, 15]. In contrast, data capturing systems with a high level of detail detect and track whole body movements. Often used in film productions optical motion capturing systems

allow this detection and tracking [16], but are not applicable for crowded scenes because of occlusion. The highest possible level of detail would be desirable for data capturing in crowds. However, there is currently no computer vision system available that provides tracking data of the whole locomotor system and further personal data for crowded scenarios.

Typically, individual trajectory information is provided by data capturing systems used in pedestrian experiments [17–26]. A high temporal and spatial resolution of these trajectories is needed to allow the application of methods for extracting crowds' properties [27] and the development of microscopic models [28].

Besides basic trajectory data, personal information using individual codes [29] or shoulder orientation with the help of markers on the shoulders [30–32] have been gathered. However, automatic shoulder tracking with conventional camera systems by detecting and tracking markers on the shoulders is restricted by occlusion. An infrared system as used in [30, 31] offers the possibility to precisely capture shoulder movements, but suffers from marker losses and reflections. Furthermore, the tracking range of these systems is severely limited and for these reasons, it is not applicable for large-scale experiments to analyze the movement of crowds in a natural setting. Therefore, there is still a need for additional tracking technologies to extend camera systems in order to provide more accurate or additional movement data. As laboratory pedestrian experiments are usually conducted indoors in simulated environments to ensure optimized conditions for an improved tracking accuracy [2], these additional techniques must be applicable indoors as well.

Due to the growing interest in location awareness in various situations such as rescue, tourism, or sports many Indoor Positioning Systems (IPSs) have been developed that can be utilized in pedestrian experiments. Basically, IPSs are separated into these categories [33]:

- Wireless localization technologies use wireless communications such as Ultra-wideband (UWB), Radio-frequency identification (RFID) or Bluetooth, or a standalone infrastructure provided in the building such as Wireless Local Area Networks (WLAN). At least one signal transmitter and one receiving unit must be available. Based on the transmitted and received signals proximity and triangulation techniques can be applied to calculate a location of an object or person. When applying the proximity technique the object that should be tracked is sending signals that are received by dedicated target objects. The tracked

object is assumed to be close to the target object that receives the strongest signal. More complex localization methods are realized with the triangulation approach where the object's position is estimated based on distances (triangulation) resulting from travel time measurements or angles (angulation) to target objects. More details on wireless IPS techniques are described in [34].

- Dead reckoning localization technologies process data of motion sensors or odometers that are attached to the tracked object. No additional infrastructure is needed, but an error accumulation needs to be handled since there are no absolute reference points available while tracking. In the area of Pedestrian Dead Reckoning (PDR) inertial sensors are widely used which are introduced in Sec. 1.2.2.

- In video scene analysis, location information is extracted using methods for tag detection, scene matching, or tracking moving objects. This is already realized by computer vision systems discussed in the beginning of this Section.

Since modern smartphones contain many of the above mentioned sensors/techniques that provide data for localizing the user (such as Wi-Fi, Bluetooth, or inertial sensors) various methods utilizing these data with positioning purposes have been developed [35]. Detailed reviews on indoor positioning systems, methods, and their applications are beyond the scope of this work and provided in [33, 36].

1.2.2 Tracking with Inertial Measurement Units

Inertial Measurement Units (IMUs) basically consist of an accelerometer and a gyroscope. Measuring the relative movements of linear and angular kinematics, a reconstruction of absolute values such as movement direction and position is possible. In addition, many inertial sensors also contain a magnetometer and are often referred to as MARG (Magnetic, Angular Rate, and Gravity) sensors. However, this distinction is not made in this thesis. As magnetometer data allow the application of extended tracking algorithms. Most of the modern inertial sensors provide 9 degrees of freedom (DOF) measurements (3-axis accelerometer, 3-axis gyroscope, 3-axis magnetometer) and are still referred to as IMUs.

Primarily used for navigation of ships and airplanes, the changed architecture of inertial sensors resulting in smaller size and low cost made them applicable in a broad range. They are available as Micro Electro-Mechanical Systems (MEMS) that are highly portable and have been used next to navigation systems in the fields of

robotics, industry quality control, medical rehabilitation, and sports learning, among others [37]. As IMUs are usually integrated in modern smartphones, they are also widely used for indoor navigation of pedestrians. A detailed review on PDR experiments using IMUs and the used tracking methods is provided in [38] where a classification in Inertial Navigation Systems (INSs) and Step-and-Heading Systems (SHSs) is proposed. The development of essential parts of these algorithms was partly driven by research in the field of robotics. As the movement of a sensor attached to a person is more complex and non-controllable, the localization of pedestrians brings new challenges to the tracking algorithms.

An **Inertial Navigation System** provides full trajectory information (3D) at any given time. The use of INSs is not limited to tracking of pedestrians. Usually, the sensor components are packed in a hard frame and attached to the person being tracked. Based on accelerometer and gyroscope data (and magnetometer data if available) the orientation of the sensor is tracked and the changes in position are calculated based on double integration of the acceleration values [39]. A crucial step of INS algorithms is to find the relation of the local sensor frame regarding the global world frame which is changing with the movement of the person. Before double-integrating the acceleration data the influence of gravity needs to be removed from the data. In order to do this, it must be known how the gravitation is distributed on the local axes as the person and therefore also the sensor is moving. As low-cost MEMS inertial sensors suffer from noise, they do not provide highly accurate measurements, which can lead to a cubic growth of the error in time (drift) [38]. Dedicated algorithms are needed to limit the drift whose approaches are explained later on.

A **Step-and-Heading System** is a specialized system that is tailored to the tracking of pedestrians only. The three basic steps are: the recognition of steps or strides, the estimation of the step length, and the estimation of heading. Steps are basically detected by investigating movement patterns and searching for stance phases or step cycles. This is mostly done by applying threshold-based algorithms or peak detection on the movement data. For estimating the step length different methods have been developed such as constant length depending on the height of a person or varying length depending on step frequency while walking. The heading estimation can be calculated in the same way as for the INSs. Details on the tracking algorithms and conducted experiments can be found in [38].

PDR techniques have various applications and thus, many tracking algorithms have been developed and experiments were conducted whose detailed description is beyond the scope of this work. Next to the listings of algorithms in [38], many different algorithms for pedestrian tracking based on the data of foot-mounted sensors [40–47] or other positions [48–50] have been developed and validated. Also, a wide range of methods exists for tracking pedestrians with the help of inertial data provided by smartphones [51–54]. Often a strict separation in INSs and SHSs is not possible as combinations of these algorithms have been developed where step patterns are used to limit the drift when double integrating accelerometer measurements.

Reference data sets of IMUs mounted to the foot [55] and attached to several positions while walking [56] and for several activities [57] have been published providing ground truth data for validating PDR algorithms.

Apart from basic methods of SHSs and INSs, various approaches for limiting the drift in position have been examined. A popular approach for this when tracking pedestrians are Zero Velocity Updates (ZUPTs) [58]. If the sensor is attached to the foot, stance phases can be detected while walking for which the sensor is assumed to be stationary. Since a zero velocity is assumed for the stance phase, the drift accumulation occurs during the swing phase only and can therefore be limited. Additionally, external measurements or information of the environment are considered while tracking. Coming from the field of robot techniques particle filters and Simultaneous Localization and Mapping (SLAM) algorithms or a combination of both are applied [38]. When applying particle filters a set of particles is propagated and weighted of which each particle represents a possible position and heading as in [59–61]. In SLAM algorithms, typically, additional sensor signals are used (such as cameras or laser rangefinders) to calculate the position and a map of the building to improve the accuracy as in [62]. Assuming the geometry of a building is known map-matching techniques can be applied as well [63] which are often combined with particle filters [64, 65]. Apart from this, by fusing data of several IMUs an improved tracking quality has been achieved [66–68].

In addition, **hybrid tracking systems** are a popular approach to overcome tracking inaccuracies with IMUs by fusion with additional data provided by another tracking technology as already described above for SLAM algorithms as an example. When it comes to the gapless detection of pedestrians while moving in- and outdoors a combination of the Global Positioning System (GPS) and INS are often used. Basically,

IMU signals are used when the person is moving in GPS signal degraded environments as in [58, 69, 70]. For navigation purposes in buildings, additional sensors and other technology have been employed to limit the drift as in [71] by combining foot mounted IMUs and RFID tags. A foot mounted IMU and Light Detection and Ranging (LIDAR) sensor have been utilized in [72], so that the distance to walls can be measured and used to improve tracking. Bluetooth-beacons in addition to IMUs contained in smartphones are used in [73]. In [74–76] approaches for fusing inertial and WLAN signals are proposed.

Besides, many hybrid systems fusing camera and IMU data exist. By attaching a smart-camera on an IMU an approach for fusing image processing techniques and IMU data is presented in [77]. A system for navigating visually impaired people utilizing inertial and visual sensors is proposed in [78] where IMU sensors were attached to Google Glasses. Further, IMUs have been used as an extension for the camera system to reconstruct 3D images [79], to provide rotational information for motion capturing [80] or to improve pose estimation with a depth camera [81].

Additionally, multisensor systems have been used in [82] (IMU, GPS, UWB) and [83] (IMU, camera glasses, WiFi). In [84] fusion techniques of inertial data with camera, UWB, or GPS data are discussed.

Capturing of additional movement data with IMUs next to trajectory information was also realized by many research groups. Starting from recognizing different activities such as standing, sitting, or stair climbing [85, 86], inertial sensors allow recognition of gait phases [87] and their detailed inspection at different speeds [88, 89]. Also, tracking of the movement of limbs and body parts with IMUs was realized in [90–96]. By placing several IMUs on specific positions on the body of a person the motion of the body can be reconstructed based on displacements and movement angles of the sensors [97]. Furthermore, full body motion capturing suits consisting of IMUs have been developed [98, 99].

Moreover, tablets containing inertial sensors were used to measure the body rotation [100] and to investigate the collision avoidance [101] in uni-, bi- or multi-directional streams. Furthermore, inertial sensors have been used to estimate crowd properties (velocity and density) based on the angular velocity or acceleration data [102, 103].

Position tracking of wheelchair users with IMUs is not common and only a few studies have been conducted so far. In [104, 105] inertial sensors were used

to reconstruct wheelchair kinematics in court sports. For this purpose, IMUs were attached to the wheels and the rotation of the wheels was calculated. Presuming a known geometry of the wheelchair the traveled distance was reconstructed. Furthermore, a related research area is the tracking of wheeled robots. INS algorithms have been applied in [106] with a 6 DOF IMU showing the need for methods to restrict the drift in position. To improve the tracking quality, hybrid tracking systems for wheeled robots consisting of IMUs and additional odometry sensors have been used in [107, 108].

1.3 Objectives, Approach and Limitations

The main objective of this work is the extension of a camera tracking system by another indoor positioning technique in order

1. to enable tracking of people, especially wheelchair users, that are temporarily occluded and
2. to provide additional data (in this case the rotation of the upper body) that are difficult to extract with cameras only.

Thus, a hybrid tracking system was designed and applied for data capturing in laboratory pedestrian experiments. Methods for tracking pedestrians based on data of IMUs and for the fusion of the data of both systems have been developed and implemented. Further, the tracking quality of these methods was validated to ensure a sufficient accuracy for the analysis of pedestrian dynamics. In the following, an overview of the main approaches and challenges regarding the design of the hybrid tracking system, the methods for distance tracking, and the capturing of the rotation of the upper body is given.

The **hybrid tracking system** was motivated by new studies conducted in 2017 investigating the movement of heterogeneous crowds (SiME studies [109]). Especially, participating wheelchair users were likely to get occluded by surrounding people due to their low height and the perspective view of the cameras. Therefore, their full trajectory information could not be ensured using the camera system only and additional data were needed to close gaps in case of temporal occlusions. For the extension of the camera system, specific inertial sensors were used in this work.

The use of inertial sensors keeps the extension of the camera system simple. In contrast to other PDR systems such as UWB, Bluetooth or Wi-Fi, no additional infrastructure in the experiment environment is needed. The sensors are self-contained devices that need to be attached to persons intended to be tracked. The optimization of the sensors' hardware resulted in small, light-weighted, and durable MEMS so that they can be worn by a person without restricting their movement [110, 111]. As inertial sensors are available with local storage, no data needed to be transferred wirelessly which reduces the risk of data loss. Besides, other PDR techniques are rarely tested in crowds where accuracy problems due to interferences, signal losses or multipaths could occur when applying proximity and triangulation techniques. Furthermore, IMUs have been used in many experiments to gather additional information such as rotations next to basic position data which opens new analysis possibilities. A major disadvantage of low cost MEMS is noisy measurements which means that considerable effort needs to be made for improving the tracking accuracy.

The proposed combination of an overhead camera system and IMUs worn by participants has been used in a similar way in [103] where the participants were equipped with tablets or smartphones. However, the inertial data were not used to derive individual data on absolute position and rotation. Therefore, the technical realization and application of the tracking system presented in this work is a novel approach.

Studies on the **position tracking of wheelchair users** are not common, even if there is a broad range of tracking algorithms utilizing IMUs as presented in Sec. 1.2.2. Especially the tracking in crowds has not been studied so far. Compared to tracking approaches in [104, 105] the tracking algorithms should not depend on special properties of the wheelchairs such as the dimensions of the wheels. As many different kinds of wheelchairs (manual, electric, custom-made) were expected for the SiME studies a more general tracking approach is aimed for. Due to the homogeneous movement of wheelchair users, INS approaches are applicable for tracking their traveled distance.

In this work, high tracking accuracy is required in case of occlusion of the wheelchair users and therefore, for a limited time range only. The fact that the wheelchair users move in a crowd opens up new possibilities for limiting the drift in position. In order to achieve high accuracy, the movement data provided by the camera system of the surrounding people (that have lead to the occlusion of the wheelchair users) can be utilized and appropriate methods must be developed.

Besides, the fusion of the data of two IMUs is promising which was investigated for a rigid body in [66, 68] for simplified and restricted movement processes but not for the movement of pedestrians.

The **capture of rotation data** of participants' upper bodies is another main objective of this work. The analysis of past experiments for bottleneck scenarios with high densities has increased the interest in rotation data. With studies presented in [112] the movement of a group entering a concert guided by two different spatial barrier structures was investigated. The analysis was based on trajectory information and a questionnaire asking for perception and evaluation of both scenarios. The video recordings showed regions of densely crowded people. Based on the questionnaire data this was accompanied by a low level of comfort. In these studies, the knowledge about the rotation of the participants' trunks would have been valuable information to quantify the level of comfort or the individual space requirements.

Details on the above-mentioned studies are beyond the scope of this thesis but they have motivated the goal of collecting rotation data in pedestrian experiments which was realized with IMUs in this work. Various orientation tracking algorithms (as a part of INSs and SHSs) exist that are fusing the different measurements of inertial sensors which can be used to keep track of the orientation of the upper body. However, the calculation of the absolute rotation of the upper body in crowds utilizing IMUs is a novel approach.

To enable both, position and rotation tracking, methods for the fusion of IMU and camera data need to be developed. Both data sets must be provided for the same person, at the same time step and in a common coordinate system. Appropriate requirements for the experiment procedures must be formulated and realized.

Based on the presented objectives and considerations, the work presented in this thesis can be broken down into the following packages:

1. Technical extension of the camera tracking system: After a comprehensive requirements analysis, the decision for a sensor system, and a specific manufacturer must be made. The choice fell on IMUs since no additional technical infrastructure is needed and much research on pedestrian tracking indoors with IMU has already been done.

2. Tracking algorithm: Methods for processing IMU data must be designed to provide the desired additional information. Furthermore, techniques for fusing camera and IMU data need to be developed to provide a consistent and accurate database.

3. Implementation: A framework for automatic data extraction and fusion must be implemented.

4. Wheelchair tracking: Experiments with participating wheelchair users should be conducted using the hybrid tracking system for data capturing. The developed and implemented methods should be applied and an analysis of the tracking quality should be undertaken.

5. Heading tracking: Experiments with a 3D capturing system should be conducted to investigate different rotational movements and to validate the heading tracking accuracy.

6. Rotation in crowds: The approach for heading tracking can be used to measure the rotation of the upper body of pedestrians. Analysis of a crowds' movement should be done based on data provided by the hybrid tracking system.

As it would be too complex to consider and implement all desirable aspects, this work has limitations. First, the proposed hybrid tracking system can be used for laboratory studies only since pedestrians need to be equipped with selected inertial sensors. An investigation of real-life scenarios is not possible with this approach. Additionally, the processing of tracking data is realized offline which means that calculations are undertaken after the completion of relevant experiments. Therefore, there is no need in optimizing the performance e.g., for real-time tracking of the methods implemented in the framework.

Besides, fusion and tracking methods are specifically tailored to extend a camera system for capturing movement data in pedestrian experiments conducted in a 2D plane. Vertical movements (such as stair climbing) were not considered. Furthermore, distance tracking methods are applied for wheelchair users only. They might be applicable for walking participants as well but this would require methods for analyzing step patterns which are not part of this work.

For a deeper analysis of the movement of the crowd, inertial sensors were used to track the rotation of the upper body in the presented studies. A reconstruction of full body motion based on low-cost IMUs is desirable, however not within the scope of this work.

1.4 Thesis Outline

This thesis has been divided into seven Chapters. Chapter 1 already addressed the motivation, objectives, and limitations of this work. Furthermore, a review on the current state of the art regarding data capturing systems for pedestrian experiments and especially tracking techniques with inertial sensors was given. In addition, the advantages of using inertial sensors as an extension of the camera system were presented.

The context of Chapters 2 to 6 is visualized in Fig. 1.2. The hybrid tracking system consisting of a camera system as a basis and inertial sensors as an extension is introduced in Chapter 2. Conducted laboratory experiments with heterogeneous crowds (referred to as SiME studies) and studies with another camera system (referred to as Optitrack studies) are described in that Chapter. In the SiME studies the movement of a crowd involving wheelchair users has been recorded with the hybrid tracking system. In contrast, the Optitrack studies were small-scale experiments using a 3D camera tracking system to validate the heading tracking for different movement processes.

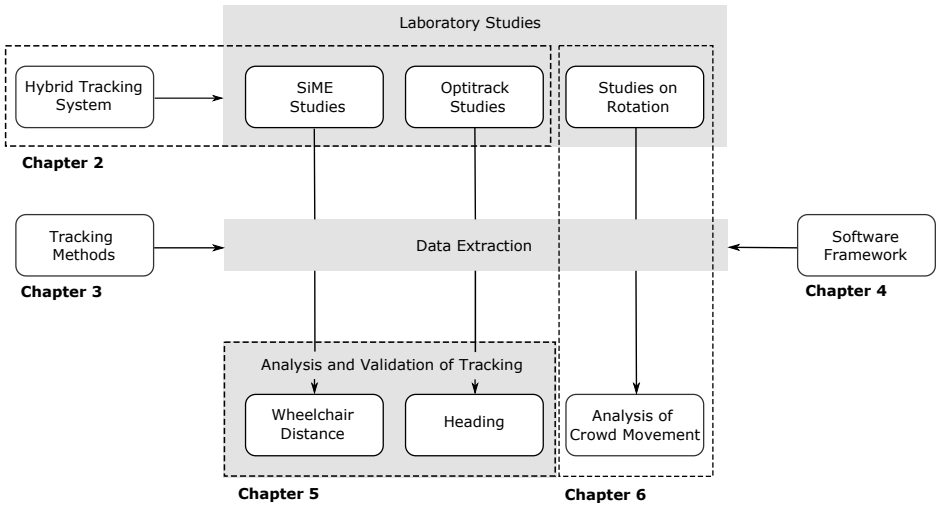

Figure 1.2: Overview of the outline of this thesis.

In Chapter 3 the tracking methods are described. To calculate a position based on IMU data, the orientation of the device needs to be calculated first. For this purpose, measurements of the accelerometer, gyroscope, and magnetometer were fused. To improve the distance tracking, which suffers from error accumulation over time, the

data of the camera system were used for corrections, and the data of two IMUs were fused. Additionally, techniques for the fusion of camera and IMU data are described so that uniform, calibrated and synchronized data in the same frame of reference and for the same time step can be calculated.

The developed software framework for automatically extracting the desired data for given IMU data and trajectories provided by the camera system is presented in Chapter 4. The framework was implemented following certain software engineering guidelines to keep the code clearly structured and open for extensions.

Data gathered in the studies introduced in Chapter 2 were processed with the framework explained in Chapter 4. The resulting tracking data were analyzed and are presented in Chapter 5, focusing on the validation of the distance tracking accuracy for wheelchair users (based on the SiME studies) and the validation of the heading tracking accuracy (based on the Optitrack studies).

As the validation of heading accuracy indicated only a small error, the data capturing method was applied for new studies investigating the rotation of the upper body in bottleneck scenarios. These studies are described in Chapter 6 to illustrate the added value in the analysis of crowd movement that arises from the use of inertial sensors in conjunction with a camera system.

To conclude this thesis, the main results and potential approaches for future improvement are given in Chapter 7.

Chapter 2

Data Capture

For gathering movement data of a crowd, a tracking system is needed that provides gapless trajectories for all pedestrians in this crowd. Based on the positional information at a given time, important characteristics for pedestrian dynamics can be determined such as velocity and density. The basis of this thesis is a data capturing system that not only records position data but also relative movement data (such as acceleration and rotational information) to enable an extended analysis of the crowd's movement. In the following, this novel tracking system is introduced. In addition, conducted studies are described in order to demonstrate the use of the system and to provide data for the analysis and validation of the tracking methods.

2.1 Hybrid Tracking System

The tracking system used consists of two capturing techniques that complement each other. A set of cameras provides overhead recordings of the crowd's movement from which trajectories of each participating person can be extracted based on the detection and tracking of their heads. Additionally, movement sensors are attached to the participants providing individual relative movement data. While the camera system provides accurate trajectory data of participants' heads, IMU sensors allow the capturing of movements not visible to the cameras (due to occlusion) and the calculation of movements that are difficult to reconstruct based on camera data only (such as the rotation of the upper body).

2.1.1 Camera System

A grid of cameras on the ceiling was used as a basic tracking system for gathering trajectory information of pedestrians' heads. By using an overlapping camera grid

a large experimental area can be covered. The cameras need to be synchronized, calibrated, and aligned in a way that overlapping areas enable the concatenation of trajectories from the individual coverage areas. Experiments are usually performed indoors to ensure uniform lighting conditions. All data were recorded from above, and trajectories were then extracted by detecting and tracking participants' heads. This automatic extraction was undertaken with the software PeTrack [113] which is well-established and used by many researcher groups such as [26, 114–118]. With PeTrack the sample images are searched for markers attached to participants' heads (detection) which represent a pedestrian. These pixels are sequentially tracked across images to determine the trajectories [2, 119].

Usually, participants wear caps (markers) to make the detection process easier. These makers enable a link to additional information to the detected person. Since the distance from the person to the camera needs to be known to calculate their actual position, participants typically wear caps (markers) that encode their height. With the known height of the camera and the height of the participant/marker, the perspective distortion can be corrected. While colored caps stand for different height ranges, additional information such as the head orientation can be encoded with structured markers [119, 120]. Besides, individual codes make it possible to personalize each trajectory and connect it to a questionnaire that is filled out by each participant [29].

Figure 2.1 shows processing steps with a sample image for a bottleneck study. In this study, the participants wore colored caps encoding different height ranges. The colors of the caps are very bright so that they were in contrast from the rest of the image. After considering the camera-specific distortion (see Fig. 2.1b) the detection and tracking of the markers provides individual trajectories colored according to the marker (see Fig. 2.1c). The resulting trajectories of all participants can be seen in Fig. 2.1d. After the extraction, information for each frame about the x-, y- and z-position for each detected person is provided where the z-position represents the height. Since the heads were tracked the swaying while walking is visible in the extracted trajectories which can provide information about steps. Straight pink trajectories can be observed for wheelchair users wearing pink caps in Fig. 2.1c.

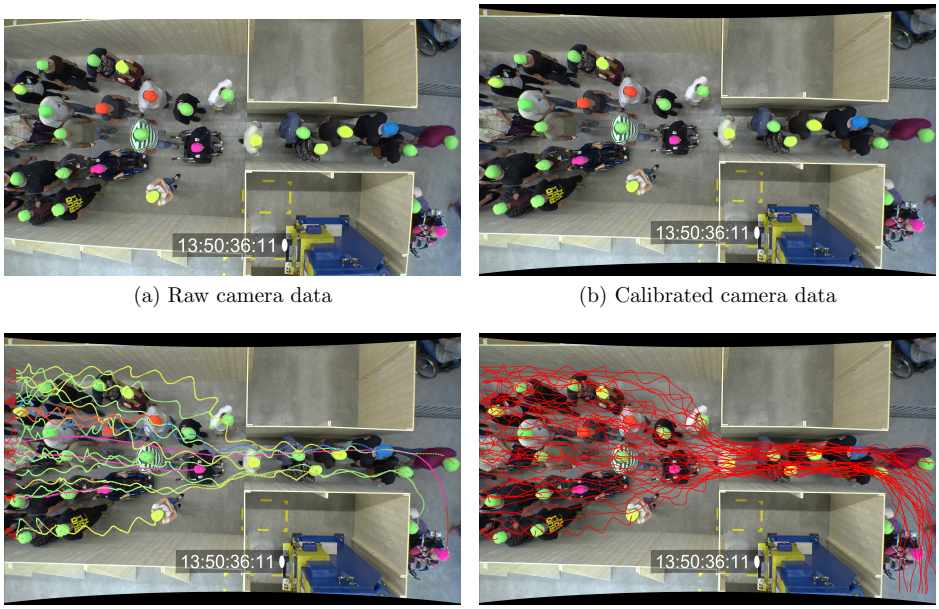

(a) Raw camera data

(b) Calibrated camera data

(c) Trajectories of visible participants

(d) Trajectories of all participants

Figure 2.1: Different steps of processing the camera data.

With the camera system and PeTrack it is possible to gather trajectory information of pedestrians in crowds with a high temporal and spatial resolution. Based on errors when correcting the camera distortion and unknown accurate heights (when using no individual markers) a positional error of a few centimeters must be expected [120]. The error increases from the center to the edge of the image. Nevertheless, the system provides data that are reliable for the analysis of the movement of a crowd. The overhead recordings (perpendicular to the floor) allow for accurate detection and tracking without occlusion for a broad range of body heights. However, when getting closer to the border of the recording area small people are more likely to get occluded due to taller surrounding participants and the perspective view, especially for the shown studies where wheelchair users attended.

2.1.2 IMU System

The SABEL Sense system of SABEL Labs [121] shown in Fig. 2.2 was chosen for the extension of the camera system. Based on the following requirements, this system is the most suitable.

- Technical components: Next to a 3 DOF accelerometer and 3 DOF gyroscope, a 3 DOF magnetometer should be integrated into the sensor as well. This makes it possible to apply tracking algorithms that are based on sensor fusion approaches considering the magnetic field.
- Handling: The sensor should be easily attachable to the body. It should not restrict the movement of the person wearing it. The devices should be housed in a durable case with minimal control elements only so that they cannot be triggered accidentally by the participants.
- Battery life: Usually, when conducting pedestrian experiments many studies are conducted with different configurations one after the other without letting the participants wait long. The battery power should be sufficient for a usage of several hours.
- Storage: Since the transmission of the signal might be affected by large crowds or the geometry, the recorded data of the IMU must be stored locally on the devices. Sufficient storage for recording several hours must be available.
- Affordability and scalability: It should be a low cost system so that it is possible to equip a high number of participants. Additionally, simultaneous data gathering for several participants wearing a sensor must be possible.
- Synchronization mechanisms: A mechanism for synchronizing the sensors with each other must be available. Besides, a synchronization method (not only via movement patterns) is desirable.
- Software: Software for controlling the sensor system and calibrating and processing to IMU data is necessary.

The SABEL sensors contain an accelerometer, gyroscope, and magnetometer measuring the acceleration, angular velocity, and magnetic field along three axes. The sensor components are highly sensitive with a measurement range of $\pm 16\,\mathrm{g}$, $\pm 2000\,^{\circ}\,\mathrm{s}^{-1}$, and ± 8 gauss. A stable housing protects the hardware. The system comes with a software for controlling and synchronizing the sensors wirelessly via a hub device [122]. The sensors can be synchronized with each other and with a camera using an LED signal from the system's hub device. Besides, manual synchronization with the help of movement patterns is possible by searching for significant data in the camera and IMU data.

Figure 2.2: IMU sensors and hub device with an antenna.

With the provided software the sensors need to be calibrated on-site according to [123] to achieve as exact measurements as possible. Tools for data processing and visualization are also available [124]. Each device has local storage from which the recorded data can be downloaded after the capture period. The limiting factor for the data collection is not the available local storage but the battery life of five hours which means the sensors need to be charged during longer studies. Data are usually recorded with a sample rate of 100 Hz. Controlling of the sensor such as start recording, end recording, and synchronization is only possible via the network. In this way, up to 35 sensors can be controlled with one hub device. This can be increased if needed.

As the sensors have been used by other researcher groups to monitor and quantify human motion in the field of sports [125, 126] and even for wheelchair tracking [105], they appeared to be suitable for extending the tracking system.

2.2 Conducted Studies

In the following, the configuration of two studies and technical details on using inertial sensors in combination with a camera system is described. The hybrid tracking system consisting of the camera and IMU system was used for the first time in large-scale pedestrian studies under laboratory conditions investigating the movement of a heterogeneous crowd. As the heading tracking provided promising results additional studies to particularly determine the heading tracking accuracy of the IMU system were conducted with a 3D camera tracking system (Optitrack).

Results and analysis of the position and heading tracking are not discussed here but are described in Chapter 5 (Sec. 5.1 and 5.2).

2.2.1 Movement Studies with Heterogeneous Crowds

Within the scope of the project SiME[1] [109] large-scale pedestrian experiments have been conducted in June 2017 in which the hybrid tracking system was used for capturing movement data. That studies aimed to gather data of the movement of a heterogeneous crowd consisting of people with and without disabilities. Since there is a lack of data in terms of age and mobility for the movement of pedestrians in dense crowds [127], the SiME studies aimed to give new insights in order to make pedestrians' environment safer, especially for pedestrians with disabilities.

Spread over two days 145 studies with 252 participants were conducted investigating their movement in a corridor and bottleneck geometry with varying widths. For the configuration of the crowd (number of participants with and without disabilities or kind of disabilities) a score was developed [128]. Sample images of the movement of a crowd with wheelchair users are shown in Fig. 2.3. Participants wore colored caps to encode different height ranges for improved data extraction (see Sec. 2.1.1).

(a) Corridor run (b) Bottleneck run

Figure 2.3: Sample images of the conducted studies with heterogeneous crowds. Wheelchair users wearing pink caps participated.

Overall, eight wheelchair users participated in the studies who used different types of wheelchairs (mechanical or electric) and with different abilities to move (such as in the need of being pushed or operating the wheelchair with a lever). Due to their low height with a mean of $1.29 \pm 0.10\,\mathrm{m}$ compared to the other participants with a mean height of $1.74 \pm 0.10\,\mathrm{m}$, wheelchair users were likely to be occluded in the crowd.

[1] SiME is a German acronym for "Safety for people with physical, mental or age-related disabilities" and was funded by the German Federal Ministry of Education and Research (BMBF).

Therefore, IMUs were used in addition to provide movement data in case of occlusion. Their wheelchairs were equipped with two IMUs on the backrest aligned centrally and vertically (see Fig. 2.4). Additionally, labels were attached to the shoulders of the wheelchair users to enable the correct assignment of worn sensors (IMU data) and tracked wheelchair users (camera data). The temporal synchronization of IMU and camera data was realized with the help of an LED signal which is explained in detail in Sec. 3.3.1.

Figure 2.4: Participant sitting in a wheelchair that is equipped with IMUs.

Since the focus of this thesis is on tracking methods, the analysis of the SiME studies is not addressed here. However, fundamental diagrams and time-space relations were analyzed specifically for wheelchair users, but also for participants with other disabilities such as walking or visual impairments. Details on this are beyond the scope of this work but have been published in [129–132]. Low densities occurred due to mutual consideration and low motivation in front of the bottleneck, which meant that complete IMU and camera data were available for all wheelchair users (no occlusion occurred) so that data fusion and tracking techniques could be validated. The extracted camera and IMU data have been published and can be found in [133].

2.2.2 Validation with a 3D Camera Tracking System

Since the basic camera tracking system that is used for recording pedestrian experiments (see Sec. 2.1.1) can provide ground truth information of the trajectory of the participant's head only, additional studies were performed to validate the orientation tracking with additional position data. For this purpose, an Optitrack capturing system [134] was used to track several specific points of a person and wheelchair. By attaching optical reflecting markers to these points their 3D positions over time can be calculated based on the recordings of multiple infrared cameras.

The studies were conducted in July 2018 in cooperation with a research group from SABEL Labs at the Charles Darwin University, Darwin, Australia [121] with the purpose to validate the orientation calculation of the IMUs (and therefore of the tracked object) based on their data for the movement of a wheelchair and a walking person. The attachment of IMUs and Optitrack markers is shown in Fig. 2.5. Using the Optitrack system allowed to gather ground truth data of the rotation of a wheelchair and the upper body of a walking person by placing markers on the handles of the wheelchair or shoulders (marked red in Fig. 2.5). In this way, it was possible to track the axis that is moved when the wheelchair/person is rotating and it can be compared with calculated rotation based on data of the attached IMUs. To minimize the reflection sources reflecting parts of the wheelchair were covered with tape. The additional optical markers on the sensors and head (marked orange in Fig. 2.5) were attached for possible future analysis but were not required for the validation of the heading tracking.

(a) Preparation of the wheelchair (b) Preparation of the walking person

Figure 2.5: Attachment of the IMUs and optical markers.

A 12 camera system was used (Optitrack Flex 3 cameras) for the conducted studies. The cameras were placed at different heights around the capturing area to capture a distinct view of the area (see Fig. 2.6). Each camera recorded 2D images and with methods of triangulation in overlapping capturing areas, 3D positions can be reconstructed. An accuracy of sub-millimeters has been reached with an optimal configuration of the system. The aim in such a capture configuration is for at least three separate cameras to detect all markers at any given time. The larger the number of cameras detecting a marker, the higher the accuracy of the marker position.

Figure 2.6: Optitrack cameras spread around capturing area.

The basic configuration of the studies is illustrated in Fig. 2.7. The same person participated in all runs. The tracked person was moving from a starting area to a turning area and back again to the start which is equal to the end area. The start/end and turning points were marked with tape on the ground. The movement from start to end including the turning back is considered as one run. Since overstepping was possible, the tracking range varied but was approximately 3.5 m. Five different scenarios have been investigated:

1. Movement in a **wheelchair using arms** to move forward
2. Movement in a **wheelchair using feet** to move forward
3. **Standing** on a fixed position **and twisting** the upper body to the right and left side
4. **Normal walking**: straight movement and zigzag
5. **Walking in a crowd**: walking with strong rotation of the upper body, doing sidesteps

Five runs were conducted for each scenario, except for the second scenario which was stopped after the fourth run as the participant was struggling with this unfamiliar movement and progressed only slowly. The wheelchair was moved forward by using

arms and feet to investigate the effect of different movement patterns on the heading accuracy. Studies with a wheelchair that is being pushed could not be realized due to the occlusion of markers on the backrest. To investigate the influence of bobbing (up and down movement while walking) the rotation while standing and walking was recorded. The studies of walking with strong rotation and sidesteps have been conducted to represent the movement of a person in a crowd since due to occlusion the movement through an actual crowd cannot be recorded with the Optitrack system.

To synchronize the data of the IMUs and camera system a specific movement was conducted before each run resulting in significant movement patterns in both data sets. This approach is explained in detail in Sec. 3.3.1. The captured data have been published and are available in [135].

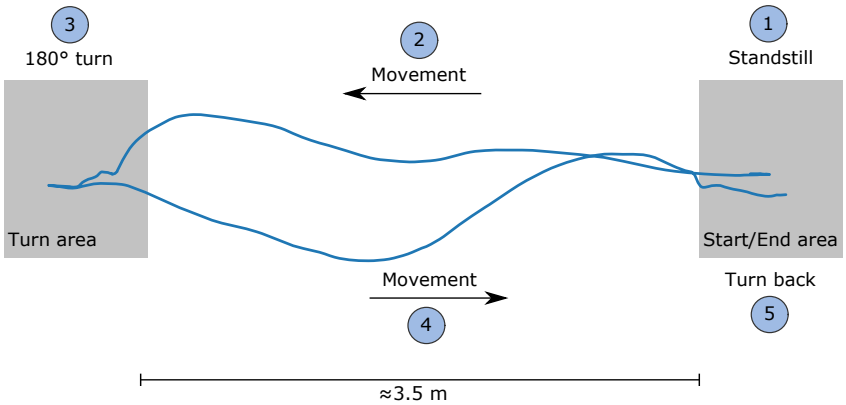

Figure 2.7: Setup of the Optitrack experiments. The person was moving from the starting area (right) to the turning area (left) and moved back to the starting area again.

Chapter 3

Methodology

The individual IMU data captured from a participant were used to derive information about the rotation and position of the sensor and thus, of the person being tracked. In this Chapter, the corresponding methods for heading and distance tracking are described. To use both, IMU and camera data for tracking, mechanisms for synchronizing and calibrating the data are proposed. To limit the drift when calculating positions based on IMU data, several approaches are introduced using data of surrounding people (provided by the camera system) or fusing the data of two IMUs to improve the tracking accuracy.

3.1 Overview

3.1.1 Frames of Reference

When operating with IMU and camera data, the two must be described in the same frame of reference (coordinate system). Since the camera data must be enriched with additional information based on IMU data, the reference frame of the camera trajectories is the desired common reference.

While applying tracking methods, the data were provided in or transformed to three different reference frames which are shown in Fig. 3.1. Reference frame I describes the local coordinate system of the inertial sensors. IMU data were provided in that frame. The sensors were supposed to be attached vertically to the wheelchair or person with the z-axis orientated anteriorly (direction of movement). With W, the world's reference frame is denoted which is a global reference frame based on the earth's magnetic field and gravity which is important during the orientation tracking process. The camera data were given in a global camera frame C which is independent of W and I. The camera frame can be chosen arbitrarily and was typically aligned

with the geometry setup when extracting the trajectories from the video recordings. Figure 3.1c shows an example for the SiME studies.

Basically, the local IMU data needed to be transformed from reference frame I to W and then to the desired reference frame C. As the sensor (or the object/person wearing it) was moving over time, the relation between I and W changed as well and needed to be recalculated over time. In contrast, the relation between W and C remained the same over time and needed to be calculated only once. In the following Sections, it is explained how I, W, and C are related to each other and how transitions between them can be established.

3.1.2 Data Flow and Processing

An overview of the applied tracking methods and the flow of data given in different reference frames is shown in Fig. 3.2. Operations above the dashed line are necessary for heading tracking. Processes below that line belong to the distance tracking methods. The methods for heading tracking can be used as a stand-alone algorithm if only the rotation of the sensor is of interest without the need for distance tracking.

The algorithm starts with preprocessing IMU data and applying the orientation filter to calculate the orientation of the device in the world reference frame W. By calculating the ground truth (GT) heading for a particular part of the camera trajectory, camera and IMU data can be aligned. After the alignment process, the relation of the reference frames W and C, and therefore I and C is known which completes the heading tracking and provides necessary information for the subsequent distance tracking. Afterward, it is possible to rotate the local acceleration data to the camera reference frame C. The gravity is subtracted and various double integration approaches can be applied. Additional camera data of a person nearby were used to limit error and improve the tracking quality.

The temporal synchronization of the IMU and camera data is not visualized in Fig. 3.2 but is described in Sec. 3.3.1. After applying Madgwick's orientation filter [136], only 2D acceleration data in xy-plane were used, so distance tracking also provides 2D position data. Since the gravity is affecting the z-axis only, subtraction of gravity is not necessarily needed for the applied tracking approaches but facilitates analysis of 3D acceleration data without the influence of gravity.

By applying a Measurement-Augmented Kalman Filter [137] the data of two IMUs are fused. For this purpose, the steps leading to the linear acceleration are applied for two different IMU data sets, respectively.

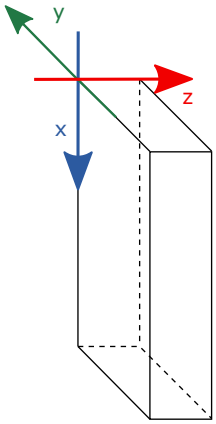

(a) Local IMU frame I

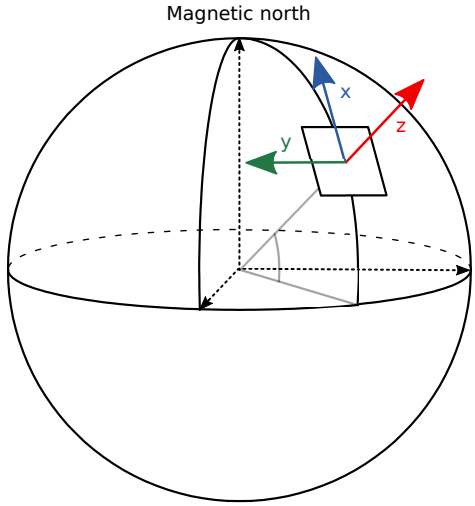

(b) Global world frame W

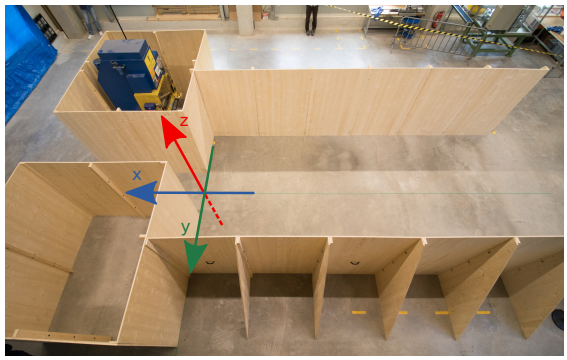

(c) Global camera frame C placed on the floor in the middle of the bottleneck entrance with z pointing up

Figure 3.1: Different reference frames that are important for data processing.

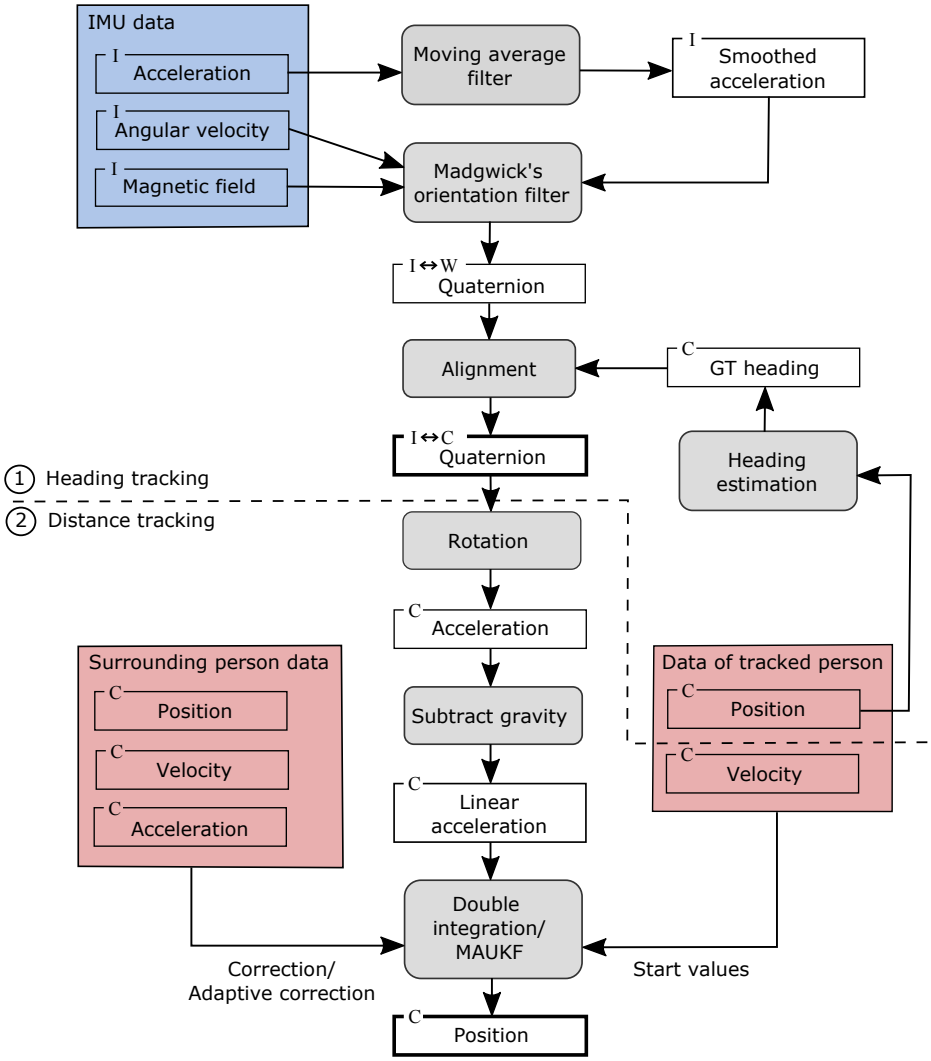

Figure 3.2: Overview of the data flow and processing. IMU data are highlighted in blue, camera data in red, and methods or operations in grey. Frame of reference is indicated with I, W, or C for each data set. The main result of heading and distance tracking is marked bold.

3.2 Tracking with Inertial Sensors

In the following, it is described how absolute information about the orientation and traveled distance of the sensor are determined based on the locally measured acceleration, angular velocity, and magnetic field.

3.2.1 Data Preprocessing

To ensure accurate measurements, IMU sensors need to be calibrated at the location of studies before capturing data. For this purpose, the calibration method provided by the SABEL Sense Software is used [123]. When the sensor is in a stationary state the vector sum of the measured acceleration should be equal to the gravity vector. The calibration aims to estimate a scale factor and offset for each axis which are used to adjust the accelerometer output accordingly. To do so, the sensor must be oriented in six different positions (on each side) and stationarily for each. Specifically, the sensor measures the effect of gravitational acceleration in each of the three axes (x, y, and z) and the opposite direction of each axes. This results in a positive and negative output for each of the three channels. Then by solving a non-linear system of equations the scale factors and offsets are calculated.

Before applying orientation and distance tracking methods the acceleration is smoothed with a moving average filter using a window size of 25 samples to reduce noise. This smoothing filter is applied because the signal measuring the actual acceleration is low compared to the high superimposed noise for slow or constant motion. This is especially important when the tracked person is stationary or moving at a constant speed. The acceleration is expected to be low for the homogeneous movement of a wheelchair user or when rotating the upper body. Since the participants of pedestrian experiments are typically asked to move at a moderate pace, but not fast, a window size of 25 samples which is equal to 0.25 s was chosen. According to [130] the unimpeded speed of the wheelchair users that participated in the SiME studies was $0.96 \pm 0.35\,\mathrm{m\,s^{-1}}$. The average amount of distance covered within 25 samples at that speed is 0.24 m. For the movement in a crowd, the covered distance is even smaller as the participants influence each other's movement. Therefore, no actual fast movements are expected for this period which could be incorrectly smoothed out. Smoothing of gyroscope data did not result in better tracking results and therefore is not applied.

3.2.2 Orientation Tracking

Accelerometer and gyroscope sensors provide information about the relative changes in movement only. The magnetometer measures the absolute magnetic field but only in a local frame. However, when an IMU sensor is not moved an initial absolute orientation regarding the world reference frame can be calculated based on the gravity and earth's magnetic field. When moving the sensor the relation of the local reference frame I to the world reference frame W changes. Starting from an absolute orientation the measurements can be used to calculate a new orientation for each data sample. For this purpose, an orientation filter is applied that fuses data of the individual components of the IMU sensor, using their strengths and compensating for their weaknesses. In this way, an optimized estimate for the orientation of the sensor in a global reference frame is calculated and the local data can be rotated to the desired frame.

3.2.2.1 Orientation Representation

In the first step, the orientation of the device needs to be represented in an appropriate form that allows the application of rotation operations. Common representations for that purpose are Euler angles, quaternions, and direction cosine matrices. For the proposed method quaternions were chosen as they are unaffected by the problem of singularities and no trigonometric functions are required. Quaternions have been used in many orientation tracking algorithms in different research areas such as for pedestrian navigation purposes [42, 43, 46, 52], tracking of human body motions [91, 138], and tracking of vehicles or aircrafts [139–142].

As shown in Eq. 3.1 quaternions describe a rotation by a rotation angle θ around an axis $\boldsymbol{r} = \begin{pmatrix} r_x & r_y & r_z \end{pmatrix}^\intercal$. Frames of reference are specified here by leading subscripts. By ${}^A_B\boldsymbol{q}$ a quaternion is denoted that describes the orientation of frame B relative to frame A. The rotation axis $\boldsymbol{r}$ is given in frame A.

$$ {}^A_B\boldsymbol{q} = \begin{bmatrix} q_0 & q_1 & q_2 & q_3 \end{bmatrix} = \begin{bmatrix} cos(\theta/2) & -r_x sin(\theta/2) & -r_y sin(\theta/2) & -r_z sin(\theta/2) \end{bmatrix} \tag{3.1} $$

The conjugated quaternion is marked with * and describes the contrary rotation as defined in Eq. 3.2. To rotate a vector $\boldsymbol{x}$ given in frame A to frame B by a quaternion Eq. 3.3 can be applied where $\otimes$ defines a quaternion product [143].

$$ {}^A_B\boldsymbol{q}^* = {}^B_A\boldsymbol{q} = \begin{bmatrix} q_0 & -q_1 & -q_2 & -q_3 \end{bmatrix} \tag{3.2} $$

$$^{B}\boldsymbol{x} = {}^{A}_{B}\boldsymbol{q} \otimes {}^{A}\boldsymbol{x} \otimes {}^{A}_{B}\boldsymbol{q}^{*} \tag{3.3}$$

Since the initial orientation is based on gravity and the earth's magnetic field the algorithm provides quaternions in the form ${}^{I}_{W}\boldsymbol{q}$ which relates IMU data to the world frame (see Fig. 3.1a and 3.1b). More details regarding quaternions and their operations can be found in [143].

3.2.2.2 Madgwick's Orientation Filter

For calculating the orientation of the sensor, Madgwick's orientation filter is applied which is introduced in [136, 144]. That filter fuses measurements of the magnetometer, accelerometer, and gyroscope to calculate an optimized orientation estimation. With a validation study, a filter accuracy with a root mean square error of less than 1° could be achieved with an Xsens sensor [136]. Besides the high accuracy of the filter, its application on data of SABEL Labs sensors [105] with promising results contributed to the choice of this orientation tracking procedure.

The basic idea of the filter is to calculate the sensor's orientation by fusing the measurements of its various components. Basically, two estimators of the orientation are calculated using measurements of the different sensor components and considering their specific strengths and weaknesses. Afterward, these two estimators are weighted and fused resulting in an optimized orientation estimation. The first estimation is based on gyroscope measurements only, while the second is calculated considering accelerometer and magnetometer measurements. Based on [136, 144] a basic introduction of the orientation filter is given in the following.

As a first estimate for the orientation, the measurement output of the gyroscope is used. The angular velocity ${}^{I}\boldsymbol{w}$ (see Eq. 3.4) can be used to calculate the quaternion derivative ${}^{I}_{W}\dot{\boldsymbol{q}}$ as in Eq. 3.5 describing the rate of change of orientation of the world reference frame W relative to the IMU reference frame I.

$$^{I}\boldsymbol{w} = \begin{bmatrix} 0 & w_x & w_y & w_z \end{bmatrix} \tag{3.4}$$

$$^{I}_{W}\dot{\boldsymbol{q}} = \frac{1}{2}\, {}^{I}_{W}\boldsymbol{q} \otimes {}^{I}\boldsymbol{w} \tag{3.5}$$

Assuming that initial conditions are known the actual orientation ${}^{I}_{W}\boldsymbol{q}_{\boldsymbol{w},\boldsymbol{i}}$ can be calculated by numerically integrating the quaternion derivative as in Eq. 3.6 and 3.7 for time t_i with i indicating the time step and a sampling period $\Delta t = t_i - t_{i-1}$.

The notation $\boldsymbol{q_w}$ specifies that the quaternion was calculated based on the angular velocity $\boldsymbol{w}$.

$$ {}_{W}^{I}\dot{\boldsymbol{q}}_{\boldsymbol{w},i} = \frac{1}{2}\, {}_{W}^{I}\boldsymbol{q}_{i-1} \otimes {}^{I}\boldsymbol{w}_i \tag{3.6} $$

$$ {}_{W}^{I}\boldsymbol{q}_{\boldsymbol{w},i} = {}_{W}^{I}\boldsymbol{q}_{i-1} + {}_{W}^{I}\dot{\boldsymbol{q}}_{\boldsymbol{w},i}\Delta t \tag{3.7} $$

The second approach for estimating the orientation uses the accelerometer and magnetometer measurements. The measurements of one of these components cannot provide a unique orientation. However, both can be combined for this purpose.

An initial assumption is that the sensor is stationary so that the accelerometer measures gravity and the magnetometer measures the earth's magnetic field only. To find the quaternion ${}_{W}^{I}\boldsymbol{q}$ (see Eq. 3.8) that rotates a reference direction in the world frame ${}^{W}\boldsymbol{d}$ (see Eq. 3.9) to the measured direction in the IMU frame ${}^{I}\boldsymbol{s}$ (see Eq. 3.10) an optimization problem is defined as in Eq. 3.11 and 3.12.

$$ {}_{W}^{I}\boldsymbol{q} = \begin{bmatrix} q_1 & q_2 & q_3 & q_4 \end{bmatrix} \tag{3.8} $$

$$ {}^{W}\boldsymbol{d} = \begin{bmatrix} 0 & d_x & d_y & d_z \end{bmatrix} \tag{3.9} $$

$$ {}^{I}\boldsymbol{s} = \begin{bmatrix} 0 & s_x & s_y & s_z \end{bmatrix} \tag{3.10} $$

$$ \min_{{}_{W}^{I}\boldsymbol{q}} \boldsymbol{f}({}_{W}^{I}\boldsymbol{q}, {}^{W}\boldsymbol{d}, {}^{I}\boldsymbol{s}) \tag{3.11} $$

$$ \boldsymbol{f}({}_{W}^{I}\boldsymbol{q}, {}^{W}\boldsymbol{d}, {}^{I}\boldsymbol{s}) = {}_{W}^{I}\boldsymbol{q}^{*} \otimes {}^{W}\boldsymbol{d} \otimes {}_{W}^{I}\boldsymbol{q} - {}^{I}\boldsymbol{s} \tag{3.12} $$

This is solved with a gradient descent algorithm which general form is defined in Eq. 3.13 for n iterations, step size μ and ${}_{W}^{I}\boldsymbol{q}_0$ as an initial guess for the orientation.

$$ {}_{W}^{I}\boldsymbol{q}_{k+1} = {}_{W}^{I}\boldsymbol{q}_{k} - \mu \frac{\nabla \boldsymbol{f}({}_{W}^{I}\boldsymbol{q}_k, {}^{W}\boldsymbol{d}, {}^{I}\boldsymbol{s})}{\|\nabla \boldsymbol{f}({}_{W}^{I}\boldsymbol{q}_k, {}^{W}\boldsymbol{d}, {}^{I}\boldsymbol{s})\|}, \qquad k = 0, 1, 2 \ldots n \tag{3.13} $$

By substituting ${}^{W}\boldsymbol{d}$ with the direction of the gravity and magnetic field, and ${}^{I}\boldsymbol{s}$ with the corresponding sensor measurements a specified optimization problem is defined. It is assumed that the gravity ${}^{W}\boldsymbol{g}$ affects only the z-axis of the accelerometer (see Eq. 3.14) while the earth's magnetic field ${}^{W}\boldsymbol{b}$ influences only one horizontal and

the vertical axes of the magnetometer in world frame W (see Eq. 3.15). These assumptions allow a simplification of the objective function introduced in Eq. 3.18 in order to solve the optimization problem.

$$^{W}\boldsymbol{g} = \begin{bmatrix} 0 & 0 & 0 & 1 \end{bmatrix} \tag{3.14}$$

$$^{W}\boldsymbol{b} = \begin{bmatrix} 0 & b_x & 0 & b_z \end{bmatrix} \tag{3.15}$$

The measurements of the accelerometer $^{W}\boldsymbol{a}$ and magnetometer $^{W}\boldsymbol{m}$ can be distributed to all axes (see Eq. 3.16 and 3.17).

$$^{I}\boldsymbol{a} = \begin{bmatrix} 0 & a_x & a_y & a_z \end{bmatrix} \tag{3.16}$$

$$^{I}\boldsymbol{m} = \begin{bmatrix} 0 & m_x & m_y & m_z \end{bmatrix} \tag{3.17}$$

Substituting $^{W}\boldsymbol{g}$ and $^{W}\boldsymbol{b}$ for the general direction $^{W}\boldsymbol{d}$ and by substituting the actual sensor measurements $^{I}\boldsymbol{a}$ and $^{I}\boldsymbol{m}$ for $^{I}\boldsymbol{s}$, respectively, two objective functions are defined and combined (see Eq. 3.18). With Eq. 3.19 the second orientation estimator $_{W}^{I}\boldsymbol{q}_{\nabla,i}$ based on the measurements of the accelerometer $^{I}\boldsymbol{a}_i$ and magnetometer $^{I}\boldsymbol{m}_i$ sampled for time step i is calculated.

$$\boldsymbol{f}_{\boldsymbol{g},\boldsymbol{b}}(_{W}^{I}\boldsymbol{q}, {}^{I}\boldsymbol{a}, {}^{W}\boldsymbol{b}, {}^{I}\boldsymbol{m}) = \begin{bmatrix} \boldsymbol{f}_{\boldsymbol{g}}(_{W}^{I}\boldsymbol{q}, {}^{I}\boldsymbol{a}) \\ \boldsymbol{f}_{\boldsymbol{b}}(_{W}^{I}\boldsymbol{q}, {}^{W}\boldsymbol{b}, {}^{I}\boldsymbol{m}) \end{bmatrix} \tag{3.18}$$

$$_{W}^{I}\boldsymbol{q}_{\nabla,i} = {}_{W}^{I}\boldsymbol{q}_{i-1} - \mu_i \frac{\nabla \boldsymbol{f}_{\boldsymbol{g},\boldsymbol{b}}(_{W}^{I}\boldsymbol{q}_{i-1}, {}^{I}\boldsymbol{a}_i, {}^{W}\boldsymbol{b}, {}^{I}\boldsymbol{m}_i)}{\|\nabla \boldsymbol{f}_{\boldsymbol{g},\boldsymbol{b}}(_{W}^{I}\boldsymbol{q}_{i-1}, {}^{I}\boldsymbol{a}_i, {}^{W}\boldsymbol{b}, {}^{I}\boldsymbol{m}_i)\|} \tag{3.19}$$

Finally, the orientation estimators defined in Eq. 3.7 and 3.19 are weighted and fused to calculate an estimator for the orientation. In this way, the measurements of all components of the IMU are used. While the gyroscope is affected by measurement noise, the accelerometer might not be completely stationary and the magnetometer might be exposed to interferences. Thus, the fusion of all data channels is an error-resistant approach. Further details on the choice of the step size μ_i for the optimization problem and the weights for fusing the quaternion estimations can be found in [136]. Applied methods for compensating magnetic distortion and gyroscope bias drift have also been explained in this publication. Besides, an alternative version of this algorithm is described that is not considering magnetometer measurements since the tracking can suffer from disturbances of the magnetic field.

The only parameter that needs to be adjusted is the filter gain that represents all mean zero measurement errors of the gyroscope. This filter gain is sensor-specific and is provided by SABEL Labs so that no parameter tuning is required for this orientation tracking approach.

3.2.3 Distance Tracking

Due to the participating wheelchair users in the SiME studies (see Sec. 2.2.1) the focus of the distance tracking method is the reconstruction of the trajectories of wheelchair users only. Their characteristic homogeneous movement allows integrating the acceleration data to calculate their traveled distance according to INS algorithms. The basic approach of double integration is expanded by fusing the data of two sensors to improve the tracking quality. The described methods use IMU data only. Improved tracking approaches with the help of camera data are described in Sec. 3.3.2.

Since acceleration data in the camera frame are needed for distance tracking, the orientation calculation explained in Sec. 3.2.2.2 is a required preceding step and provides information about the quaternions.

3.2.3.1 Application of Double Integration

The first and simple approach is to calculate the position data out of the acceleration with numerical integration methods. Once the local acceleration data ${}^{I}\boldsymbol{a}$ were transformed to a global acceleration ${}^{W}\boldsymbol{a}$ for each time step i by Eq. 3.20, the gravity was subtracted as in Eq. 3.21 resulting in linear acceleration data ${}^{W}\boldsymbol{a}_{\text{linear}}$ that were measured due to the actual movement of the wheelchair.

$$ {}^{W}\boldsymbol{a}_i = {}^{I}_{W}\boldsymbol{q}_i \otimes {}^{I}\boldsymbol{a}_i \otimes {}^{I}_{W}\boldsymbol{q}_i^{*} \tag{3.20} $$

$$ {}^{W}\boldsymbol{a}_{\text{linear},\,i} = {}^{W}\boldsymbol{a}_i - \begin{pmatrix} 0 \\ 0 \\ 9.81 \end{pmatrix} \tag{3.21} $$

After rotating the acceleration data into global space, only x- and y-values are used for trajectory construction. By double integrating the acceleration data the velocity $\boldsymbol{v}_i$ and position $\boldsymbol{s}_i$ can be calculated as in Eq. 3.22 and 3.23 with $\Delta t = t_i - t_{i-1}$. Applying higher order numerical methods for this purpose does not provide better results since the data have been smoothed before (see Sec. 3.2.1).

$$ \boldsymbol{v}_i = \boldsymbol{v}_{i-1} + \frac{\Delta t}{2} \cdot ({}^{W}\boldsymbol{a}_{\text{linear},\,i-1} + {}^{W}\boldsymbol{a}_{\text{linear},\,i}) \tag{3.22} $$

$$\boldsymbol{s}_i = \boldsymbol{s}_{i-1} + \frac{\Delta t}{2} \cdot (\boldsymbol{v}_{i-1} + \boldsymbol{v}_i) \tag{3.23}$$

3.2.3.2 Application of a Kalman Filter

While the double integration approach uses the data of one sensor only, a Kalman filter (KF) is applied to fuse the data of two IMUs for distance tracking. The KF is a linear filtering approach that calculates estimates of unknown variables considering statistical noise and other inaccuracies [145]. Based on the ideas in [66] and [68] a Measurement-Augmented Kalman Filter (MAUKF) was designed that fuses the data of two IMUs by using the knowledge that both sensors are tracking the same movement when attached to a wheelchair as in Fig. 2.4. Due to the nature of placement constraints, the MAUKF is a non-linear KF. The system is described by the following state transition equation

$$\boldsymbol{x}_{i+1} = A \cdot \boldsymbol{x}_i + \boldsymbol{w}_i \tag{3.24}$$

and the measurement equation

$$\boldsymbol{y}_i = C \cdot \boldsymbol{x}_i + \boldsymbol{v}_i \,. \tag{3.25}$$

The modeled system limited to the x-y plane of motion is a 12 state system consisting of 2D acceleration $\boldsymbol{a}$, velocity $\boldsymbol{v}$, and position data $\boldsymbol{s}$ of two sensors that were attached to the same wheelchair. The state vector $\boldsymbol{x}_i$ and measurement vector $\boldsymbol{y}_i$ for time t_i with i indicating the time step are defined in Eq. 3.26 with $\boldsymbol{s}_1, \boldsymbol{v}_1$, and $\boldsymbol{a}_1$ belonging to the first sensor and $\boldsymbol{s}_2, \boldsymbol{v}_2$, and $\boldsymbol{a}_2$ belonging to the second sensor. The proposed filter is similar to the work reported in [68] but computes the position in 2D using the global linear acceleration data based on Madgwick's orientation filter instead of processing local acceleration data as input. Therefore, the rotation calculation is not part of the implemented MAUKF.

$$\boldsymbol{x}_i = \begin{pmatrix} \boldsymbol{s}_1 \\ \boldsymbol{v}_1 \\ \boldsymbol{a}_1 \\ \boldsymbol{s}_2 \\ \boldsymbol{v}_2 \\ \boldsymbol{a}_2 \end{pmatrix} \in \mathbb{R}^{12}, \qquad \boldsymbol{y}_i = \begin{pmatrix} \boldsymbol{a}_1 \\ \boldsymbol{a}_2 \end{pmatrix} \in \mathbb{R}^4 \tag{3.26}$$

The state transition matrix A implements the double integration process and is given by Eq. 3.27 and 3.28 with $\Delta t = t_{i+1} - t_i$. I_m denotes the identity matrix and $0_{m \times n}$ the zero matrix with the dimensions m and n.

$$A = \begin{pmatrix} A_1 & 0_{6\times6} \\ 0_{6\times6} & A_1 \end{pmatrix} \tag{3.27}$$

$$A_1 = \begin{pmatrix} I_2 & \Delta t \cdot I_2 & \frac{\Delta t^2}{2} \cdot I_2 \\ 0_{2\times2} & I_2 & \Delta t \cdot I_2 \\ 0_{2\times2} & 0_{2\times2} & I_2 \end{pmatrix} \tag{3.28}$$

The measurement transition matrix C is given by Eq. 3.29 and relates the state vector to the measured acceleration.

$$C = \begin{pmatrix} 0_{2\times4} & I_2 & 0_{2\times4} & 0_{2\times2} \\ 0_{2\times4} & 0_{2\times2} & 0_{2\times4} & I_2 \end{pmatrix} \tag{3.29}$$

Up to this point, the filter would be a conventional KF estimating the separate states of the two IMUs. Knowing that the calculated positions $\boldsymbol{s}_1$ and $\boldsymbol{s}_2$ must be the same for each step since both IMUs were attached on the same vertical axis on the wheelchair the calculations can be restricted. By implementing this non-linear placement restriction the filter becomes MAUKF where the distance $D = |\boldsymbol{s}_1 - \boldsymbol{s}_2|$ between both sensors was calculated as in [68] by:

$$D^2 = \boldsymbol{x}_k^T \cdot G \cdot \boldsymbol{x}_k \tag{3.30}$$

with

$$G = \begin{pmatrix} I_2 & 0_{2\times4} & -I_2 & 0_{2\times4} \\ 0_{4\times2} & 0_{4\times4} & 0_{4\times2} & 0_{4\times4} \\ -I_2 & 0_{2\times4} & I_2 & 0_{2\times4} \\ 0_{4\times2} & 0_{4\times4} & 0_{4\times2} & 0_{4\times4} \end{pmatrix}. \tag{3.31}$$

Since the distance between the reconstructed positions should be zero, the new measurement vector $\tilde{\boldsymbol{y}}$ is defined as in Eq. 3.32 which leads to the varied measurement equation (see Eq. 3.33). A detailed description of the forecast and projections steps and the choice of sigma points and weights can be found in [137].

$$\tilde{\boldsymbol{y}}_i = \begin{pmatrix} \boldsymbol{y}_i \\ 0 \end{pmatrix} = \begin{pmatrix} \boldsymbol{a}_1 \\ \boldsymbol{a}_2 \\ D^2 \end{pmatrix} \in \mathbb{R}^5 \tag{3.32}$$

$$\tilde{\boldsymbol{y}}_i = \begin{pmatrix} C \cdot \boldsymbol{x}_i \\ \boldsymbol{x}_i^T \cdot G \cdot \boldsymbol{x}_i \end{pmatrix} + \begin{pmatrix} \boldsymbol{v}_i \\ 0 \end{pmatrix} \tag{3.33}$$

Due to the slow movement of the wheelchair users, small changes must be noticed by the filter and cannot be smoothed out. Therefore, the measurement noise matrix R was created with smaller values (based on the standard deviation of the accelerometer

noise $\sigma = 0.004\,g$) than the process noise matrix Q (see Eq. 3.34) which results in more uncertainty for the modeled process. Besides, the acceleration data are smoothed by a moving-average filter at the beginning and Madgwick's orientation filter and the fixed distance between the tracked position ($D^2 = 0$) can be considered as a noiseless value. Process noise is given due to the assumption that both sensors are measuring the same movement which cannot be guaranteed since the sensors are not exactly vertically aligned or might suffer from different magnetic disturbances and external impacts due to their different attachment positions.

$$R = \begin{pmatrix} \sigma^2 & 0 & 0 & 0 & 0 \\ 0 & \sigma^2 & 0 & 0 & 0 \\ 0 & 0 & \sigma^2 & 0 & 0 \\ 0 & 0 & 0 & \sigma^2 & 0 \\ 0 & 0 & 0 & 0 & 0 \end{pmatrix}, \qquad Q = I_{12\times 12} \tag{3.34}$$

A comprehensive analysis of tuning Q and R could be done to improve the results. Additionally, an adaptive Kalman filter as in [146] might be suitable and could be investigated in the future.

3.3 Fusion of IMU and Camera Data

Since inertial data must be provided in camera reference frame C, camera and IMU data need to be synchronized in time and the frame of reference must be aligned. Afterward, it is possible to apply distance tracking algorithms as explained in Sec. 3.2.3 and to use camera data during that process to improve the tracking quality.

In the following Sections, IMU data given for one time step are referred to as samples (with a sample rate of 100 samples per second) while measurements of the camera system for one time step are referred to as frames (with a frame rate of 25 frames per second). Reference frames denoted by I, W, or C are still standing for coordinate systems as defined at the beginning of this Chapter (see Fig. 3.1).

3.3.1 Synchronization and Calibration

The first step for synchronizing IMU and camera data is to find the samples and frames that were recorded for the same time range (typically the time of a study/run). Two approaches are applied for this purpose. While the data sets for the SiME studies (see Sec. 2.2.1) are synchronized with an LED signal, data of the validation studies (see Sec. 2.2.2) are synchronized with a significant movement. Usually, the synchronization

points are generated at the beginning and end of an experiment so that start and end samples/frames can be found.

For the SiME studies synchronization signals were triggered from the hub device of the IMU system. This added a record to the IMU data and initiated a flashing of an LED which was visible to the camera system. In order to synchronize the data sets, the corresponding frames and samples of the signals are extracted out of the data (frame of first appearance of LED, sample of LED record).

For the validation studies with the infrared camera system, the synchronization was done with the help of a vertical movement according to [88]. A heel drop was conducted at the start and end of a run (plantarflexing to stand on the toes and drop on the heel). Figure 3.3 shows an example of acceleration spike data of a heel drop. The sample of the first negative peak (local minimum) on the x-axis of the local acceleration is chosen as the significant sample here. For the corresponding frame, the lowest position on the vertical movement axis of the marker on the sensor is searched for. The same synchronization approach is also applicable to the movement of the wheelchair. For this purpose, the wheelchair was slightly lifted and dropped to receive significant signals.

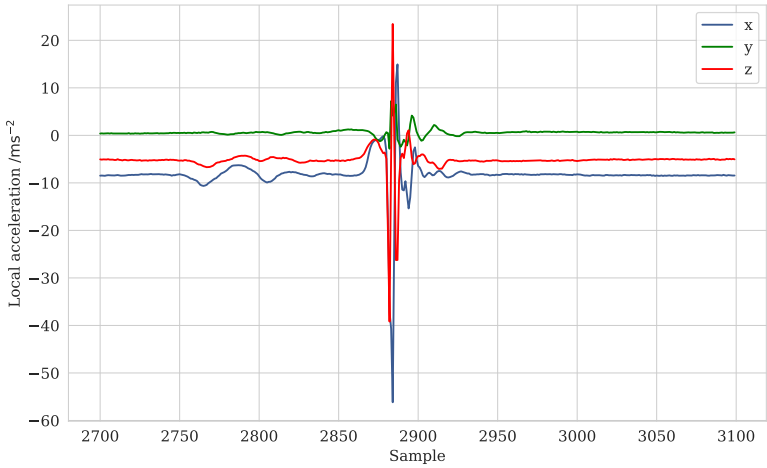

Figure 3.3: Acceleration data for a heel drop. Data of the heel drop itself clearly stand out.

As a next step for the temporal synchronization, a sample needs to be assigned to the corresponding frame and vice versa. Since camera and IMU data were recorded with a different frame and sample rate, the recordings need to be mapped to each

other. The determined start and end samples/frames are relative timestamps only. Based on the number of frames/samples recorded between the synchronization points the elapsed time can be estimated. Due to inaccuracies when recording the data, the elapsed time based on the IMU data and the elapsed time based on the camera data must not be the same. To overcome this issue a scale factor is used to find the corresponding frame for a sample. This scale factor S is the ratio of the number of recorded frames N_f and the number of recorded samples N_s between the synchronization points as defined in Eq. 3.35.

$$S = \frac{N_f}{N_s}, \qquad i = \lfloor S * j + 0.5 \rfloor \tag{3.35}$$

Assuming the frames are available for equidistant time steps i and the samples are given for equidistant time steps j within the synchronized period, time steps i for a given j can be assigned using the scale factor. Typically, the i and j do not start at zero so that offsets must be considered.

For the SiME studies, the sampling rate was higher than the frame rate. Therefore, a group of samples is available for the same frame. The first sample of that groups is assigned to the frames. An illustration of the assignment process is shown in Fig. 3.4 with a sampling rate that is twice the frame rate. For the same time, 15 frames and 32 samples were recorded which means that two extra samples were recorded. When processing IMU and camera data to improve tracking the same frame is assigned to two or three consecutive samples according to Eq. 3.35. The scaled assignment ensures that the extra recorded samples are spread over time. If the data of an IMU sample are needed for a camera frame, the samples marked in blue are assigned. This direction of assignment is only needed to find the start and end samples of the IMU data for a given camera trajectory.

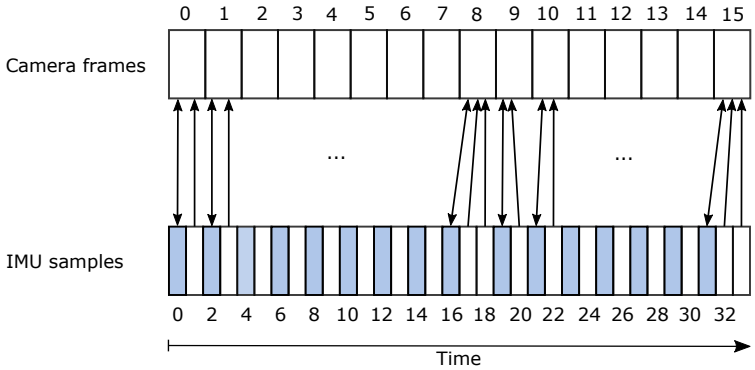

Figure 3.4: Assignment of camera frames and IMU samples recorded for the same period.

After synchronizing camera and IMU data, the IMU data must be provided in camera frame C. When applying Madgwick's orientation filter the sensor data are aligned in global world frame W.

It is assumed that the reference frames W and C share the same z-axis. Therefore, a rotation angle around the z-axis of reference frame W needs to be found to align the x- and y-axes. For this purpose, the direction of movement is calculated based on IMU data in world frame W and based on camera data in camera frame C. To calculate these heading angles the tracked person is supposed to move without abrupt changes in the direction of movement. Camera and IMU data must be available for the same time range which could be before or after the IMU tracking range.

As a condition for the alignment, the local z-axis of the IMU must point in the direction of movement. Thus, the local z-axis ${}^{I}\boldsymbol{z}$ is rotated by quaternions to reference frame W as shown in Eq. 3.36. Since the sensors were attached vertically to the wheelchair or person the rotated z-axis ${}^{W}\boldsymbol{z}$ should be in the global xy-plane. The heading angle α_{imu} is then calculated by Eq. 3.37.

$$ {}^{W}\boldsymbol{z} = {}^{I}_{W}\boldsymbol{q}_i \otimes {}^{I}\boldsymbol{z} \otimes {}^{I}_{W}\boldsymbol{q}_i^* = {}^{I}_{W}\boldsymbol{q}_i \otimes \begin{pmatrix} 0 \\ 0 \\ 1 \end{pmatrix} \otimes {}^{I}_{W}\boldsymbol{q}_i^* \tag{3.36} $$

$$ \alpha_{\text{imu}} = \arctan\left(\frac{{}^{W}z_y}{{}^{W}z_x}\right) \tag{3.37} $$

To achieve a sufficient estimate for the heading angle from the camera data, the person should move with a constant velocity and their trajectory should be linear for several consecutive frames to get the best estimate. Based on a start frame i and end

frame $i+r$ the corresponding positions of the trajectory ${}^{C}\boldsymbol{s}_j$ are given for a person and a movement direction ${}^{C}\boldsymbol{d}$ and heading angle α_{camera} are estimated as in Eq. 3.38. A constant speed is necessary to ensure that the person is moving and not the swaying of their head while standing is used for this calculation.

$$ {}^{C}\boldsymbol{d} = {}^{C}\boldsymbol{s}_{i+r} - {}^{C}\boldsymbol{s}_i, \qquad \alpha_{\text{camera}} = \arctan(\frac{{}^{C}d_y}{{}^{C}d_x}) \tag{3.38} $$

The difference angle $\alpha_{\text{diff}} = \alpha_{\text{camera}} - \alpha_{\text{imu}}$ is used to create a quaternion that represents the rotation around the z-axis as shown in Eq. 3.39. Using this quaternion the acceleration data in camera frame C can be calculated by rotating the data from Eq. 3.21 as in Eq. 3.40.

$$ {}^{W}_{C}\boldsymbol{q} = \begin{bmatrix} \alpha_{\text{diff}} & 0 & 0 & 1 \end{bmatrix} \tag{3.39} $$

$$ {}^{C}\boldsymbol{a}_i = {}^{W}_{C}\boldsymbol{q} \otimes {}^{I}_{W}\boldsymbol{q}_i \otimes {}^{I}\boldsymbol{a}_i \otimes {}^{I}_{W}\boldsymbol{q}_i^* \otimes {}^{W}_{C}\boldsymbol{q}^* \tag{3.40} $$

3.3.2 Utilizing Camera Data while Tracking

3.3.2.1 Processing Camera Data

To calculate a trajectory in reference frame C tracking methods described in Section 3.2.3 are applied with the acceleration data resulting from Eq. 3.40 as input. In order to improve the tracking quality velocity and acceleration data are calculated from the camera trajectories so that these additional data can be used while tracking. The basic idea is that the velocity or acceleration of the wheelchair based on IMU data must be similar to the velocity or acceleration based on camera data of people that are moving close to the wheelchair user and causing the occlusion. For reasons of simplification, data of wheelchair users who were pushed by another person are taken into account only (with the pushing person as the surrounding person). However, this approach is also applicable for any surrounding persons of wheelchair users.

The velocity $\boldsymbol{v}_i$ based on camera data for frame i is determined by calculating the covered distance within $2 * j$ frames (to smooth out swaying) using the extracted position data $\boldsymbol{s}_i$ (see Eq. 3.41) with a frame rate of $fr = 25\,s^{-1}$.

$$ \boldsymbol{v}_i = \frac{\boldsymbol{s}_{i+j} - \boldsymbol{s}_{i-j}}{\frac{2*j}{fr}} \tag{3.41} $$

Acceleration data $\boldsymbol{a}_i$ can also be derived from the position data given by the camera system. Since acceleration is the change in velocity it can be estimated as follows:

$$\boldsymbol{a}_i = \frac{\boldsymbol{v}_i - \boldsymbol{v}_{i-1}}{\frac{1}{fr}} \tag{3.42}$$

Since the velocity data are already smoothed (within $2*j$ frames), the acceleration is calculated based on the velocity for two consecutive frames only. For estimating the velocity $j = 6$ is chosen which is a period of nearly 0.5 s. This short range is chosen to gain better estimates when the direction of the trajectory was changing quickly. However, this leads to the problem of instability of the velocity vector when the person is moving slowly or even waiting in front of the bottleneck. Due to stronger swaying or moving of the head while standing the velocity vector would change considerably and would not represent the actual movement speed and their direction. As the start position and velocity for $i = 0$ are taken from the camera data, the tracking approach is very sensitive to the initial velocity and the start time of tracking. When the person was moving at a steady speed the best results have been seen.

The velocity and acceleration data from Eq. 3.41 and 3.42 have been used to restrict the IMU tracking data when double integrating or applying MAUKF. Two different approaches have been investigated for the double integration and MAUKF method respectively and are described in the following.

3.3.2.2 Correction

As a first simple approach, the velocity of the IMU $\boldsymbol{v}_{\text{imu}}$ (calculated based on IMU data) is set to the velocity of the pushing person $\boldsymbol{v}_{\text{pusher}}$ (calculated based on camera data) when their difference exceeded a predefined range $\boldsymbol{v}_{\text{range}}$. The difference in velocity $\boldsymbol{v}_{\text{diff}}$ is calculated for each time step i as in Eq. 3.43. If its norm exceeds a range of $\boldsymbol{v}_{\text{range}}$ at time step k as in Eq. 3.44 $\boldsymbol{v}_{\text{imu}}$ is set to $\boldsymbol{v}_{\text{pusher}}$ and the calculation is continued normally until the next reset.

$$\boldsymbol{v}_{\text{diff},\,i} = \boldsymbol{v}_{\text{imu},\,i} - \boldsymbol{v}_{\text{pusher},\,i} \quad \forall i \in \{1, ..., n\} \tag{3.43}$$

$$|\boldsymbol{v}_{\text{diff},\,k}| > \boldsymbol{v}_{\text{range}} \tag{3.44}$$

For the MAUKF approach, the velocities of both sensors are considered by choosing the larger difference as in Eq. 3.45 with $\boldsymbol{v}_{1,i}$ denoting the velocity of the first IMU and $\boldsymbol{v}_{2,i}$ denoting the velocity of the second IMU. If the norm of $\boldsymbol{v}_{\text{diff}}$ exceeds $\boldsymbol{v}_{\text{range}}$

the velocities of both sensors are reset. In addition to this, the acceleration data of the pushing person (based on the camera data) are used as input for one step of the KF to read in the corrected measurements as well. The adapted measurement vector $\boldsymbol{y}_k$ is defined in Eq. 3.46 and replaced in Eq. 3.32.

$$\boldsymbol{v}_{\text{diff},\,i} = \begin{cases} \boldsymbol{v}_{1,\,i} - \boldsymbol{v}_{\text{pusher},\,i} & \text{if } |\boldsymbol{v}_{1,\,i} - \boldsymbol{v}_{\text{pusher},\,i}| > |\boldsymbol{v}_{2,\,i} - \boldsymbol{v}_{\text{pusher},\,i}|\,, \\ \boldsymbol{v}_{2,\,i} - \boldsymbol{v}_{\text{pusher},\,i} & \text{otherwise.} \end{cases} \tag{3.45}$$

$$\boldsymbol{y}_k = \begin{pmatrix} \boldsymbol{a}_{\text{pusher},\,k} \\ \boldsymbol{a}_{\text{pusher},\,k} \end{pmatrix} \tag{3.46}$$

As an estimate for $\boldsymbol{v}_{\text{range}}$ the averaged absolute difference in velocity for a wheelchair user and the pushing person is calculated based on the camera data for all runs and data sets resulting in $0.12\,\text{m}\,\text{s}^{-1}$.

3.3.2.3 Adaptive Correction

As a second approach acceleration data were corrected based on the velocity to improve tracking quality. For this purpose, the difference in velocities $\boldsymbol{v}_{\text{diff}}$ is calculated as in Eq. 3.43 and 3.45. If the difference becomes too large, the IMU acceleration data are corrected assuming a faulty offset e.g., due to biases or a faulty orientation calculation. The basic idea is to estimate which difference in acceleration has led to the existing (faulty) difference in velocity and to adjust the acceleration values accordingly and restart the calculation.

If $|\boldsymbol{v}_{\text{diff}}|$ exceeds $\boldsymbol{v}_{\text{range}}$ at time step k as in Eq. 3.44 the corresponding difference in acceleration ${}^{C}\boldsymbol{a}_{\text{diff}}$ is calculated as in Eq. 3.47 with Δt defining the time since the last correction from step k_{prior} to k. By adding ${}^{C}\boldsymbol{a}_{\text{diff}}$ as in Eq. 3.48 the global acceleration ${}^{C}\boldsymbol{a}$ is corrected for previous and future time steps starting after the last correction k_{prior} and $\boldsymbol{v}_{\text{imu}}$ is calculated again based on the corrected acceleration values $\boldsymbol{a}_{\text{new}}$. The distance tracking calculations between the corrections remain unchanged.

$${}^{C}\boldsymbol{a}_{\text{diff},\,k} = \boldsymbol{v}_{\text{diff},\,k}/\Delta t \tag{3.47}$$

$${}^{C}\boldsymbol{a}_{\text{new},j} = {}^{C}\boldsymbol{a}_{j} + {}^{C}\boldsymbol{a}_{\text{diff},\,k} \quad \forall j \in \{k_{\text{prior}} + 1, ..., n\} \tag{3.48}$$

The correction approach of the acceleration based on calculated velocities is presented in Fig. 3.5. The velocity components of the pushing person and the IMU are exemplified with their corresponding difference $|\boldsymbol{v}_{\text{diff}}|$. The threshold $\boldsymbol{v}_{\text{range}}$ is exceeded at the vertical lines. The drift of IMU velocity values between the adaption points is

visible. When reaching an adaption point the acceleration data are adjusted accordingly for the data up to the previous adaption point. It can be seen that a correction can be triggered by a deviation of the IMU velocity x- and y-component, but also by only one of them.

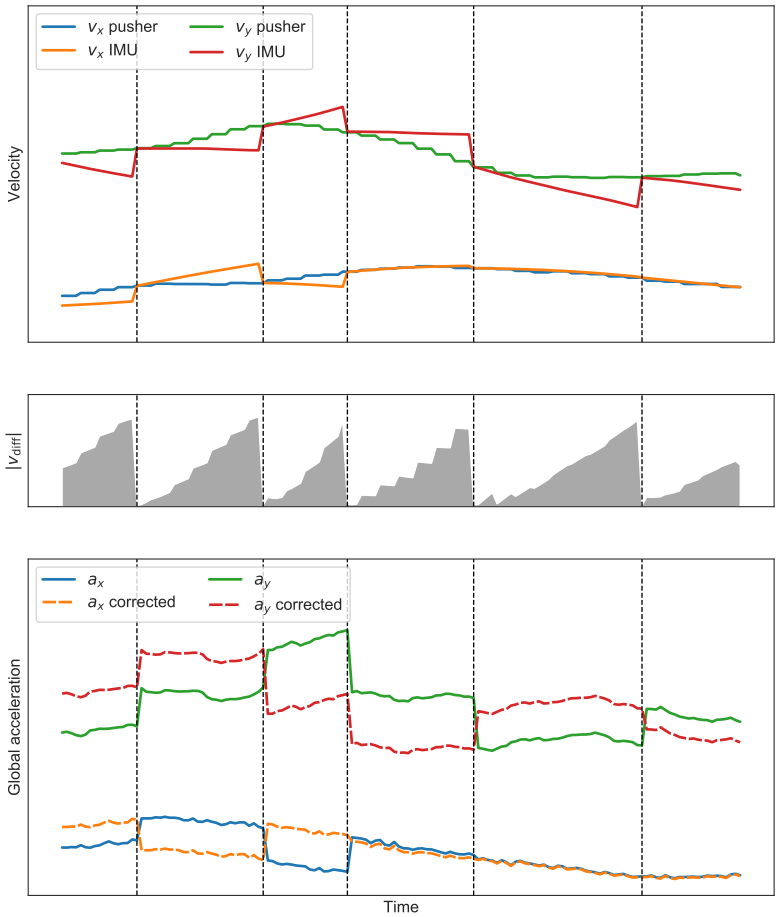

Figure 3.5: Qualitative example of the adaptive correction of acceleration based on velocity data. All plots share the same time axis. Adaption points are marked with vertical lines and appear based on the calculated $\boldsymbol{v}_{\text{diff}}$ (middle). Between two consecutive adaption points the uncorrected velocity IMU values are shown (top) which start at an already corrected value. When an adaption point is reached, the acceleration values are retrospectively adjusted (bottom) so that the desired velocity is achieved when they are double-integrated again.

Chapter 4

Framework

Methods for heading and distance tracking, and approaches for fusing camera and IMU data are explained in Chapter 3. For an application to large data sets, the implementation of a framework for automatically processing the data is required as a next step. In the following, an overview of the structure of the developed framework, its functionalities, and steps of data processing is given. The framework is open source and can be found in [147].

The framework is supposed to read in data of different data capturing systems introduced in Chapter 2 and to apply the proposed methods explained in Chapter 3 so that the tracking results can be analyzed in Chapter 5.

4.1 Code Structure

The developed framework is a set of well-structured python scripts. Python is a popular and open source interpreted programming language that comes with comprehensive libraries for data analysis [148]. Providing constructs and approaches for object-orientated programming it is possible to write clear code [149]. A disadvantage of python might be the slower run time compared to other languages like Java or C. As the run time is not a crucial factor because data are processed after the conduction of experiments, the advantages, especially the facilitated data processing, were decisive for the choice of python.

For the implementation of the desired functions, well-established design guidelines were followed to improve especially the readability and extensibility of the code. Using an object-orientated design the source code complies with the SOLID principles [150]:

- **S**ingle-responsibility principle: states that classes or functions must be independent and should have a specified single purpose

- **O**pen-closed principle: states that the code is open for extension, but closed for modification
- **L**iskov substitution principle: states that a base class can be easily substituted with a subclass without changing the code
- **I**nterface segregation principle: states that interfaces must have a single, well-defined purpose
- **D**ependency inversion principle: states that it is better to depend on abstractions than on concrete implementations

To develop a well-structured framework the required operations and data structures were elaborated in order to implement the methodology described in Chapter 3. Based on the algorithm overview shown in Fig. 3.2 and following the concept of object-oriented programming, several classes were implemented to read in and fuse camera and IMU data, to apply the different algorithms, and to provide the calculated tracking data.

An overview of the created main class `ImuTracker` and its dependencies is given in the class diagram shown in Fig. 4.1. The `ImuTracker` uses classes that provide input data (grey area) and classes that offer algorithms that can be applied to these data (blue area). The `ImuTracker` itself acts as a kind of coordinator and defines the concrete interaction of the different data, and which specific algorithms are used and how. As a result (shown as green area) it provides new objects representing information on calculated trajectories and additional tracking data.

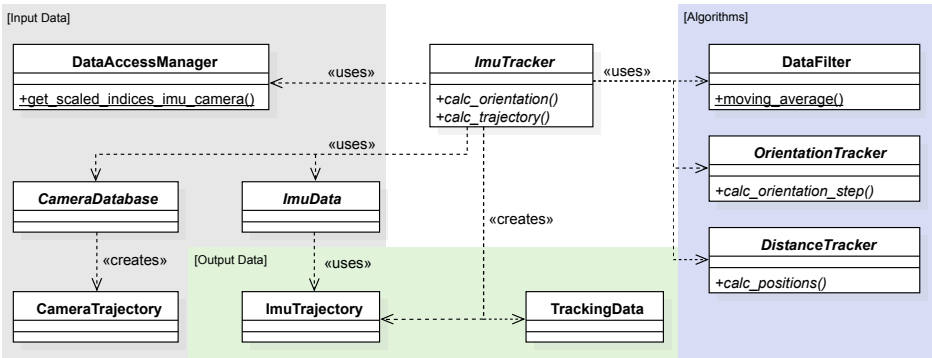

Figure 4.1: Overview of the implemented main classes and their dependencies. For the sake of clarity, no attributes are listed and only the most important methods are presented.

To keep the code extensible and to make it easy to choose from different specified algorithms and data sets abstract classes have been used which are marked italic. The abstract classes declare different methods that must be implemented by inheritance. With the extracted information of a camera tracking system a `CameraDatabase` can be created. This class is defined as abstract since different read-in procedures need to be implemented as the trajectory information is provided in various formats by different camera systems. In `CameraDatabase` objects of `CameraTrajectory` are created that store the data for the trajectories such as the ID for a person and the position given per frame. With IMUs recorded data are stored in objects of `ImuData` which is also an abstract class declaring the needed data but keeping the read in procedure abstract again. The `DataAccessManager` is used to synchronize the access to objects of `ImuData` and `CameraTrajectory` to get the sensor and camera data for a corresponding sample and frame for the same time step.

The code is open for further heading or distance tracking approaches by declaring the `OrientationTracker` and `DistanceTracker` classes abstract. Currently implemented classes for the `DistanceTracker` are shown in Fig. 4.2. They realize the different distance tracking approaches according to Sec. 3.2.3 with the possibility to apply the correction and adaptive correction method as described in Sec. 3.3.2. Different approaches for calculating distances (such as step length estimation) can be added by implementing a new class that inherits from the `DistanceTracker`. Another class for processing the data is provided with the `DataFilter` which can be used by the `ImuTracker` e.g., to smooth data.

After reading in and processing the data the `ImuTracker` is providing the results in form of `ImuTrajectory` and `TrackingData`. If distance tracking is enabled the calculated trajectory based on IMU data is stored in an `ImuTrajectory` object. If fusion is enabled also camera data are used to calculate the trajectories. Additionally, the processing of two different IMU data sets is coordinated in the `ImuTracker` when MAUKF methods are applied. For this purpose, an object of `TrackingData` is created for each initialized IMU data set during the tracking process. It stores all data that are important for or calculated during the tracking process such as the global acceleration and the calculated quaternions.

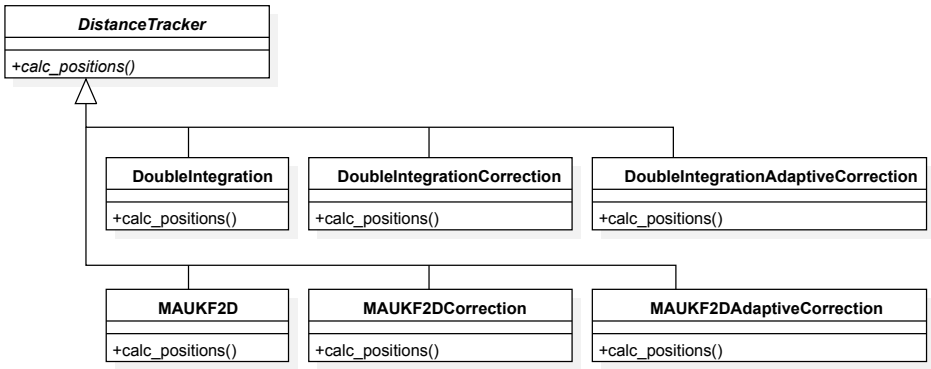

Figure 4.2: Overview of distance tracker classes.

Additional classes that are used but not shown in Fig. 4.1 or 4.2 are described in the following:

- `ImuCameraTracker`: Inherits from `ImuTracker` and implements the interaction of the other classes to provide results according to the algorithm presented in Fig. 3.2. This is a specific implementation of the data flow and processing realized in this work.
- `MadgwickFilter`: Inherits from `OrientationTracker` and implements Madgwick's orientation filter according to Sec. 3.2.2. This is currently the only implemented approach for orientation tracking.
- `SabelImuData`: Inherits from `ImuData` and defines the read-in procedure for the data of SABEL Labs sensors specified in Sec. 2.1.2.
- `PeTrackDatabase`: Inherits from `CameraDatabase` and defines the read-in procedure for the data of the basic camera system introduced in Sec. 2.1.1.
- `OptiTrackDatabase`: Inherits from `CameraDatabase` and defines the read-in procedure for the data of the OptiTrack camera system used in the experiments explained in Sec. 2.2.2.
- `Plotter`: Collection of methods for visualizing the data.
- `Analysis`: This class provides methods for validating the results such as calculating the difference between the ground truth heading and the calculated IMU heading.

The specific `ImuCameraTracker` used in this work can be adapted and extended in order to apply other tracking or fusion techniques. Currently, its implementation provides the IMU-IMU fusion (MAUKF) for the data of two IMU sensors only. The implementation can be extended to handle data from more IMUs. By additionally reading in another IMU data set, managing a corresponding `TrackingData` object and providing appropriate tracking techniques, this adaption can be implemented. For major changes a new implementation of the abstract `ImuTracker` should be realized. This can be useful, for example, to enable an exchange of data during orientation and distance tracking, as these are currently calculated completely separately from each other.

4.2 Data Flow and Processing

With the developed framework it is possible to choose from several algorithms based on the provided input data. The framework allows to apply distance tracking techniques with these different types of input data:

- Data of only one IMU are provided. Distance tracking is possible with a defined absolute start position. No fusion techniques (neither IMU and IMU nor IMU and camera data) are available.
- Data for two IMUs are provided. Distance tracking is possible with a defined absolute start position. Fusion of the data of both IMUs is possible.
- Data of one IMU and a camera database are provided. Basic distance tracking with correction and adaption methods is applicable.
- Data of two IMUs and a camera database are provided. All distance tracking approaches are applicable.

Based on the provided input data, fusion techniques are applied by choosing the corresponding `DistanceTracker`. For the above-listed types of input data, it is also possible to only perform the orientation tracking per IMU data set.

A basic `ImuTracker` has to be initialized with at least one `ImuData` object and an algorithm configuration file that defines the details of the tracking algorithm such as the chosen tracking methods that should be applied. Additionally, configuration information about external dependencies and experiment conditions has to be provided

containing information on file names and the assignment of pedestrians and sensors. Details on the input files can be found in App. B.

An overview of the data flow and processing realized in the `ImuCameraTracker` is shown in Fig. 4.3. As an example, the application of the double integration with correction approach is illustrated. During this tracking process, data provided by the SABEL Labs sensors and trajectory data provided by the camera system are used. The `ImuCameraTracker` can be initialized with the help of the `DataAccessManager`, the definition of an `ImuData` and `CameraDatabase` object, and algorithm and run configuration data. A `DataFilter` object is used to smooth the acceleration data which are forwarded to the orientation tracker implemented in the `MagdwickFilter`. The orientation tracker provides quaternions that are needed for aligning camera and IMU data and to calculate the linear acceleration. Based on this, the `DoubleIntegration-Correction` tracker calculates the position that is used for creating a trajectory as the final output.

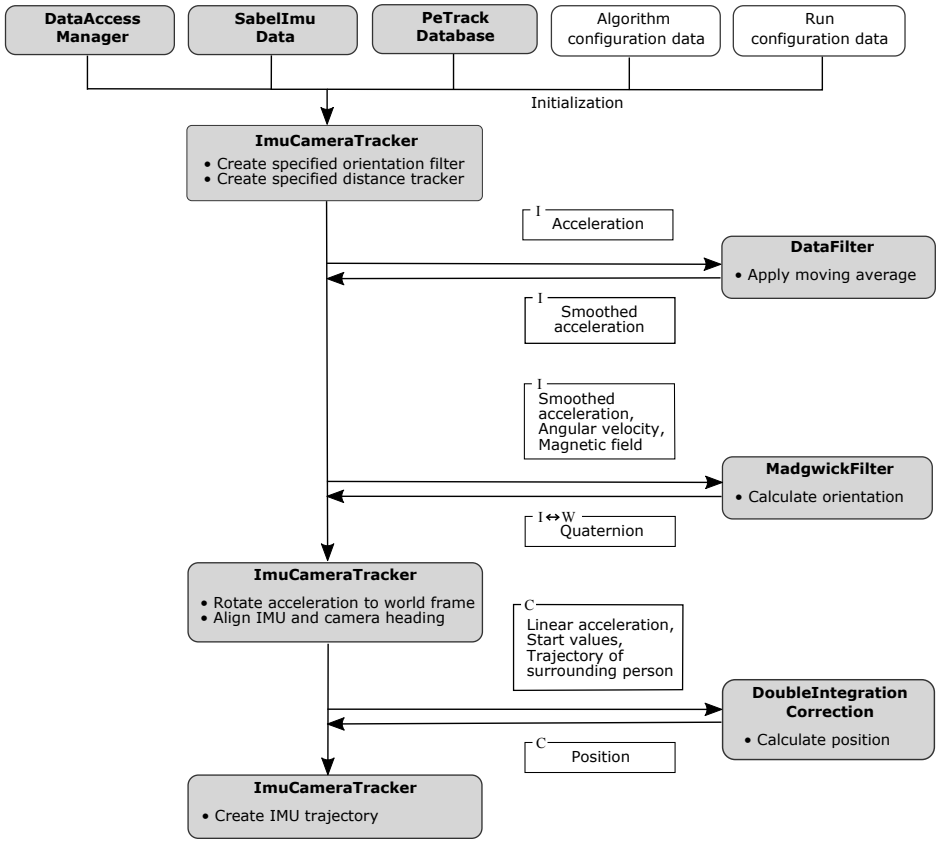

Figure 4.3: Overview of the data flow and processing based on the implemented classes for the example of double integration with correction approach. Classes are highlighted in grey with a list of basic operations. Data sets transferred between the classes are represented in rectangles with their frame of reference (I, W, or C).

Chapter 5

Analysis and Results

In the first Section of this Chapter the proposed methods for distance tracking are applied to the wheelchair data provided by the SiME studies (see Sec. 2.2.1). Results of the different distance tracking algorithms and correction approaches are analyzed and compared. The analysis of the studies using the Optitrack system described in Sec. 2.2.2 is given in the second Section of this Chapter. A detailed analysis of the rotation for different movement processes using the data of the infrared camera system is presented.

5.1 Distance Tracking

The analysis of the SiME studies is limited to the bottleneck studies in which wheelchair users have participated. Since the trajectories of the corridor studies are mainly straight without any significant movement changes, they do not provide data of additional movement types and thus are not part of the following analysis.

Due to low densities in the crowd no problematic occlusion occurred. Thus, camera data are available for each participant. The camera data of wheelchair users are considered as ground truth (GT) and are used for validating the wheelchair trajectories calculated based on IMU data. Next to the overall tracking quality, the different processing steps of the IMU data are shown using an example data set.

5.1.1 IMU Data Example

For a better understanding of the movement data of a wheelchair user and the related challenges of tracking, the IMU data of a wheelchair user are analyzed as an example in the following. Since the different distance tracking approaches result in a high

quality for this data set, it is very suitable for a detailed inspection of the derived data such as rotated IMU data, velocity, and position.

Figure 5.1 shows the ground truth trajectory of a wheelchair user and the corresponding IMU data. The IMU was attached vertically at the backrest with the local z-axis pointing in the direction of movement. The local linear acceleration was calculated by rotating the global gravity vector to the IMU frame I and followed by subtracting the result from the acceleration data. Therefore, the shown data should represent the actual movement only.

For the first part of the trajectory, the acceleration data are very small and fluctuate around zero. It is difficult to determine the main direction of movement which should be along the z-axis until the person leaves the bottleneck. The acceleration along the local x-axis should be zero since it is pointing upwards and the height of the wheelchair is not changing. But especially when the person is moving straight forward the measured x-values are not zero and rather similar to the y- and z-values. A possible reason for this is the tilted attachment of the sensor. This would be due to the character and shape of the backrest which means that the local x-axis of the sensor is slightly misaligned and does not match the global z-axis in camera frame. Furthermore, the data may be affected by noise which is more dominant in comparison to the actual low measurement values. Additional errors in the data may be caused by influences on the sensor that are not related to the actual movement of the wheelchair e.g., a person in the wheelchair moves their upper body which affects the backrest which in turn affects the sensor. At this point, it can be seen that it is challenging to calculate position data via double integration of acceleration measurements and that further restrictions or additional knowledge regarding the movement are required.

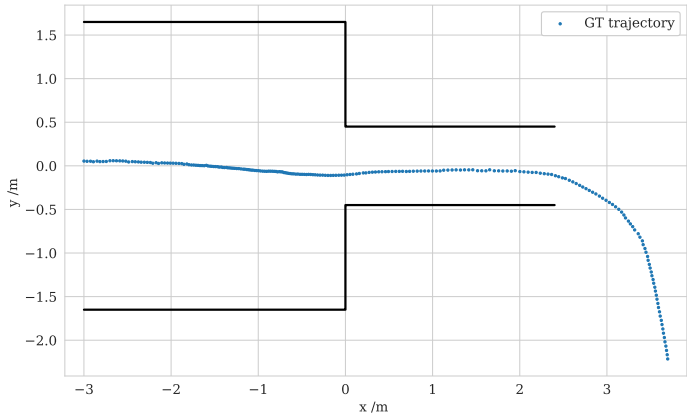

(a) Ground truth trajectory of a wheelchair user (blue) moving through a bottleneck (black) from the left to the right

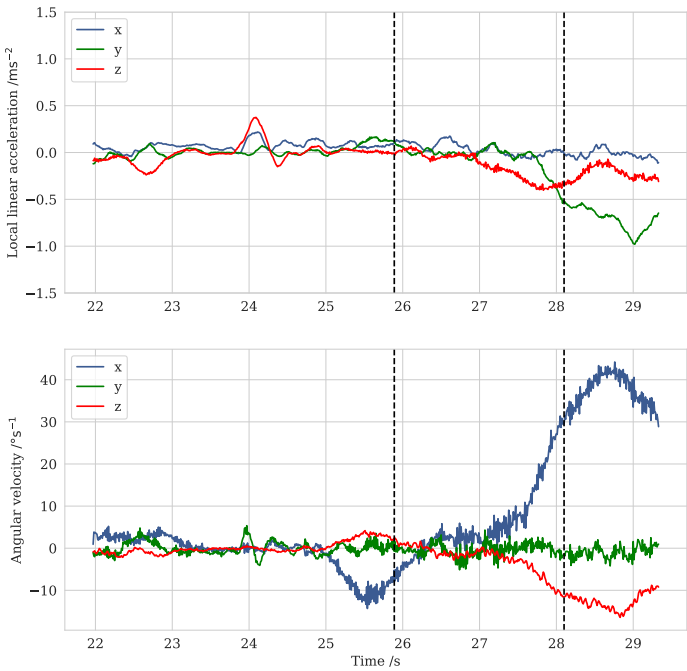

(b) Data of the accelerometer and gyroscope in local reference frame I

Figure 5.1: Trajectory of a wheelchair user and corresponding local IMU data. The first dashed line (bottom) represents the timestamp when the person enters the bottleneck (x = 0 m) and the second one when the person leaves the bottleneck (x = 2.4 m).

Nevertheless, the curve of the trajectory when leaving the bottleneck is clearly visible in the acceleration and gyroscope data as the acceleration along the local y-axis is decreasing. Furthermore, data analysis has shown that it is possible to detect a standstill phase at the beginning of each run (not visible in the shown diagrams). When the magnetometer values are constant, and accelerometer and gyroscope measurements are close to zero followed by a rapid change of their measurements, the start of the run could be detected. This standstill is needed for heading tracking so that the orientation filter converges.

Since it is difficult to interpret unprocessed measurements of the magnetometer, these values are not presented here but can be found in App. C.2. Basically, it can be said that magnetometer measurements are in contrast to the gyroscope data not sensitive to local noise but do suffer from magnetic disturbances which justifies the use of an orientation filter.

5.1.2 Validation of Heading Accuracy

Even though a detailed validation of the orientation tracking algorithm is given in Sec. 5.2.2 the orientation calculation is validated for the SiME experiments as well to make sure that the subsequent distance tracking is not strongly biased. For this purpose, the movement of the wheelchair is compared with the movement of the head of the person sitting in the wheelchair. This validation is not as accurate as in Sec. 5.2.2 since the calculation of a ground truth heading is more difficult but allows to identify any major discrepancies. Therefore, this analysis assures that no severe errors occurred in the orientation calculation which may have a large impact on the distance calculation.

For validating the orientation calculation, a ground truth direction is needed which is calculated out of the position data given by the camera system. The ground truth direction is represented by a velocity vector that was calculated as in Eq. 3.41 with $j = 6$. To avoid instability of the ground truth heading which occurred when the person was standing or waiting, the heading validation is performed starting at 2 m in front of the bottleneck to ensure that the participant is in motion. This is a suitable approach for the conducted experiments since no high densities were observed directly in front of the bottleneck, meaning that wheelchair users could enter the bottleneck effectively unimpeded within that range. To validate the overall quality of heading tracking the absolute difference of the IMU and ground truth heading angle in the plane of motion was calculated for 54 data sets resulting in an average absolute error of 6.20° ($\sigma = 2.65$). An example with a mean heading error of 3.7° is shown in Fig. 5.2.

Note that the trajectory in this figure and for the following results is shorter than in Fig. 5.1a since a period at the start and end is needed for calculating the velocity out of the camera trajectory.

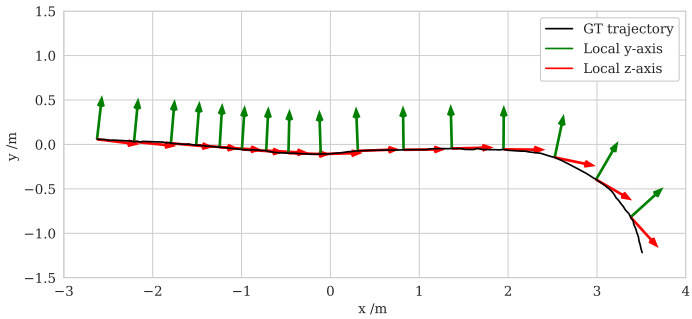

Figure 5.2: Trajectory of a wheelchair user and local IMU frame of the attached sensor after orientation calculation. Local z-axis points in the direction of movement.

Besides, the analysis has shown that usually 2 s of standstill are sufficient for convergence of the algorithm to calculate an initial orientation as described in Sec. 3.2.2.2. The sample ranges for the stationary phases are different for each wheelchair and were searched manually by investigating the data. Mostly, a period before the run started was chosen as stationary phase. The analysis of the orientation in 3D has shown that due to a tilted backrest the local z-axis of the IMU is not strictly in the plane of motion. This error was neglected. As explained in Sec. 3.3.1 a linear part in the camera trajectory needs to be found for aligning the IMU data in camera frame C. This linear part was always found inside the bottleneck.

5.1.3 Double Integration

The double integration based on IMU data without any corrections described in Sec. 3.2.3.1 works satisfactorily for a few data sets only (7 %) with an absolute mean error in position of 0.3 m to 0.5 m. The overall absolute mean error was 6.92 m ($\sigma = 13.73$) which shows that the application of correction methods is needed.

For the IMU data shown in Fig. 5.1b, a mean error of 0.47 m with a maximum error of 0.91 m was achieved. Calculated velocity and position data for the same data set are shown in Fig. 5.3 and the resulting trajectory is presented in Fig. 5.4a. The wheelchair user was moving with a nearly constant velocity through the bottleneck followed by a curve at the end.

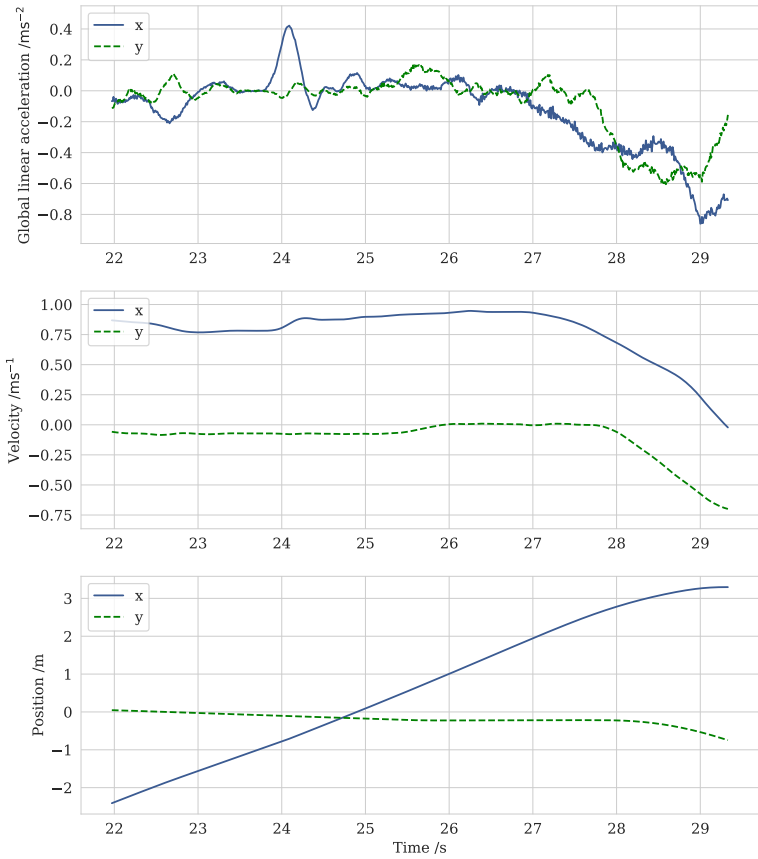

Figure 5.3: Overview of the global linear acceleration (top), the corresponding velocity (middle) and the position data (bottom) based on the data shown in Fig. 5.1b.

The velocity was overestimated before the turn at the end, which led to the maximum error in distance. When turning, the velocity was slightly underestimated since the traveled distance of the IMU trajectory in x- and y-axes was too short. While the shape of the trajectory matched the ground truth for this example, the same tracking procedure was applied to the data of the second sensor that was attached to the same wheelchair at a higher position resulting in less accurate tracking quality (see Fig. 5.5a). Even though the heading tracking quality for the upper sensor was slightly more accurate with an error of 3.65° the raw IMU data show a higher noise and more fluctuations. While the applied orientation filter can handle this noise, the distance tracking based on double integration appears to be too sensitive to that higher noise.

That example indicates that an accurate heading calculation is necessary for sufficient quality of distance tracking but it cannot be ensured.

By applying the correction methods described in Sec. 3.3.2.2 the tracking quality for both sensors could be improved. The maximum error in position could be decreased from 7.06 m to 0.18 m for the upper sensor with the adaptive correction (see Fig. 5.5c). Nevertheless, the adaptive correction of acceleration data based on velocity of the pushing person did not show the desired effect. Several corrections were necessary (often in short intervals) so that the drift in double integration of the acceleration data cannot be attributed to an offset error only. The average time between successive corrections was less than one second. The maximum period without any needed corrections was approximately 6 s. Besides, the adaptive correction did not consistently lead to a better result than the basic correction approach as for the lower sensor (see Fig. 5.4b and 5.4c). However, for the upper sensor, the adaption demonstrates an improvement and assures that the calculated trajectory stayed close to the ground truth resulting in an absolute mean error in position of 0.14 m.

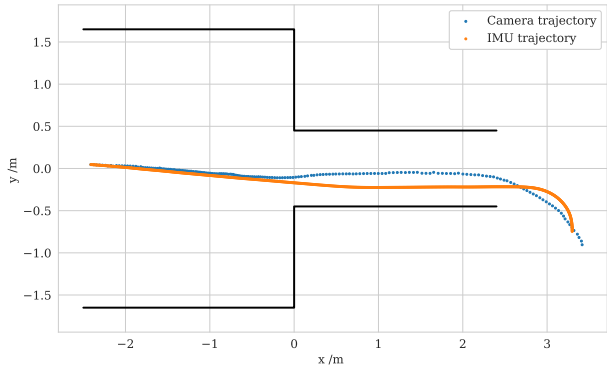

(a) Double integration

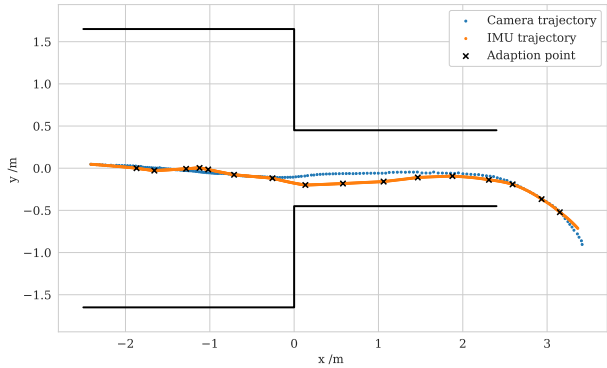

(b) Double integration with correction

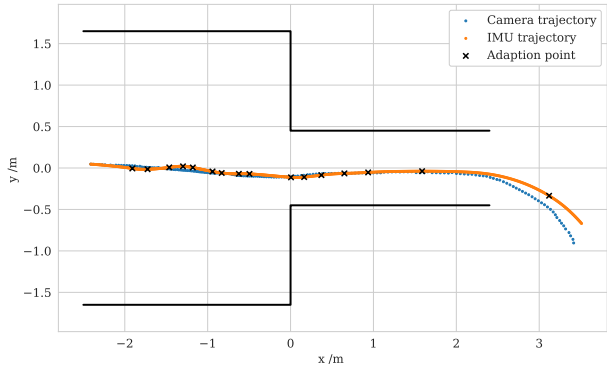

(c) Double integration with adaptive correction

Figure 5.4: Results for different distance tracking approaches for sensor attached to the lower backrest.

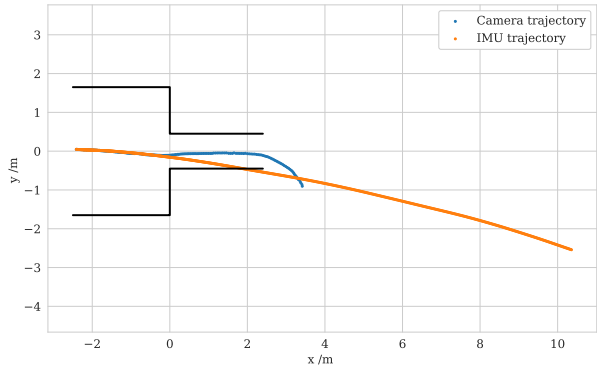

(a) Double integration

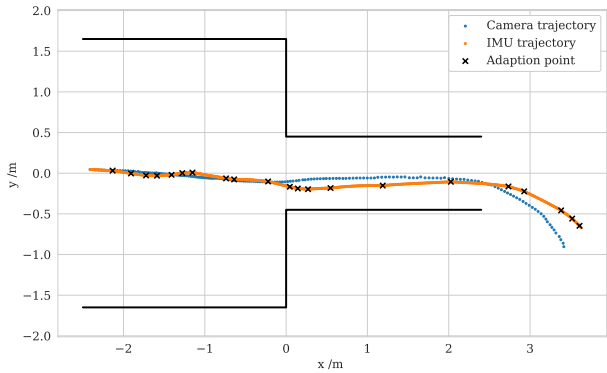

(b) Double integration with correction

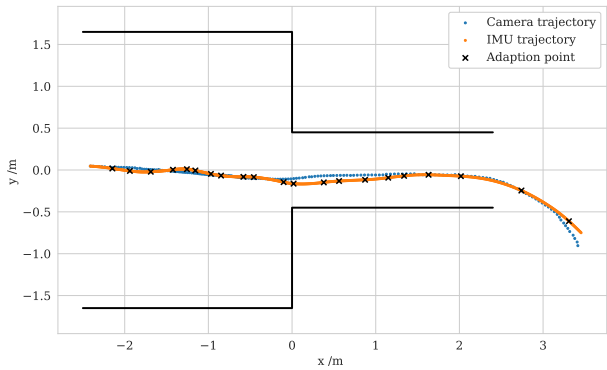

(c) Double integration with adaptive correction

Figure 5.5: Results for different distance tracking approaches for sensor attached to the upper backrest.

5.1.4 MAUKF

When applying MAUKF as explained in Sec. 3.2.3.2 and fusing the data of two sensors without corrections the overall tracking quality improved resulting in a mean error of 3.65 m for 23 data sets. Since data from two sensors of the same wheelchair are required for validation, fewer data sets are available for validating MAUKF than for the double integration approaches. Figure 5.6 shows the result for fusing the data of two sensors for which the results of double integration are given in Fig. 5.4a and 5.5a. Applying MAUKF meant an increased error in position for the lower sensor but an improvement of tracking quality for the upper sensor. Since the drift in position was still too high, correction methods were needed even when fusing the data of two sensors.

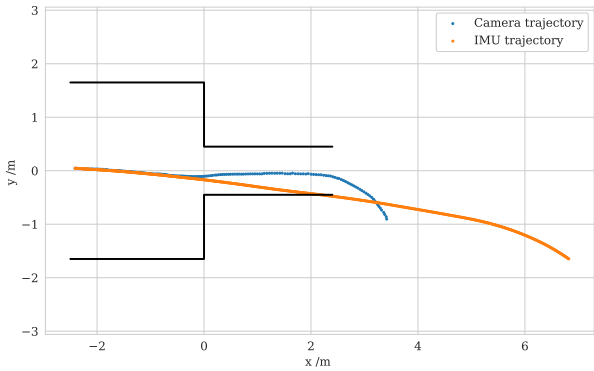

(a) MAUKF

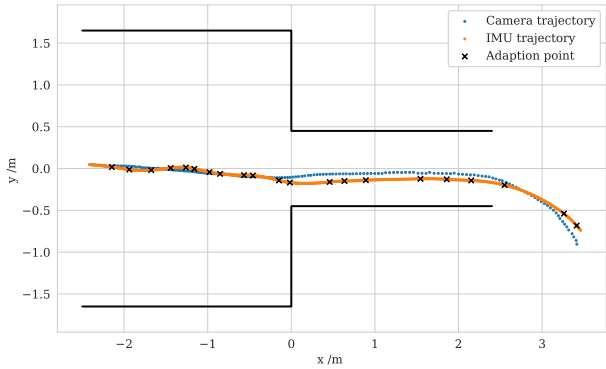

(b) MAUKF with adaptive correction

Figure 5.6: Results for tracking a wheelchair by applying MAUKF. Only with additional adaption methods the drift in position can be restricted.

Higher accuracy for both sensors compared to double integration can only be achieved when one sensor is underestimating the velocity while the other is overestimating the movement. An example of this is shown in Fig. 5.7. Correction methods were still needed to achieve a better tracking quality. For applying MAUKF with correction and adaptive correction the overall mean tracking error in position decreased to 0.14 m and 0.13 m.

5.1.5 Effects of the Correction Methods

As the correction methods changed the velocity or acceleration vector, not only the amount but also the direction is changed. Thus, the swaying of the pushing person may be transferred to the corrected IMU trajectory of the wheelchair user. This effect depends on the number and points in time of corrections. An example is shown in Fig. 5.8. The trajectory of the wheelchair user was smooth but the calculated trajectory based on IMU and camera data shows many fluctuations in direction resulting in bumps which are typical for the head's trajectory of a swaying person. For the basic correction approach shown in Fig. 5.8a, changes in direction after a correction or a series of corrections appear (marked as adaption points). Applying the adaptive correction does not solve this problem as shown in Fig. 5.8b. Adaption points are spread differently and the tracking quality was improved from 0.29 m to 0.15 m (absolute mean error) but the faulty shape of the trajectory remained the same.

This effect could be reduced by improving the calculation of the velocity and acceleration data based on the camera data (see Sec. 3.3.2.1), which was challenging especially at low speeds. This could be achieved by considering the trajectories of several surrounding people. Their information could be used to calculate an averaged main movement direction which is not as sensitive to a single individual swaying. Another approach for optimization could be an alternative smoothing method for the trajectories to reduce the impact of swaying as in [151]. Furthermore, the fusion of the corrected acceleration vector with the help of MAUKF was not sufficient to smooth and correct the position data for this example. The correction still appears as a hard reset in the trajectory. An adjustment of the measurement and process noise matrix could be investigated for this purpose.

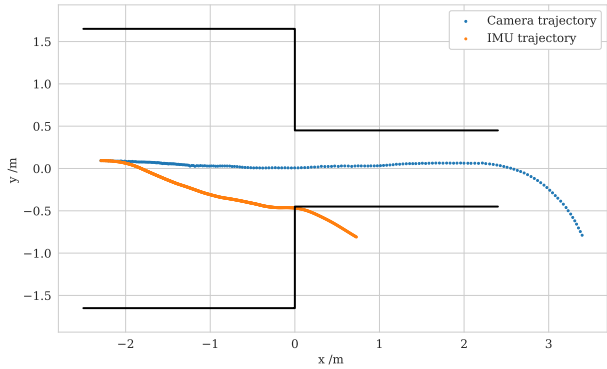

(a) Double integration for lower sensor

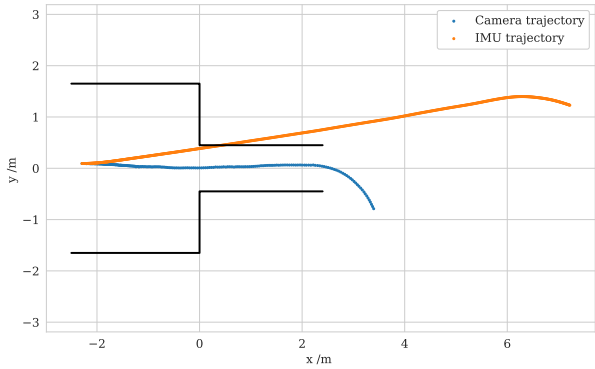

(b) Double integration for upper sensor

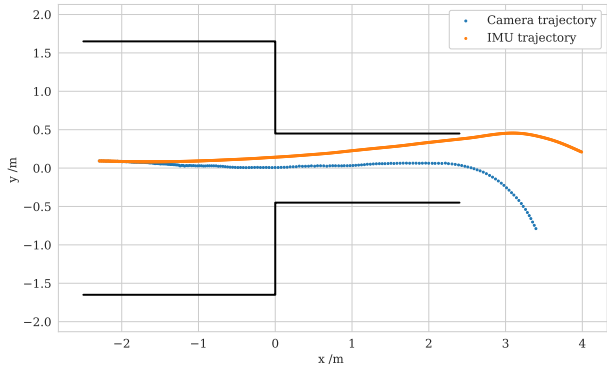

(c) MAUKF fusing data of both sensors

Figure 5.7: Improvement when applying MAUKF and fusing data of two sensors.

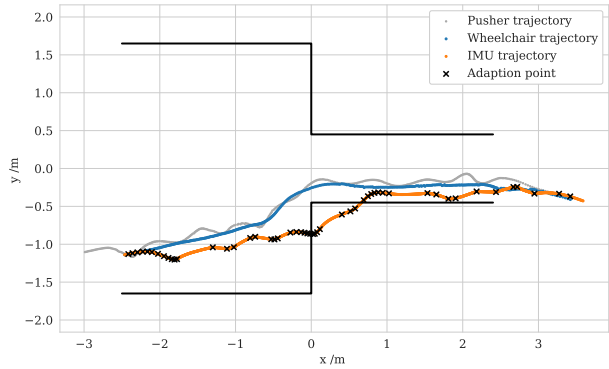

(a) Swaying after applying double integration with correction method

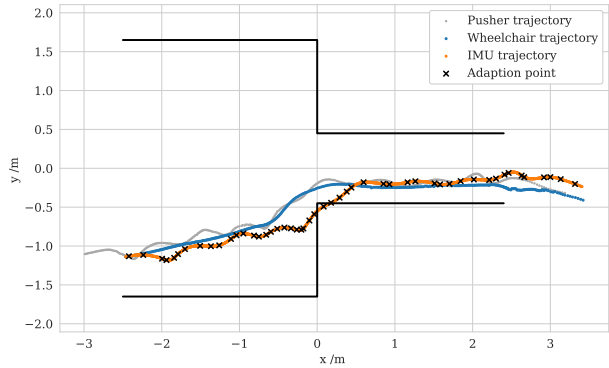

(b) Swaying remains the same when applying MAUKF with adaptive correction method

Figure 5.8: Example of swaying in a wheelchair trajectory caused by the correction method.

5.1.6 Comparison of the Different Approaches

An overview of the resulting errors in position and information about corrections is shown in Table 5.1. Details on the quantity and type of data sets used for the validation can be found in App. C.1. By fusing the data via MAUKF without any corrections the mean spatial error of 6.92 m of the double integration method could be reduced almost to half achieving an error of 3.65 m. Characteristics of the IMU data such as small values and slight changes make the trajectory reconstruction particularly sensitive to starting values and external impacts. The following external influences could be observed: shocks caused by a bag bumping against the sensor, vibrations due to changing of the sitting position or when moving the wheelchair without help

by pushing the wheels. These circumstances led to a maximum error of 47.69 m for MAUKF which was still too large and methods for restricting the drift while tracking was required.

Basically, it can be concluded that when correction methods were applied the smoothness of the trajectories was lost due to abrupt changes in movement direction. Fusing the data with MAUKF improved the overall tracking result but small fluctuations due to swaying of the pusher and the corresponding change in velocity were still visible in the calculated trajectories. Only a minimal improvement in tracking quality could be achieved when applying the adaptive correction method instead of the simple correction.

Table 5.1: Overview of tracking quality for application of double integration and MAUKF, both with and without different correction approaches. For mean values, the corresponding σ is provided in parentheses. The double integration approaches were tested for 54 data sets, MAUKF for 23.

Approach	Mean spatial error /m	Maximum spatial error /m	Mean amount of corrected samples /%	Longest period without adaption /s
Integration	6.92 (13.73)	218.91	-	-
Integration with correction	0.19 (0.09)	1.07	3.66 (2.74)	7.69
Integration with adaptive correction	0.14 (0.07)	0.96	3.03 (0.83)	6.22
MAUKF	3.65 (5.50)	47.69	-	-
MAUKF with correction	0.14 (0.06)	0.85	3.59 (1.46)	3.41
MAUKF with adaptive correction	0.13 (0.05)	0.73	3.21 (0.79)	1.76

5.2 Heading Tracking

The applied orientation filter for heading tracking was already validated with IMU sensors from the company Xsens in [136] by rotating a measurement platform resulting in a dynamic root mean square error of less than 0.8°. To validate the orientation calculation for the SABEL Labs IMUs considering the synchronization and alignment approach, the data of the studies described in Sec. 2.2.2 were analyzed. In contrast

to the analysis in [136] data of the actual movement of a wheelchair and a walking person with a shorter stationary phase are validated.

5.2.1 Method for Validation

A ground truth heading was required for validating the calculated orientation based on IMU data. For this purpose, the wheelchair and upper body of the person were equipped with several markers (see Fig. 2.5). It is difficult to estimate a ground truth heading based on consecutive position points of optical markers, especially when moving slowly or backwards. Therefore, instead of tracking the actual movement direction, the axis of the wheelchair or body was tracked.

The angle α of that axis was considered as the ground truth heading. One local axis of the sensor can be aligned with the wheelchair or body axis, depending on how the sensor is attached. For the conducted studies the local y-axis was aligned and the angle of that axis β was considered as the heading calculated based on IMU data which was validated. The angles are illustrated in Fig. 5.9.

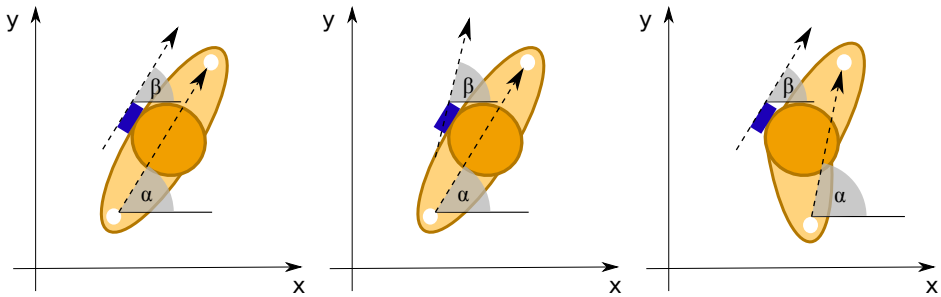

(a) α and β are the same indicating the heading calculation is accurate

(b) β is bigger than α indicating a faulty orientation calculation

(c) The person pulls one shoulder forward leading to a bigger α

Figure 5.9: Sketch of angles that are used for validating the calculated heading based on IMU data. The person has an optical marker in white on each shoulder between which the body axis is marked. The IMU on the back is marked in blue with the local y-axis. Angles are calculated with reference to the global positive x-axis.

The difference between both angles $\epsilon = \beta - \alpha$ is calculated as a measure for the accuracy of the calculated heading. Figure 5.9a shows the heading without an error, while for the example in Fig. 5.9b the error is larger than zero indicating a deviation of the calculated local y-axis counterclockwise. For this validation method, a fixed body axis is assumed. Due to the one-sided movement as in Fig. 5.9c the body axis

changes while the orientation of the sensor remained the same. For this case, an error was calculated which is not because of the faulty calculation of β. This needed to be considered when analyzing the error. Furthermore, the orientation of the IMU can be affected by local movements of the sensor as it is attached with a rigid clamp that does not adapt to the shape of the back. The same approach was chosen for validating the movement of the wheelchair as the optical markers were placed in a similar way. Since the markers were placed on the handles and had a fixed spatial relation to each other, the heading error shown in Fig. 5.9c did not need to be considered for the wheelchair scenarios. However, the orientation of the sensor was affected by the seating position of the person due to the soft backrest which had to be taken into account.

For calculating the local y-axis and thus β, the orientation filter explained in Sec. 3.2.2 was applied. The alignment approach as described in Sec. 3.3.1 was adapted in order to rule out the possibility of error when calculating the movement direction based on camera data. Furthermore, when considering a linear part in the camera trajectory as the movement direction, it would be assumed that the IMU sensor was aligned in the same direction. That could lead to an error if the sensor was tilted in the alignment phase e.g., due to the attachment or twisting while walking. Besides, this alignment approach was not applicable for the studies when the person was twisting the upper body while standing on the same position. Instead, it was decided to align the local y-axis with the wheelchair or body axis before the person started to move. It was assumed that their spatial relation to each other remained the same after the experiment started. The local y-axis was rotated so that ϵ is zero at the beginning if α and β are different at that time. In this way, an offset due to attachment could be considered. Nevertheless, it means that the consideration of a misalignment at the beginning is apparent for the whole run which is not the case, for example, when the person in the wheelchair was changing the seating position after the beginning.

Even if with the proposed validation method not only errors of the tracking methods but also errors due to the attachment and faulty assumptions are considered, information about the total error in the application in the intended field of use in pedestrian experiments is given.

5.2.2 Rotation of Wheelchair

In the following, the heading calculation for the movement of the wheelchair user is validated. Figure 5.10 shows an example of the captured 3D position data and the calculated local IMU axes based on IMU data. The movement from the starting area to the turning area in the direction of the negative x-axis is presented. The trajectories

of the handles presented in grey are at a higher z-position than the trajectory of the IMU displayed in black. The axis between the handles which is used for calculating the ground truth heading is presented for equal intervals of 0.5 s. The local axes of the IMU are presented at the IMU trajectory for the same intervals. For a correct heading calculation, the axis between the handles and the local y-axis should be parallel. The local z-axis points in the direction of movement and indicates the turning at the end of the trajectory.

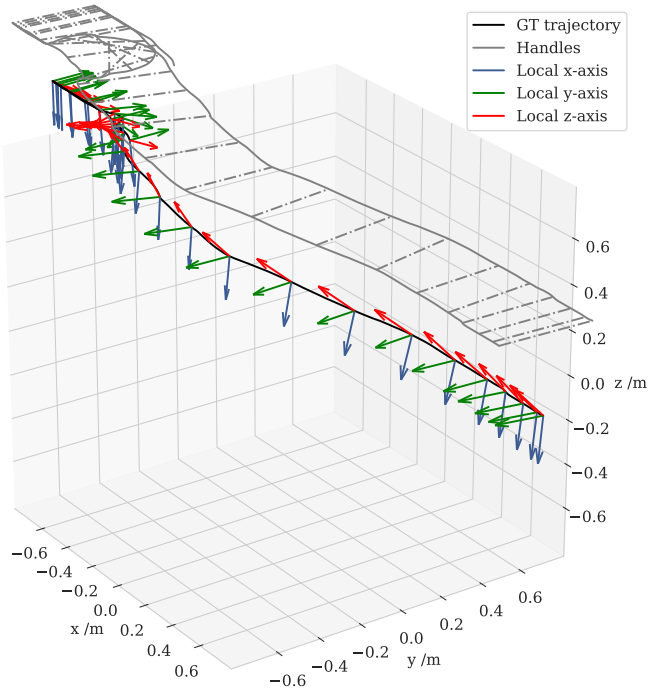

Figure 5.10: 3D position data for the movement of a wheelchair. Position data for the left and right handle and the lower IMU itself are shown. The local IMU frames and the wheelchair axis are presented for time steps of 0.5 s.

For validating the heading calculation, data in the movement plane (xy-plane) are analyzed only as shown in Fig. 5.11. For this example, the wheelchair was propelled by the person seated in it. A local displacement due to the attachment of the markers can be seen in Fig. 2.5. The axis between the handles and the local y-axis were not exactly on top of each other. When moving from the start to the turning area (see

Fig. 5.11a) the axes are parallel indicating a low tracking error and the turning at $x = -1.0\,\mathrm{m}$ is clearly visible. On the return (see Fig. 5.11b) a faulty angle between the axes was apparent.

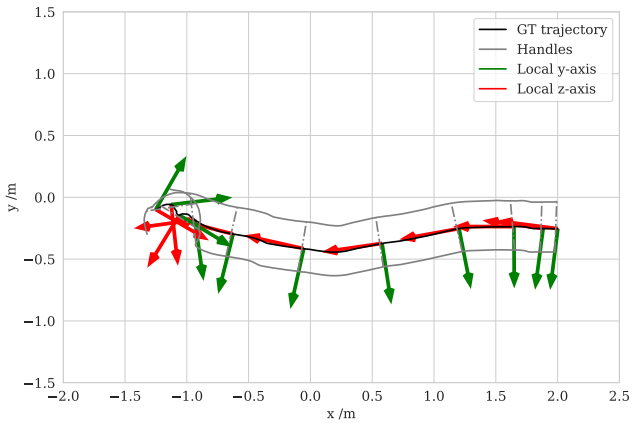

(a) Moving to the left side with sharp tun at the end

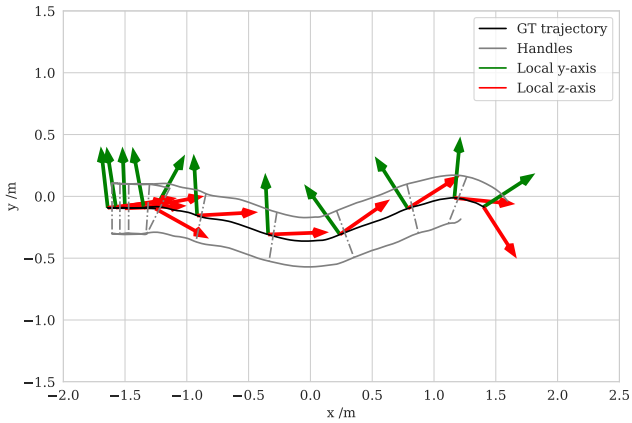

(b) Moving to the right side back to the start

Figure 5.11: Trajectory of a wheelchair user and calculated heading of the upper sensor. Axis between the handles and local IMU frame are presented for time steps of 0.5 s.

The course over time of the difference between the angles of the axis calculated as described in Sec. 5.2.1 was analyzed for all repetitions of the run. The corresponding values of the angles can be found in App. D.1. As shown in Fig. 5.12 the observed error course remained the same for all repetitions. For both sensors attached to

the wheelchair the heading calculation was more accurate for the movement from the start to the turning area at the beginning of each run. Error patterns for each sensor are similar for the conducted repetitions indicating that the similar movement is conducted and similar signals are recorded and processed. An offset in the heading calculation is visible after the first 180° turn which disappears after the second turn at the end of each run.

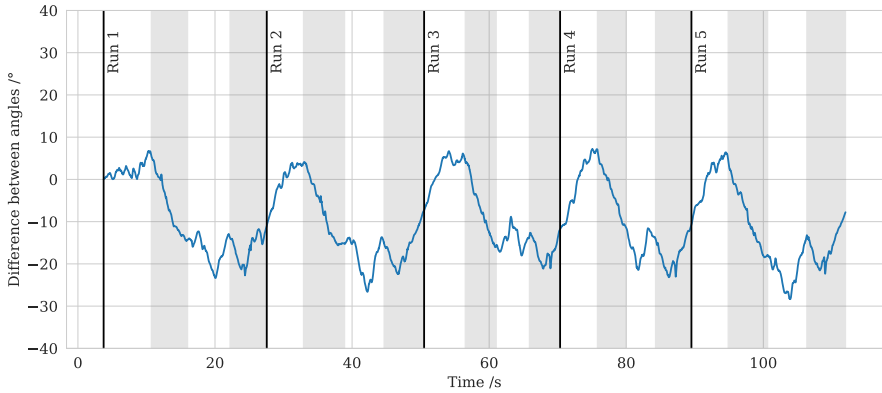

(a) Data for upper sensor

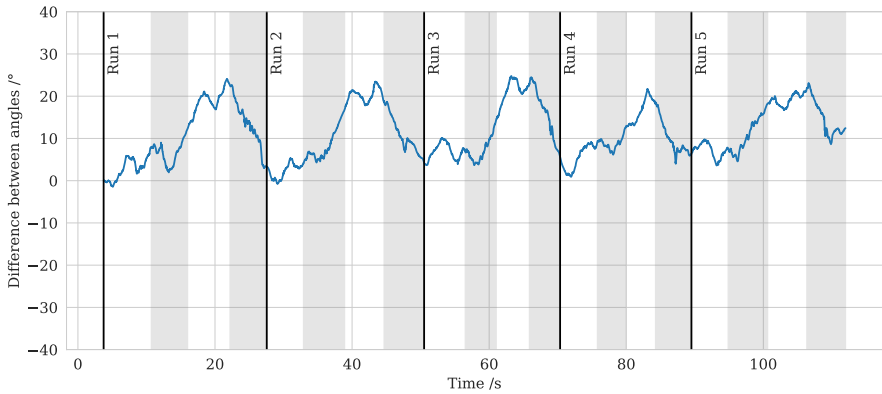

(b) Data for lower sensor

Figure 5.12: Error in heading over time for a wheelchair pushed by arms. Periods for 180° turns are marked in grey.

The local y-axis and the axis between the handles were aligned at the beginning of the first run so that the error is expected to be zero. Possible errors due to misalignment or because of measurement noise were removed for the starting scenario.

As the error patterns remain the same for each run, it is unlikely that the error was caused by a change in sitting posture on the way back. The heading tracking shows an increasing error during the first turn which is decreasing after the second turn. This was possibly caused by noise in the magnetometer measurements due to metal components of surrounding objects in the experiment location. After the first turn, the relation of the local to the global frame is turned as well leading to an increased error. When moving back to the starting point for which the alignment was done, the error decreased. This effect is visible for all captured data of the studies. The development of the error for the wheelchair user who was moving forward using their feet is provided in App. D.2. A restart of the heading calculation and an adapted alignment after the first turn was not possible since a standstill is needed for the orientation filter to calculate the initial heading.

A comparison of the heading tracking quality of the upper and lower sensor for the two different movement scenarios using feet or arms is given in Table 5.2. The mean error provides the information on whether a faulty rotation was calculated to the right (negative) or left side (positive) while the mean absolute error represents the mean error independent of the direction of rotation.

Table 5.2: Overview of heading tracking quality when applying Madgwick's orientation filter on IMU data recorded at the backrest of a wheelchair. For mean values, the corresponding σ is provided in parentheses.

Movement	Sensor position	Mean error /°	Mean absolute error /°	Maximum absolute error /°
With feet	Upper	-9.83 (9.08)	11.31 (7.14)	28.35
With feet	Lower	11.23 (6.59)	11.25 (6.55)	24.78
With arms	Upper	-15.73 (10.12)	15.87 (9.91)	34.77
With arms	Lower	0.40 (9.07)	7.59 (4.97)	18.73

Comparing the tracking accuracy for the upper and lower sensor, the attachment at the lower position on the wheelchair appears to be more suitable for tracking showing a lower mean absolute and maximum absolute error. Because of the soft backrest of the wheelchair, the upper sensor might have been more affected by local movements when the person is changing the sitting posture or when moving arms or feet to propel forward. High mean errors are apparent whose absolute value was similar to the mean absolute error except for the last data set. This indicates the offset error on the return, but also that the heading tracking on the way from start to the turning point had a low error in heading. The high maximum absolute errors only

occur when the wheelchair user was turning or during the return. When turning the wheelchair the sensor measurements were affected by more local movements. As the person sitting in the wheelchair was not familiar with using it, it was difficult for the participant to carry out the turn. On returning to the starting point, high errors were likely caused by the magnetometer noise that was already discussed. Smoothing the magnetometer measurements or focusing on accelerometer and gyroscope data could help to improve the heading tracking accuracy when magnetometer noise is apparent. Besides, when conducting laboratory studies with crowds usually several standstill phases exist so that the heading tracking can be restarted and aligned again using the movement direction of the wheelchair based on the trajectory information. Since there is potential for improving the tracking and a part of the error can be traced back to the validation method, the mean absolute errors of the lower sensors of 8° and 11° appear to be promising. Nevertheless, the results show that the heading tracking can be affected by magnetometer noise whose influence must be reduced.

5.2.3 Rotation of Upper Body

The heading tracking for the rotation of the upper body was validated for three different scenarios. For this purpose, the difference between the calculated angles is analyzed. The corresponding angles of the body axis can be found in App. D.1.

Firstly, the calculated rotation while the person was standing has been inspected. Again, the data were validated in the plane of motion only. The turning to the right side followed by a turn to the left side was considered as one run. This process is shown in Fig. 5.13 for different time steps. The initial situation at $t = 4.0\,s$ is presented in Fig. 5.13a. Due to the alignment at the beginning, the shoulder axis and the local y-axis are parallel without any error. The maximum twist to the right and left side are shown in Fig. 5.13b and 5.13d. The transition point of rotation from the right to the left side (see Fig. 5.13c) was given for the time step when the shoulder axis was equal to the initial situation (parallel to the y-axis).

When twisting to the right and left side a deviation of the axes were visible, which was also apparent for the transition phase. An inspection of the recorded position data has revealed that the shoulder axis is not fixed and the distance between the markers on the left and right shoulder varied. As previously discussed and shown in Fig. 5.9c the deviation of the axes was based on the validation method and not caused by faulty heading tracking. Even in the transition phase when moving back to the middle, one shoulder is pushed forward and is not on line with the shoulder axis in normal posture.

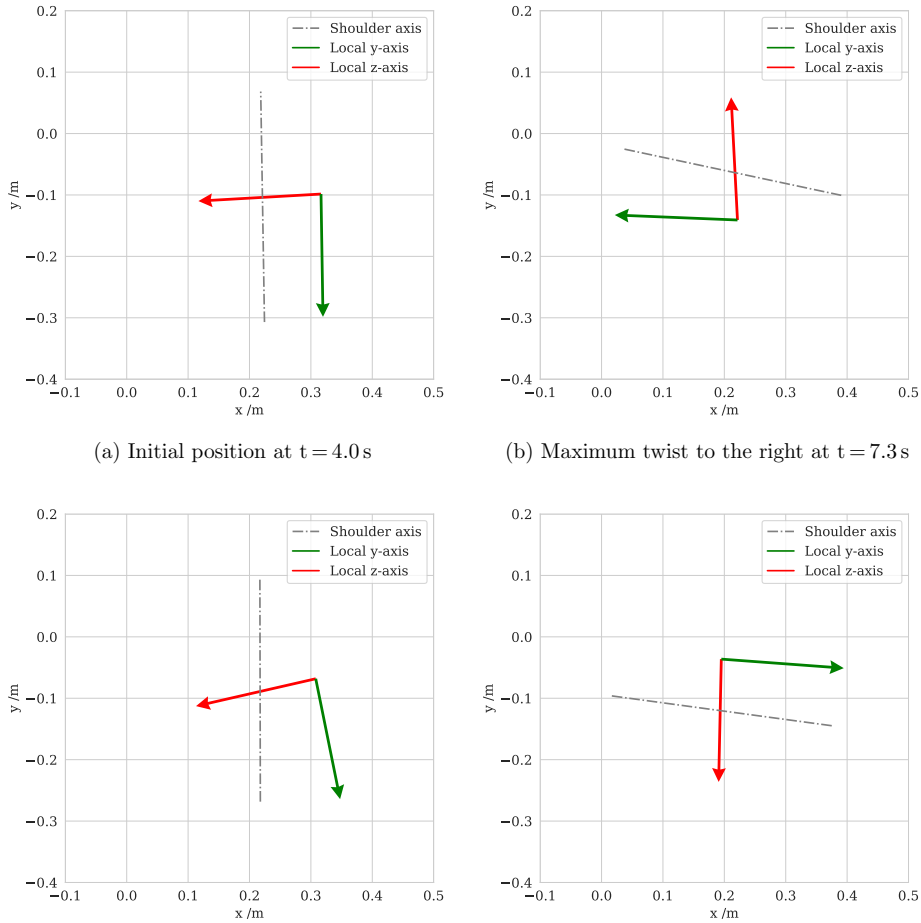

(a) Initial position at t = 4.0 s

(b) Maximum twist to the right at t = 7.3 s

(c) Passing initial position at t = 9.0 s

(d) Maximum twist to the left at t = 10.3 s

Figure 5.13: Visualization of the shoulder axis and the calculated local IMU frame when rotating the upper body to the right and left side while standing on the same position. Data for different time steps are shown.

The course of the error in heading tracking over time is shown in Fig. 5.14. The error pattern was repeating for each run showing a local maximum error of 10° to 14° just before the transition phase. The person should be instructed to rotate the upper body and keep a straight posture for a better validation of the data. However, this would lead to smaller rotation due to the limited freedom of movement.

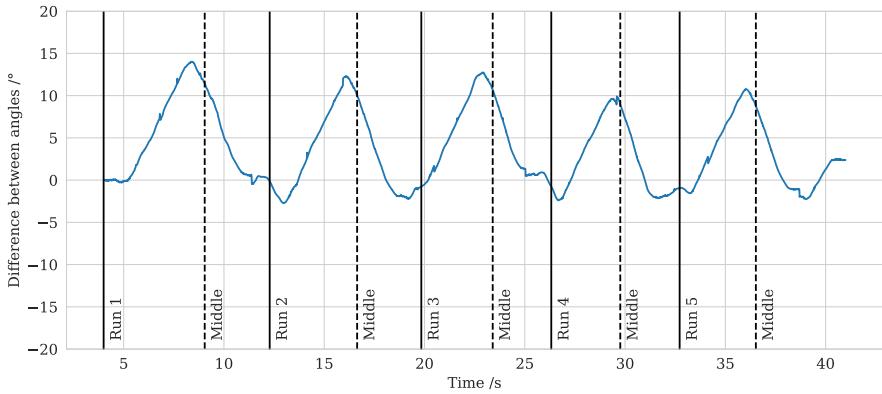

Figure 5.14: Error in heading over time for the rotation of the upper body while standing on the same position. Time of passing the initial position when rotating from the right to the left side and at which the shoulder axis is parallel to initial shoulder axis are marked with the dashed lines.

Second, the rotation while walking in x-direction was validated (Scenario 4 in Sec. 2.2.2). Due to the vertical displacement when walking (bobbing), new vertical movements have an influence on the sensor. The bobbing is visible in Fig. 5.15a as the z-values of the trajectory are slightly fluctuating. The slight increase of the z-position with decreasing x-position indicates that the optical system has not been calibrated optimally. It can be seen that the sensor on the neck was attached in a tilted way and not vertically (local x-axis). The heading calculation visualized in Fig. 5.15b does not appear to be affected by the bobbing and worked satisfactorily. The error for each run is shown in Fig. 5.16. The error increases after the first 180° turn but does not reach the maximum on the way back to the starting area. The issue with the offset caused by magnetic distortion as for the wheelchair scenarios was not apparent. It is assumed that the sensor on the neck was in a superior z-position than the sensor on the wheelchair and is therefore not as affected by magnetic distortion. High errors occur during the turns whereby errors also arise due to the validation approach (and the varying shoulder axis).

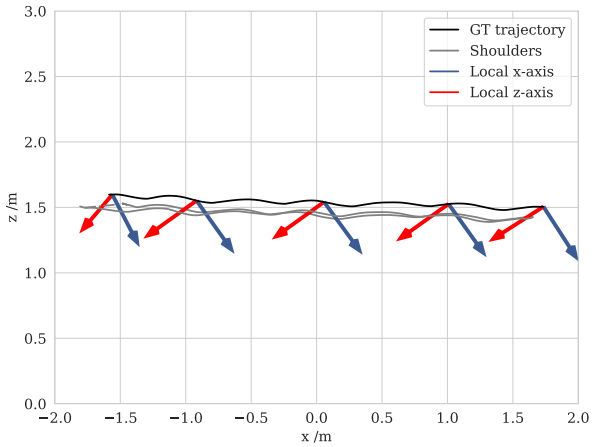

(a) Trajectory and local IMU frames projected to the xz-plane of the optical system

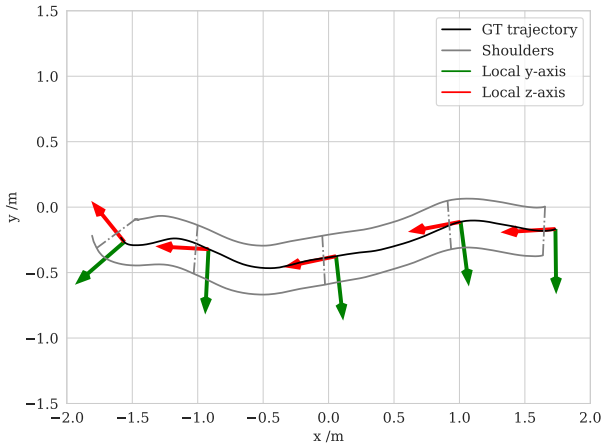

(b) Trajectory and local IMU frames in xy-plane

Figure 5.15: Trajectory of a person walking from the starting to the turning area with calculated local IMU frames. The local IMU frames are presented for time steps of 0.5 s.

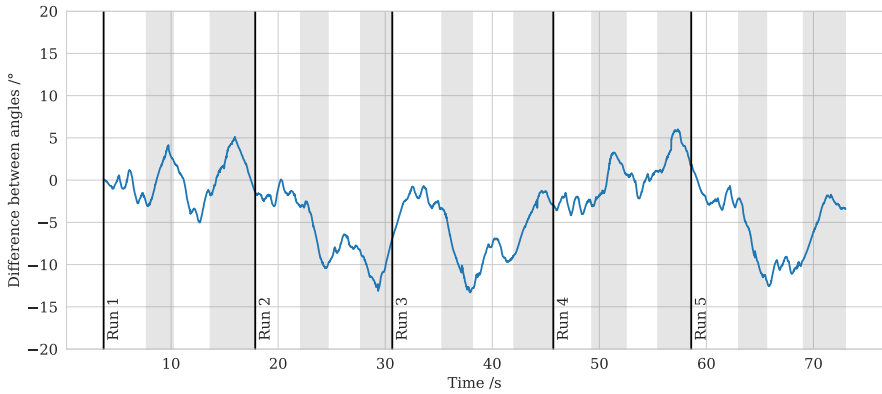

Figure 5.16: Error in heading for the normal walking scenario. Periods for 180° turns are marked in grey.

Third, the rotation calculation for the crowd walking scenario introduced in Scenario 5 in Sec. 2.2.2 was validated. Strong rotations of the upper body and walking sideways were conducted compared to the normal walking scenario. An example of a strong rotation is shown in Fig. 5.17. Around $x = 0$ the person is rotating the upper body to the left side which comes along with a strong rotation of the local y-axis of the IMU indicating a good heading tracking accuracy. The error in heading became greater during the strong rotation which again was caused by the validation approach (see App. D).

An overview of the heading tracking accuracy for the three scenarios is given in Table 5.3. Since the shoulder axis is not fixed and its length varied by 2 cm maximum, a part of the error is caused by the validation approach and not by poor tracking accuracy. Even if the variation of 2 cm appears small, it signals that one shoulder was pulled anteriorly or posteriorly, the ground truth heading changed accordingly. However, the sensor was not affected by this movement leading to a maximum absolute error of 13° to 17.5°. Comparing the results of the heading tracking while standing with the results of normal and crowd walking, the bobbing appeared to not influence the heading tracking. Mean absolute errors of 4° to 6° are highly satisfactory and sufficient to measure the rotation of the upper body of people moving in crowds.

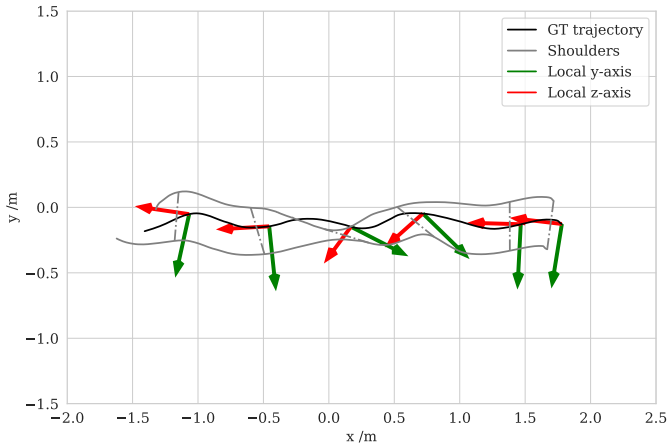

Figure 5.17: Trajectory and calculated heading of a person walking from the starting to the turning area showing a strong rotation. The local IMU frames are presented for time steps of 0.5 s.

Table 5.3: Overview of heading tracking quality when applying Madgwick's orientation filter on IMU data recorded at the neck of a person. For mean values, the corresponding σ is provided in parenthesis.

Movement	Mean error /°	Mean absolute error /°	Maximum absolute error /°
Standing	3.73 (4.60)	4.41 (3.95)	14.01
Normal walking	-3.55 (4.41)	4.41 (3.54)	13.30
Crowd walking	-5.43 (4.66)	5.69 (4.34)	17.48

Chapter 6

Application

After the development and validation of the tracking algorithms, the heading tracking approach was found to be a sufficient method to capture rotational data of pedestrians in crowds. To clarify the added value of the developed hybrid tracking system and to show new arising possibilities for the analysis of a crowds' movement, new studies using the hybrid system have been conducted.

The hybrid tracking system presented in this work was used in the following studies to measure the rotation of the upper body of pedestrians entering a bottleneck of various widths with high and low motivation. Using the provided data, the relation between the rotation and motivation as well as flow and density was analyzed. In contrast to other studies on the rotation in crowds [100, 101] the body rotation was not calculated based on the angular velocity data only but by fusing all sensor data.

6.1 Study Setup

Overall, 32 studies have been conducted with decreasing bottleneck width and two different motivations. $N = 25$ people participated in the first 16 studies with bottleneck widths of $w_b \in [1.0\,\mathrm{m},\ 0.9\,\mathrm{m},\ 0.8\,\mathrm{m},\ 0.7\,\mathrm{m}]$. Followed by $N = 8$ participants walked through the bottleneck with a width of $w_b \in [0.7\,\mathrm{m},\ 0.6\,\mathrm{m},\ 0.5\,\mathrm{m},\ 0.4\,\mathrm{m}]$. The entrance area was constructed out of wooden walls. The actual bottleneck had a depth of 0.13 m to create the impression of walking through a doorframe. Behind the bottleneck, walls were placed on the left and right sides to prevent an early turning of the participants.

For each bottleneck width, two different situations were created by instructions of the study coordinator. The participants were asked to imagine being part of a crowd that is entering a door that leads to an event location. To vary the motivation the following two instructions were given before entering the bottleneck:

- "You have tickets with a seat reservation and will reach this seat in good time before the start of the event." for low motivation and
- "Now imagine that you have a valid ticket but no fixed seat and therefore a better seat the sooner you are entering." for high motivation.

Based on these instructions the participants are referred to as low and highly motivated in the analysis. To obtain a more reliable data set, each run was conducted twice in succession with the same instruction. For technical reasons, a preparation phase was conducted before each run. This preparation phase was required to ensure the applicability of the IMU tracking algorithm and the fusion of camera and sensor data. All participants gathered in a starting area. Participants with IMUs were asked to spread evenly in the crowd and to do a heel drop to separate whole IMU data sets into the different runs for visual analysis. Then, participants were asked to standstill at the beginning so that the initial orientation of the sensors can be calculated. To make the heading alignment possible a straight part in the participant's trajectory is needed. Since winding trajectories were expected in front of and behind the bottleneck participants were asked to walk on a straight line at first and then to gather in front of the bottleneck. Afterward, the actual experiment (entrance phase) commenced and the participants passed the bottleneck.

The experiments were recorded with two cameras on the ceiling whose views can be seen in Fig. 6.1. Participants were moving from the right to the left. After standing still (see Fig. 6.1a), the participants walked on a straight line (see Fig. 6.1b), gathered in front of the bottleneck (see Fig. 6.1c), and moved through the bottleneck (see Fig. 6.1d). Participants then returned to the starting area. To improve the accuracy of trajectory extraction, participants wore orange caps with a black dot. Each person's height was measured and trajectories were extracted with the averaged height of all participants. The extracted and fused trajectories are shown in Fig. 6.1e. Due to the limited capturing range the straight walk could not be detected for all participants. Therefore some trajectories could only be extracted for one camera view. In addition, for taller persons, the overlap area of the camera perspectives was smaller so that the combining of the trajectories was not possible. In this case, only trajectories of the camera recording the entrance phase were analyzed. For combined trajectories a more accurate fusion with IMU data was assumed. This was due to the straight walk data were missing for uncombined camera trajectories. Nevertheless, a fusion could still be implemented before entering or after leaving the bottleneck, by searching for periods when participants were temporarily standing or walking without twisting.

(a) Standstill in preparation phase

(b) Straight walking in preparation phase

(c) Gathering in front of the bottleneck in entrance phase

(d) Moving through the bottleneck in entrance phase

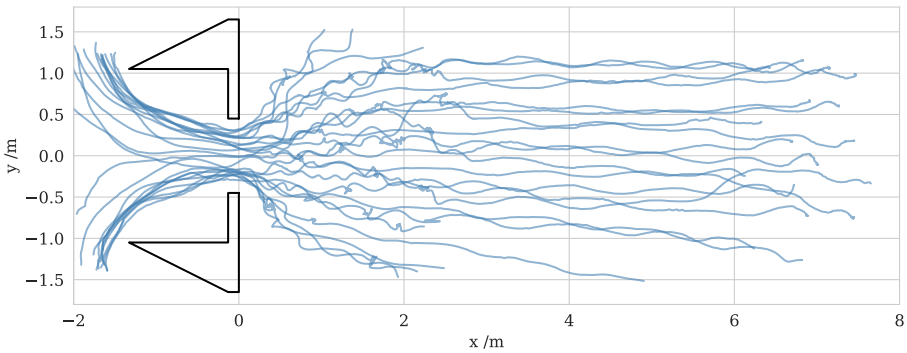

(e) Unprocessed combined trajectories of both camera recordings

Figure 6.1: Overview of the study setup. Preparation phase (top) and entrance phase (middle) were recorded with one camera respectively. Combined trajectories are shown at the bottom.

During all runs the same seven people were wearing an inertial sensor on the back and chest to measure the rotation of their trunk. Due to the limited number of available sensors only seven people could be equipped with inertial sensors. They wore sensors, positioned at two different body points. This was to investigate which

position was optimal to estimate the rotation of the upper body. Because of issues with the synchronization of IMU and camera data via the LED signal which was not seen by the cameras, the fusion and scaling were realized manually by utilizing the heel drop spikes. The captured data of the studies are provided in [152].

6.2 Twist Angle

6.2.1 Definition and Calculation

The twist angle α of a person is defined as the difference between the walking direction of the person and the rotation of the upper body. This twist angle is not the same as the twist between the upper and lower body. It can be the same for unimpeded walking but that does not usually apply when moving in a crowd or through a bottleneck. As shown in Fig. 6.2 Person A had a low twist angle. This is associated with a low twist between the upper and lower body. When passing the bottleneck like person B the upper body was rotated around 90° in relation to the direction of movement but with a low twist between upper and lower body.

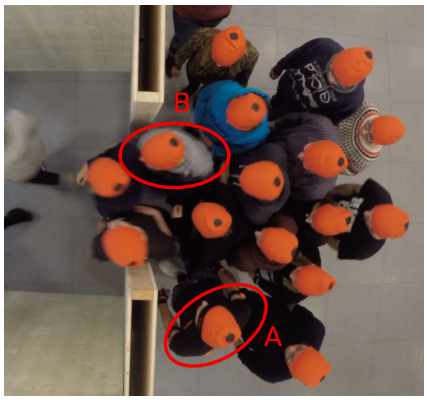

(a) Sample image of a study with high motivation and a bottleneck width of 0.8 m

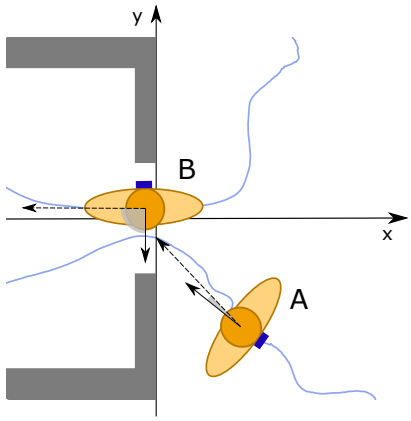

(b) Sketch for a similar situation for person A and B

Figure 6.2: Sample image (left) and sketch (right) of a similar situation of people entering the bottleneck explaining the twist angle. In the sketch the sensors are marked in blue on the back. Trajectories are presented in light blue, the orientation of the upper body by a solid vector and the preferred walking direction by a dashed vector. The twist angle α is marked in light grey.

The actual walking direction is the vector between consecutive positions within the trajectory of a person. It was decided to calculate the walking direction differently when the participants are approaching the bottleneck due to unsteadiness when a person is standing and the head is moving. Therefore, a preferred walking direction was calculated in the area in front of the bottleneck compared to the actual walking direction in the bottleneck as defined in Eq. 6.1. For each time step i the walking direction $\boldsymbol{w}_i$ is defined as the vector between the current position $\boldsymbol{s}_i$ and the future entrance point in the bottleneck $\boldsymbol{s}_{entrance}$ where the participant crosses the y-axis (see end of dashed vector of person A in Fig. 6.2b).

$$\boldsymbol{w}_i = \begin{cases} \boldsymbol{s}_{entrance} - \boldsymbol{s}_i & \text{if } s_{i,x} \in [0,3], \\ \boldsymbol{s}_{i+1} - \boldsymbol{s}_i & \text{otherwise.} \end{cases} \tag{6.1}$$

With this method a reliable movement direction is only provided when people are moving in the direction of the bottleneck and not parallel to the y-axis. This is a valid assumption since a maximum of 25 people participated in the studies and the entrance process did not last long. The participants moved directly to the entrance and did not decide to move to another position to reach the entrance faster such as walking from the left to the right side of the entrance. In the preparation phase (straight walking) and after the entrance was reached (when crossing the y-axis) the walking direction was calculated as the usual vector between the consecutive positions of the trajectory. To improve the heading alignment process in the preparation phase and to make the walking direction more steady in the entrance phase, smoothed trajectories were used for calculating $\boldsymbol{w}$. A Moving-Average-Filter with a window size of 25 (which is equal to one second) was applied to smooth the position data $\boldsymbol{s}$.

To avoid confounding complexities, the entrance phase was limited spatially to $\mathrm{x} \in [0,3]$. At $\mathrm{x}=3$ discontinuities of the movement direction and therefore also of the twist angle may occur which had no influence on the following analysis since the twist angles were examined in the bottleneck only. When reaching the bottleneck at $\mathrm{x}=0$ the change from preferred to usual walking direction was smooth and did not cause any unsteadiness. The walking direction is presented by the angle to the positive x-axis of its vector and can in this way be compared with the rotation angle of the IMU β. For each time step i the difference of both angles as defined in Eq. 6.2 results in the twist angle $\alpha_i \in [-180°, 180°]$ with $\alpha_i < 0$ describing a rotation to the right and $\alpha_i > 0$ to the left. For person A and B in Fig. 6.2 the twist angle is positive.

$$\alpha_i = \beta_i - \arctan(\frac{w_{i,y}}{w_{i,x}}) \tag{6.2}$$

The rotation angle of the sensors α_{imu} was calculated from data of the inertial sensors by applying Madgwick's orientation filter explained in Chapter 3. The participants were asked to place the sensors vertically on their chest and back so that the rotation of the sensors matched the rotation of the upper body. The sensor's x-axis was expected to align vertically with the z-axis pointing forward or backward. Even though the z-axis was not always pointing in the direction of movement, as assumed in Sec. 3.3.1, the same heading alignment approach was applied. This means that it could not be determined whether the y-axis was orientated to the left or right shoulder and the exact alignment of the local IMU frame in the global camera frame was unknown. This was not a problem since the rotation of the local z-axis to the left or right remained the same.

6.2.2 Error Analysis

While inspecting the recorded and processed IMU data it was determined that some of the data could not be used for a proper orientation calculation. A sufficient standstill phase which is required for initialization was not always given and the data of one sensor showed a gyroscope offset, both leading to faulty orientation calculations. Besides, incomplete trajectories without a straight walk resulted in difficulties to find a proper heading alignment phase. Furthermore, the participants were asked to attach the sensors by themselves resulting in varied attachment positions such as over or under their clothing or not exactly centered. Due to insufficient fixing with tape some sensors detached while moving through the bottleneck. For those reasons, it was not possible to uniformly use the sensor on the back or chest for the analysis. Instead, for each run the data of all sensors were checked manually and classified into "Good", "Acceptable" and "Unusable" data sets as described in App. E. Only good and acceptable data sets were used for calculating the twist angle. Thus, a different database was used for the analysis of each run choosing the best IMU data set per person. When comparing the data of the sensors on the back and chest, no major difference in the tracking quality of twist angles could be observed. Thus, no preferable attachment position could be named.

Furthermore, the inspection of the twist angles in the preparation phase can also give information about the quality of the rotation values. Figure 6.3 shows the relation between the Euclidean distance to the entrance and the twist angle while straight walking in the preparation phase. The twist of the upper body from one side to the other, which is step-related, is clearly visible especially for the purple and blue curves. Typically, the twist angles while walking are expected to fluctuate around

zero as for the blue curve. For the purple curve, a large offset was visible for which several sources of error are possible. The calculated twist angle was sensitive to the time step of the heading alignment for which the straight walk is needed. A posture without twisting is assumed when aligning camera and IMU data. Depending on the chosen time step for alignment, the upper body might be twisted to the left or right when taking steps. This may occur, even though the trajectory appears to be straight. This could lead to a negative or positive offset of the twist angle. Besides, the calculated twist angle was also sensitive to the placement of the sensor. The sensors might have been attached with a slight twist already resulting in an offset. Additionally, the accuracy of the calculated walking direction which was required for calculating the twist angle as in Eq. 6.2 can also affect the accuracy of the twist angle.

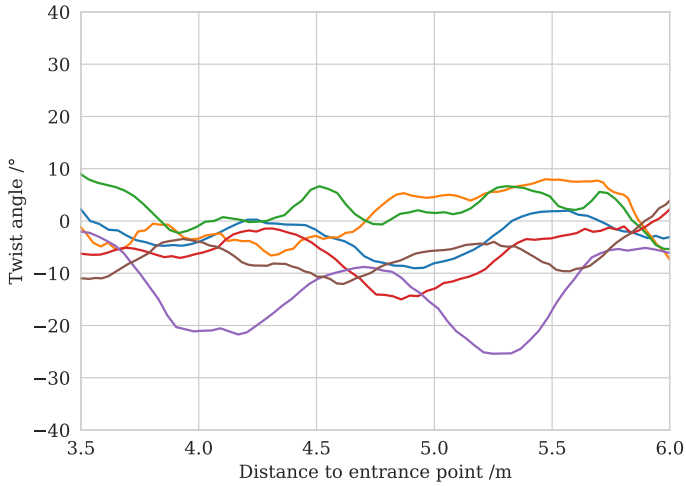

Figure 6.3: Relation of distance to entrance and twist angle in preparation phase. By the shape of the curves, twisting while walking can be observed in the data.

During the analysis of the video material, it was noticed that some rotation processes could not be mapped to the desired twist angles. Due to the chosen attachment of the sensors, there are limitations regarding the capturing of certain movements, referred to as asymmetric shoulder movements. Here, asymmetric shoulder movement describes the situation of a person moving one shoulder anteriorly or posteriorly without the opposite movement of the other shoulder. This happened, for example when one shoulder was retracted or both shoulders are pulled forward especially to pass the wall when entering the bottleneck. Two scenarios can be seen in Fig. 6.4. Both

participants moved their shoulders asymmetrically to walk through the bottleneck. Although this was not an unhindered and normal movement of the upper body, low twist angles of only 13° (top) and 22° (bottom), were measured in the bottleneck. Therefore, a detection of those special cases was not possible with the proposed method and improvements are needed (see Sec. 6.4.1).

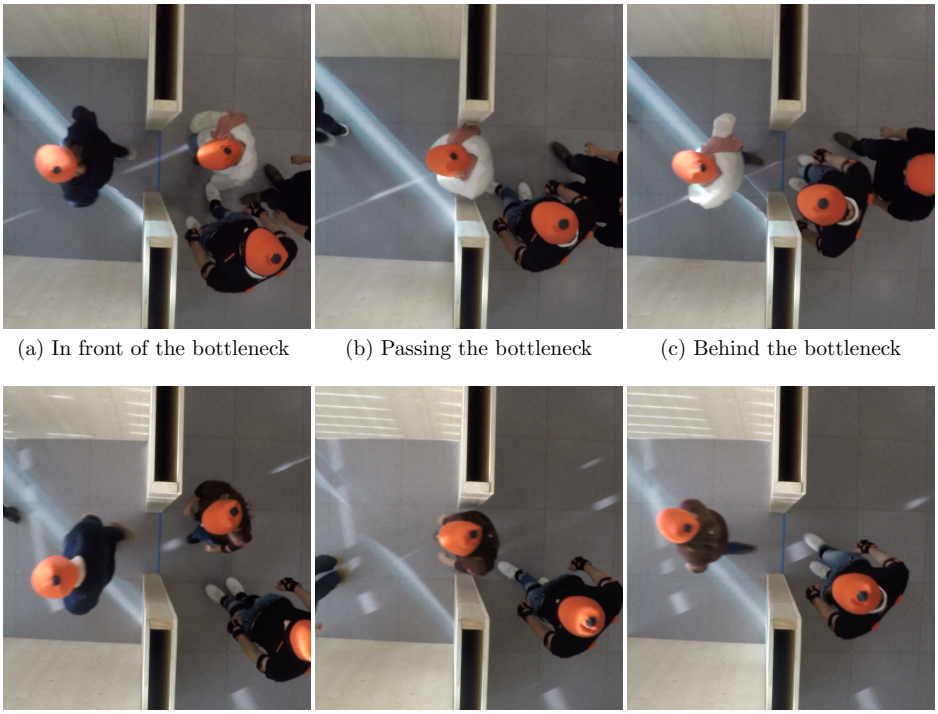

(a) In front of the bottleneck (b) Passing the bottleneck (c) Behind the bottleneck

(d) In front of the bottleneck (e) Passing the bottleneck (f) Behind the bottleneck

Figure 6.4: Example of participants walking through the bottleneck with asymmetric shoulder movement. The first person (top) pulled both shoulders forward to fit through the bottleneck without any rotation. The second person (bottom) pulled the right shoulder forward to avoid a collision with the wall.

6.3 Analysis and Results

The rotation of the upper body is influenced by several factors such as the shoulder width, the angle from which the bottleneck is approached, the personal space, existing neighborhoods, the density, or the geometry. These factors can influence each other as well and result in complex interactions. As a first approach for the analysis,

the following Sections focus on the bottleneck width, motivation, density, and flow investigating their relation with the occurred twist angles.

6.3.1 Rotation in the Bottleneck

To gain an understanding of where the participants rotated the most, the twist angles were examined depending on the distance to the entrance point. An example of a narrow and wider bottleneck is shown in Fig. 6.5. For each position of the participant's trajectories the Euclidean distance to their arrival position was calculated (when $x = 0$, see Fig. 6.1e) and the twist angle for the corresponding time step was determined. A negative distance to the entrance means that the bottleneck was reached so that the person was either moving within the doorframe or leaving it. The curves fluctuated locally at higher positive distances to the bottleneck when the participants were standing still and the preferred movement direction could not be determined reliably (due to the movement of the heads). Besides, a negative or positive offset for the twist angles was possible based on the calculation of the initial orientation of the inertial sensors as already discussed in Sec. 6.2.2.

Initially, the data of the entrance phase were analyzed. For a width of 0.4 m the process of entering the bottleneck was clearly visible based on the shape of the curves. Maximum twist angles occurred when leaving the bottleneck with absolute twist angles larger than 50° except for one person. Due to the narrow width all participants needed to rotate their upper body sideways to enter the bottleneck. The twist angles for the bottleneck with a width of 0.7 m were not homogeneous regarding the area of absolute maximum rotation anymore. The twist angle peaks were not as high as for the narrow bottleneck so that the rotation data in the bottleneck no longer differs much from the rest of the data.

The maximum occurring after the actual bottleneck in Fig. 6.5a might depend on the small depth of the bottleneck of 0.13 m. When a person was leaving the bottleneck the trailing shoulder still needed to be rotated in order to completely pass through the bottleneck. According to [32] overall smaller twist angles might occur for alternative geometries with a higher depth of the bottleneck since the uncomfortable posture with high twist angles would have to be kept longer when moving close to the wall.

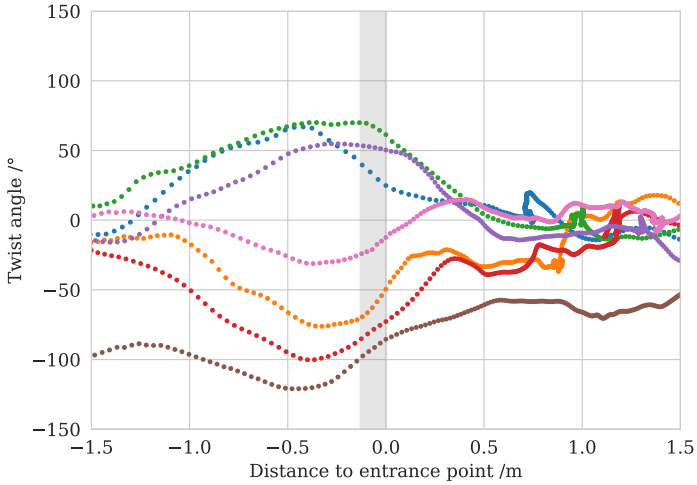

(a) Bottleneck width of 0.4 m

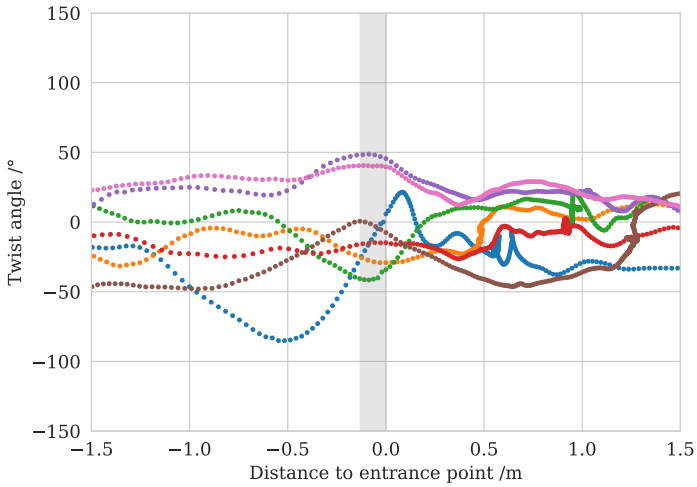

(b) Bottleneck width of 0.7 m

Figure 6.5: Relation of distance to entrance and twist angle for two bottleneck widths, low motivation, and $N = 8$. Colors are chosen based on the trajectory ID per run and do not represent the same person. The bottleneck entrance is marked in grey.

For a better understanding and illustration of the twist angles, the rotation data for one person are discussed in more detail in the following. Due to the special shape

of the blue curve in Fig. 6.5b selective twist angles (see Fig. 6.6) and the corresponding sample images (see Fig. 6.7) were investigated. The person was rotating to the left before entering the bottleneck, not rotating when reaching the bottleneck and rotating to the right when leaving it. A sharp turn in the trajectory before entering the bottleneck occurred. The person stopped briefly to let another person pass (who was wearing the white shirt) followed by an abrupt change of the twist angle. Even though the IMU data set for this person was categorized as acceptable only (due to a slight misalignment in orientation of 6°), the visual inspection indicated that the calculated twist angles are valid and match the observed movement.

The blue and green crosses were plotted to visualize the estimation of the walking direction as in Eq. 6.1 that is used for calculating the twist angle. The green cross is representing the reference point which is the entrance point ($\boldsymbol{s}_{entrace}$) for Fig. 6.7a, and the subsequent position point ($\boldsymbol{s}_{i+1}$) for Fig. 6.7b, 6.7c, and 6.7d where it is close to the green cross.

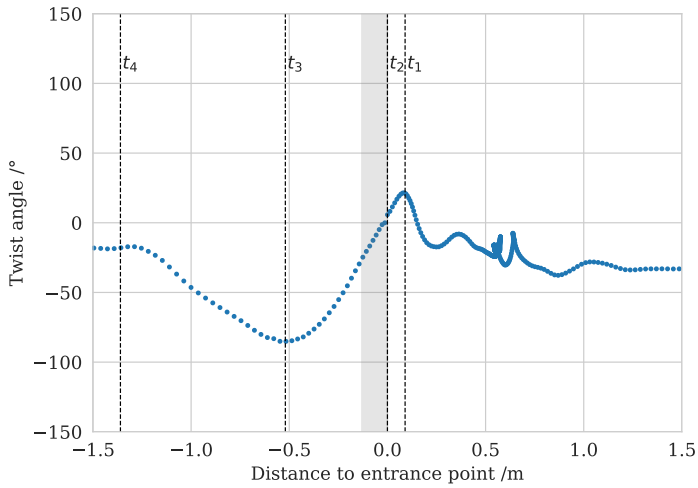

Figure 6.6: Relation between distance to entrance and twist angle for one person. The bottleneck entrance is marked in grey. Data set was chosen because of clearly visible peaks before and after entering the bottleneck and a zero twist angle when reaching the bottleneck. These striking values are marked by vertical lines (timestamps).

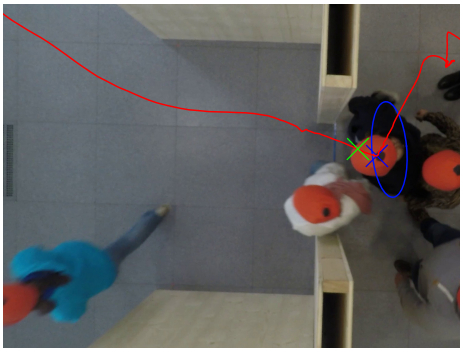

(a) Timestamp t_1: waiting for another person to pass with a slight twist to the left of 21°

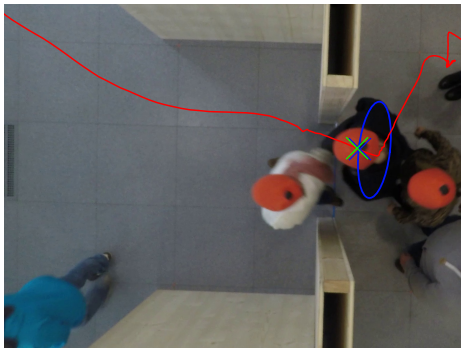

(b) Timestamp t_2: entrance point is reached with a twist angle of 6°

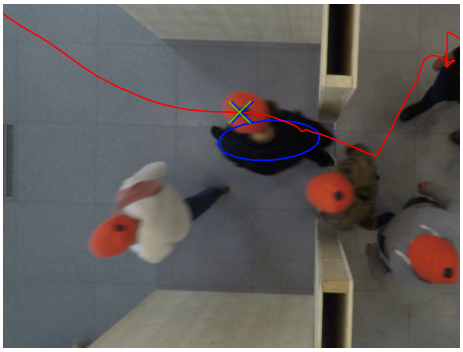

(c) Timestamp t_3: leaving the bottleneck with a high twist to the right of −85°

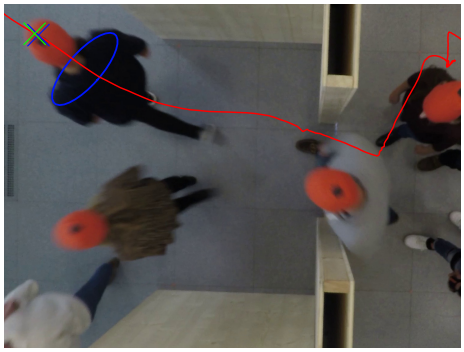

(d) Timestamp t_4: returning to normal posture with a twist angle of −18°

Figure 6.7: Sample images of rotation scenarios according to Fig. 6.6. The trajectory is shown in red plotted on the height of the participant's head and the alignment of the shoulder is marked manually with a blue ellipse. The blue cross is the current position on the trajectory while the green cross is the reference position that is used for calculating the preferred walking direction.

For further analysis of the twist angles, a temporal or local area had to be defined with the twist angles of interest, to focus on the actual process of passing the bottleneck. Both examples in Fig. 6.5 demonstrate that it was difficult to determine the start and end of the rotation for the process of passing the bottleneck with a criterion of twist angle only. Some participants approached the bottleneck already with a twist angle of more than 30° such as shown by the red, orange, and brown curve in Fig. 6.5a. Besides, people changed the direction of twisting or do have low and steady twist angles only, as for the blue and red curves in Fig. 6.5b. Moreover, it

was especially difficult to determine the end of the rotation since participants started rotating after leaving the bottleneck in order to return to the start area. Therefore, it was decided to focus on the participant's twist angles while they were moving in the doorframe when $\boldsymbol{s}_x \in [-0.13, 0]$ (see Fig. 6.1e) for further analysis.

While the maximum twist angles in combination with motivation are discussed in the next Section, at this point the twist angles in different regions of the bottleneck are investigated. For the conducted studies with a maximum bottleneck width of 1.0 m, it was observed that up to three participants entered the bottleneck at the same time. A higher rotation close to the geometry walls was expected since participants approached the bottleneck from the left or right, filled gaps, and passed sideways. Participants entering the bottleneck centrally aligned were expected to show smaller twist angles because they were less influenced by the geometry. For the analysis of this process, the bottleneck was separated into three areas: close to the left wall (maximum distance of 0.25 m), the middle, and close to the right wall (maximum distance of 0.25 m). Assuming an averaged shoulder width of 0.5 m, participants are expected to rotate their trunks when moving within 0.25 m distance to the wall. While the areas next to the wall are fixed for each run the width of the middle region varies with the width of the whole bottleneck as shown in Fig. 6.8.

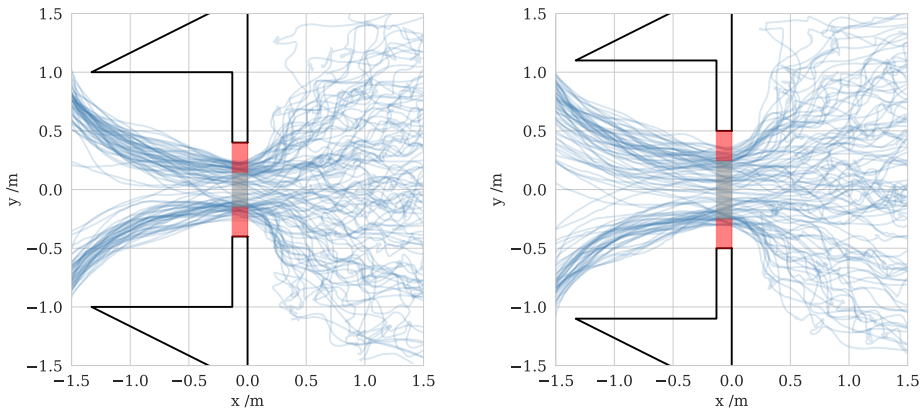

(a) Partitions for a width of 0.8 m

(b) Partitions for a width of 1.0 m

Figure 6.8: Partitioning of the bottleneck into the regions of interest. Regions close to the wall are marked in red ("Left": bottom, "Right": top), "Middle" region in grey.

Based on the participant's position when they were reaching the bottleneck with $s_x \leq 0$ the data were grouped according to the region of entrance and the absolute twist angles for that position were calculated. The results are shown in Fig. 6.9 and 6.10 for low and high motivation for the different bottleneck widths. The analysis was done for the runs with $N = 25$ participants only due to expected gaps being filled when entering the bottleneck for larger widths and higher densities.

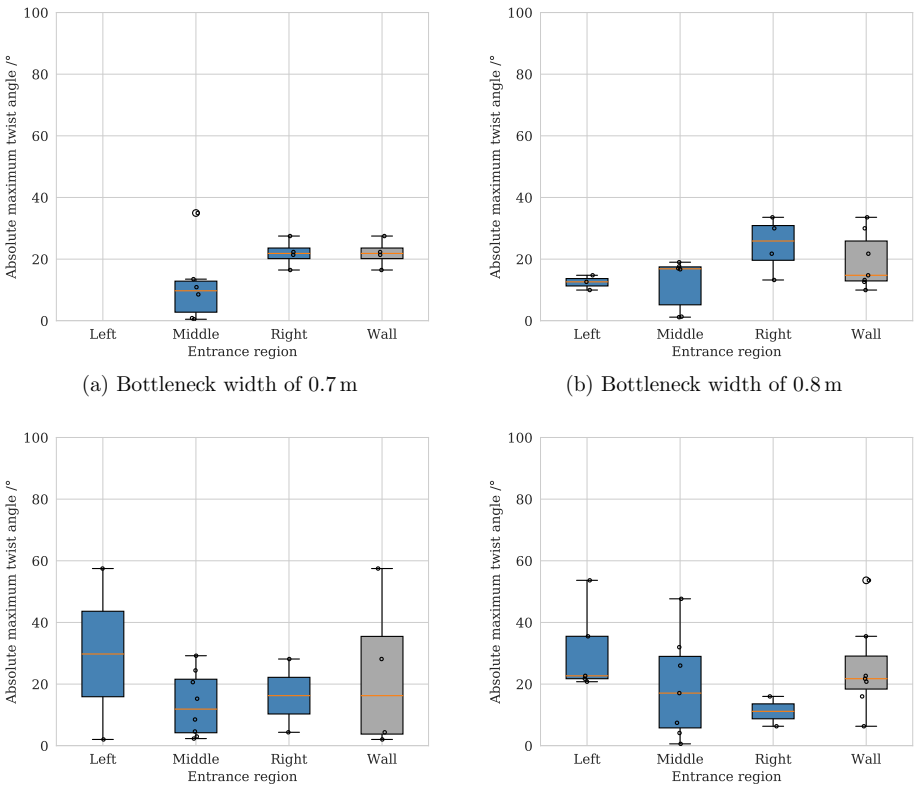

(a) Bottleneck width of 0.7 m

(b) Bottleneck width of 0.8 m

(c) Bottleneck width of 0.9 m

(d) Bottleneck width of 1.0 m

Figure 6.9: Boxplots for the calculated twist angles in different regions of the bottleneck for studies with $N = 25$ participants and low motivation. Data for "Wall" represent the merged data of "Left" and "Right". Data of both repetitions for each run are considered.

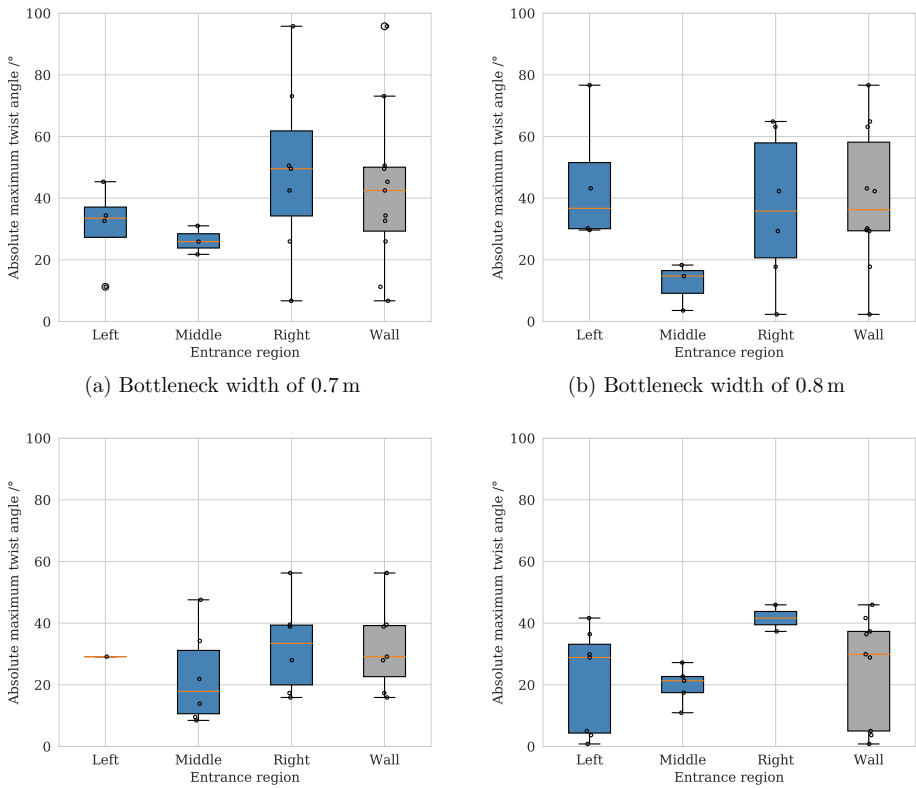

(a) Bottleneck width of 0.7 m

(b) Bottleneck width of 0.8 m

(c) Bottleneck width of 0.9 m

(d) Bottleneck width of 1.0 m

Figure 6.10: Boxplots for the calculated twist angles in different regions of the bottleneck for studies with $N = 25$ participants and high motivation. Data for "Wall" represent the merged data of "Left" and "Right". Data of both repetitions for each run are considered.

It could be assumed that twist angles are affected by many factors such as social interactions. It was observed that some participants allowed other people to pass so that the passing person did not have to rotate the upper body as much when entering from the side. Some people kept a larger distance from their neighbors and as a result, did not rotate their upper body to fill gaps especially for the low motivation scenario. Furthermore, the width of the bottleneck and the individual width of the shoulders also had an impact on their rotation. If the sum of the shoulder widths of the collectively passing persons was smaller than the bottleneck width, there was no need to rotate the upper body to a great extent even when moving close to the wall.

The expected v-shape form for twist angles values is clearly visible for the high motivation scenario meaning that the median of twist angles is higher for “Left” and “Right” than for “Middle”. This was not apparent for the low motivation scenario, since the participants were keeping a larger distance to each other without filling gaps which goes along with smaller densities (discussed in Sec. 6.3.3). The maximum difference of the medians of “Middle” and “Wall” for low motivation is 12.2° (see Fig. 6.9a) while for the high motivation scenario the maximum difference is 21.6° (see Fig. 6.10b). Additionally, a much broader range of twist angles close to the wall was observed when people were highly motivated. This applied to all bottleneck widths except for 0.9 m even though the region in the middle was increasing with an increasing bottleneck width. Although, the median for “Wall” is higher than for “Middle” very small twist angles occurred close to the wall. A high variation of twist angles close to the wall is possible depending on how many people were passing the bottleneck at the same time as shown in Fig. 6.11.

(a) Two people passing the bottleneck at the same time with low twist angles

(b) Three people approaching the bottleneck at the same time leading to high twist angles

Figure 6.11: Sample images of rotation scenarios when several participants are approaching the bottleneck with a width of 1.0 m at the same time.

Comparing the data of locally grouped twist angles with regard to the different bottleneck widths, no clear trend was apparent neither for the low nor for the high motivation scenario. In summary, it can be said that there is a much higher variation of twist angles close to the wall than in the middle of the bottleneck and that highly motivated people who were entering the bottleneck close to the wall had an overall higher twist angle.

6.3.2 Rotation and Motivation

Previous studies have shown that psychological factors such as motivation can have very strong impacts on the movement or behavior of individuals [153]. When imagining a highly motivated crowd entering a bottleneck an overall stronger rotation is expected as the participants want to reach their goal quickly and therefore exploit more possibilities to make progress.

To investigate this relation, the maximum twist angles in the bottleneck ($s_x \in [-0.13, 0]$) were analyzed for each bottleneck width for the low and high motivation studies. Only absolute values were analyzed so that the information about the direction of rotation to the left or right was neglected.

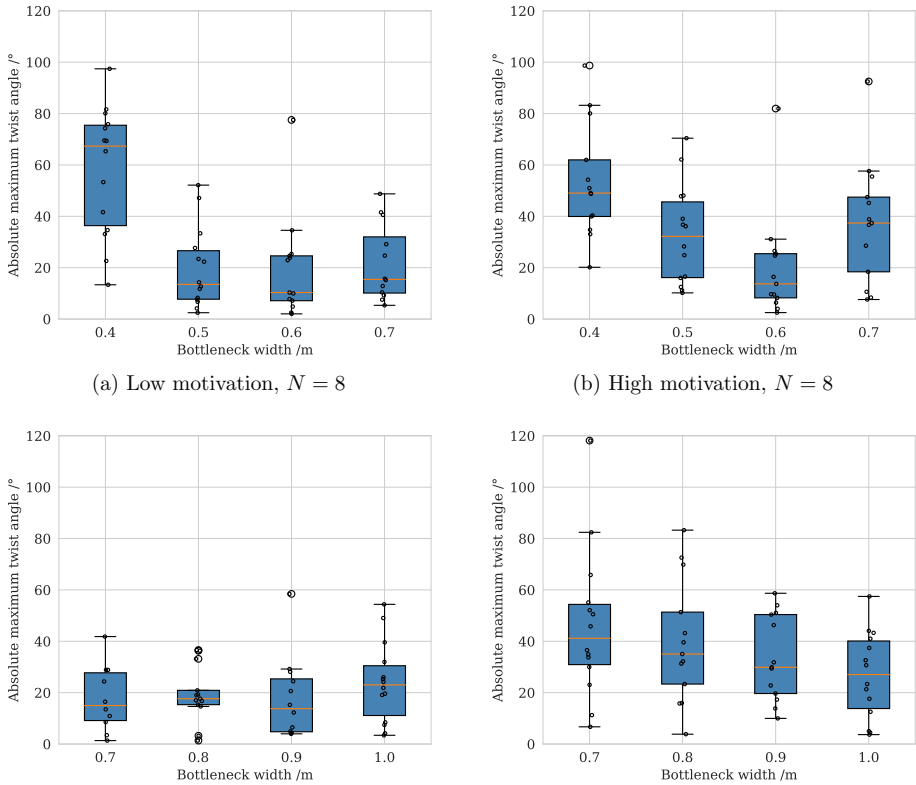

(a) Low motivation, $N = 8$

(b) High motivation, $N = 8$

(c) Low motivation, $N = 25$

(d) High motivation, $N = 25$

Figure 6.12: Relation of bottleneck width and twist angle for low and high motivation. Data of both repetitions for each run are considered (10-14 values per bottleneck width).

Figure 6.12 clearly shows that with higher motivation, a higher median twist angle in the bottleneck was likely. This means that participants were more willing to rotate their upper body when they were in a highly motivated state. This does not apply for the bottleneck width of 0.4 m for which all participants needed to rotate their upper body to pass through, even with low motivation. The range of the twist angles per width was broader for the high motivation scenario since many participants entering the bottleneck close to the wall did show higher twist angles when highly motivated (as already shown in Fig. 6.10).

Statements on the effect of different widths of the bottleneck on the twist angles were difficult to make. For the low motivation scenarios the twist median angles were similar to each other for all bottleneck widths, ranging from 10° to 23° (again except for the width of 0.4 m since everybody needed to rotate). The high motivation studies showed a broader range for the twist medians of 14° to 41° excluding data for 0.4 m. While the twist medians were decreasing for the high motivation scenario starting at 0.7 m, no trend was apparent for the low motivation. Also, decreasing twist angles for the bottleneck widths 0.4 m, 0.5 m, and 0.6 m are visible in Fig. 6.12b followed by a rise of the twist angles for 0.7 m. Given a wider bottleneck, two people can enter the bottleneck at the same time as shown in Fig. 6.13 causing the rise in the data. An increase in twist angles shown in Fig. 6.12d might also occur for higher bottleneck widths than 0.9 m when three participants are entering at the same time more often. Data for more bottleneck widths are needed to investigate this effect properly.

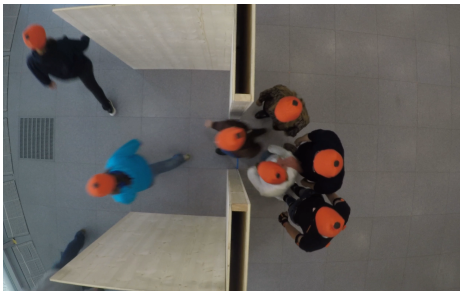

(a) Participants are entering the bottleneck one by one due to the small width

(b) Participants start to approach the bottleneck at the same time

Figure 6.13: Sample images of rotation scenarios for a bottleneck width of 0.6 m (left) and 0.7 m (right).

A summary statement can be made that with a higher motivation the width of the bottleneck had a greater influence on the occurred twist angles. This could be

the case because people were more likely to fill gaps and the bottleneck width in turn was decisive for the size of the gaps that occur especially close to the walls.

6.3.3 Rotation and Density

In the following, the relation between the maximum rotation of a person in the bottleneck and their corresponding individual density is analyzed. For calculating density, the Voronoi method [27] was applied to create Voronoi cells which provide information about the space available to each individual person for each time step. This available space was influenced by the neighbors of the person and the walls of the geometry setup. A Voronoi cell contains all points in the xy-plane that are closer to the person than to their neighbors. For density calculation unsmoothed trajectories were used to make it comparable with other studies. The density ρ for a person i for the point (x, y) was calculated as stated in Eq. 6.3 with A_i defining the area of the current Voronoi cell.

$$\rho_{i,x,y} = \begin{cases} 1/A_i & \forall (x,y) \in A_i, \\ 0 & \text{otherwise.} \end{cases} \tag{6.3}$$

Figure 6.14 shows the relation of the individual density and the occurred twist angles separated by low and high motivation for the different bottleneck widths. For each participant wearing an IMU, the first data set of density and twist angles when the bottleneck was reached ($s_x \leq 0$) was chosen. The data of the first and last two people entering the bottleneck were excluded from the analysis to consider more reliable density values. A higher density was expected for the higher motivation scenarios and can be clearly seen in the data. Due to the low number of participants the density values for runs with $N = 8$ people were not reliable and are not discussed here. Besides, for smaller bottleneck widths only one person can pass the bottleneck at a time.

Higher twist angles were expected for higher density values. This trend applied for the data shown in Fig. 6.14a and 6.14b. The effect decreased with increasing bottleneck width and a similar range of twist angles for low densities is visible (see Fig. 6.14c and 6.14d).

It was expected that a higher motivation would result in higher densities and that the participants were more likely to rotate their upper body in order to fill gaps and make faster progress in the bottleneck. However, especially for densities larger than $3\,\mathrm{m}^{-2}$ most of the twist angles were smaller than 40°. This indicates that higher densities were not necessarily associated with higher twist angles. This result is in

accordance to the findings of the cross-flow experiment in [101]. Therefore, it must be considered that with higher densities, less space between the participants and walls is available which limits the opportunity for rotation. Nevertheless, it is conceivable that the rotation increases with the density at the beginning but decreases again from a certain still to be determined threshold density value.

Nevertheless, the results show a sequence of occurrences i.e., that a higher motivation came with a higher density, which means that gaps were filled, which in turn went along with the higher willingness to rotate the upper body (see Sec. 6.3.2).

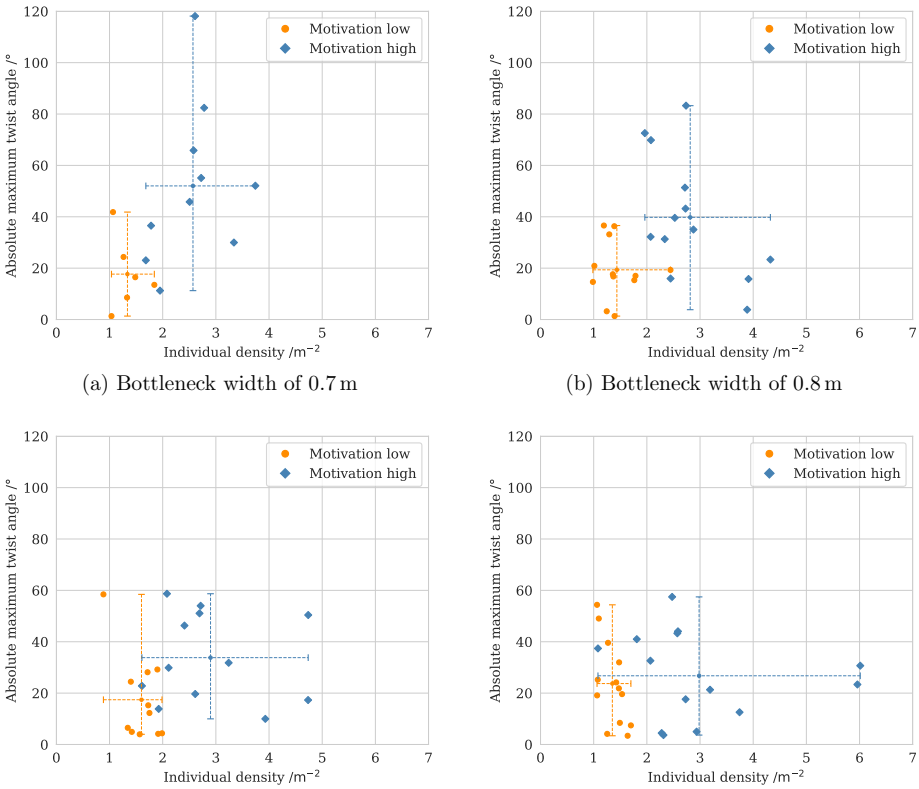

(a) Bottleneck width of 0.7 m

(b) Bottleneck width of 0.8 m

(c) Bottleneck width of 0.9 m

(d) Bottleneck width of 1.0 m

Figure 6.14: Relation of individual density and absolute twist angle in the bottleneck for $N = 25$. Data of both repetitions for each run are considered.

6.3.4 Rotation and Flow

As described in [154] a linear relationship between the width of the bottleneck and the flow is given by linear growth. Due to a zipper effect the participants can walk staggered in the bottleneck. This was observed for the conducted studies as well. Higher flows occurred for wider bottlenecks. In the following, it is investigated whether an increased flow is accompanied by higher twist angles.

Hereby, the flow is defined as the throughput at the entrance of the bottleneck at $x = 0$ and it was examined whether a higher throughput was associated with higher twist angles. The flow was visualized in form of a step function as shown in Fig. 6.15. The figures show the number of people passing the bottleneck over time and if available the twist angle data of the passing person. The steeper the step function is, the shorter the individual steps are, showing the time between successive persons passing the bottleneck. Longer steps represent a longer waiting time for the participants until they can enter the bottleneck and can be caused by waiting due to congestion or when letting someone pass. Therefore, a steeper function indicates a higher flow. The maximum number of people passing the bottleneck at the same time is invariably limited by the width of the bottleneck and the sum of shoulder widths of the participants entering the bottleneck.

The data clearly indicated that the high motivation scenarios have a higher flow than the low motivation scenarios. All twist angles for low motivation were smaller than 40°. The step functions appeared more homogeneously regarding height and width of the steps while these values have large variations for high motivation.

Depending on where a person is entering the bottleneck (middle or close to wall) a high twist angle is not necessarily needed to pass the bottleneck faster. As described in Sec. 6.3.1 participants with a high motivation occurred to have higher twist angles close to the wall. Participants approaching the bottleneck from the center showed smaller twist angles meaning a jump in the step function can be accompanied by high and low twist angles. This can be seen in Fig. 6.15d at approximately $t = 8\,s$ where twist angles of two persons entering the bottleneck at the same time are available. While one person had a high twist angle of over 65° the other person had a low twist of only 15°. A similar scenario is shown in Fig. 6.15b where twist angles of three consecutive persons are available ($t = 8\,s$ to $9\,s$). Short steps were accompanied by twist angles of 11°, 73°, and 33°.

Therefore, it can be said that high twist angles can cause an increased flow due to filling gaps. However, high twist angles are not necessarily required when the sum of the shoulder widths fits in the bottleneck width since the zipper effect needs no

rotation. Basically, the presence of high twist angles might indicate a higher flow since people are rotating their upper body in order to speed up progress. More data are needed to analyze this in detail.

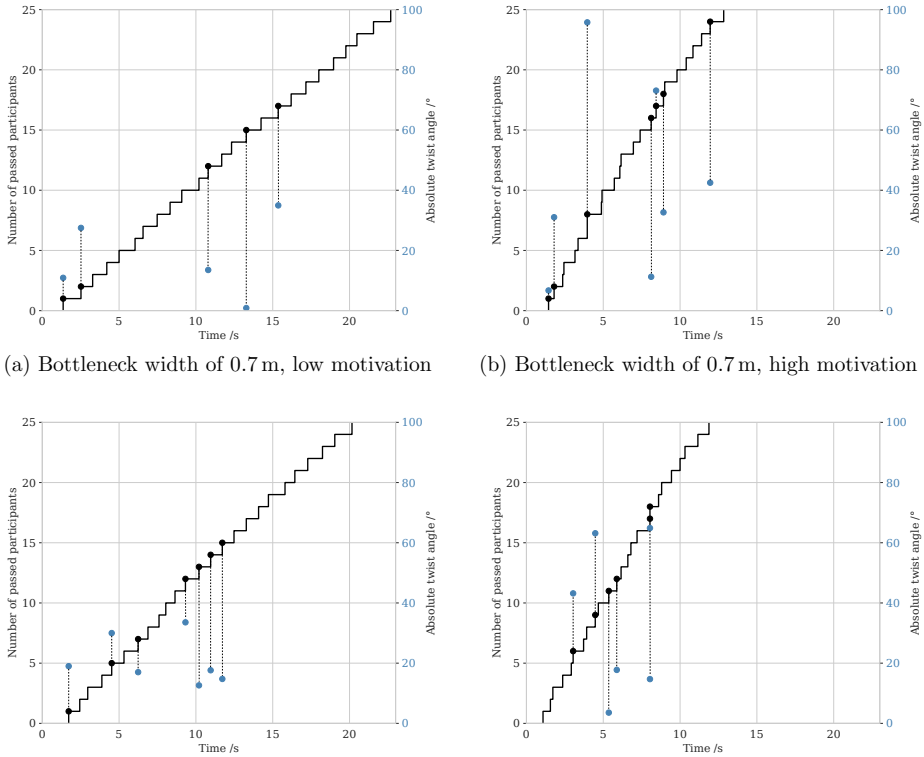

(a) Bottleneck width of 0.7 m, low motivation

(b) Bottleneck width of 0.7 m, high motivation

(c) Bottleneck width of 0.8 m, low motivation

(d) Bottleneck width of 0.8 m, high motivation

Figure 6.15: Relation of flow and twist angle.

6.4 Future Experiments

6.4.1 Suggested Improvements

In principle, the studies and validations showed that the proposed technology and data extraction technique is suitable to measure the rotation of the upper body of pedestrians in crowds. Nevertheless, some adjustments may be necessary to gather even more precise and meaningful data.

In future experiments, an adapted design of the geometry setup is suggested.

Due to limited spatial circumstances the participants had to rotate again shortly after entering the bottleneck to go back to the starting area. This made it difficult to isolate and analyze the actual rotation when passing the bottleneck. A mix of rotation in order to pass the bottleneck and to move back to the starting area occurred (see Fig. 6.1). To overcome this issue a longer corridor after the bottleneck may be beneficial.

Besides, a learning effect regarding motivation and density was observed. The instructions given before starting the entrance phase were always the same: at first, the low motivation scenario was conducted followed by the high motivation scenario. Although the instruction has not been given at that point a higher density for the high motivation scenario when gathering in front of the bottleneck could be observed for the last runs. The participants knew what to expect. To solve this issue in the future the sequence could be varied or various instructions intending the same motivation could be given.

The instruction for the standstill phase for initializing the heading calculation of the IMUs must be made more clear and precisely in the future. Insufficient initialization data made the rotation calculation difficult and at times, led to unusable data sets. It was observed that people stood still, but moved their upper body to talk to or look at each other. “Please keep your upper body still.” might be a preferred instruction. Although, the attachment of the sensors could be reconsidered to make the measurement of asymmetric rotations possible. The attachment on the scapula region may be promising.

6.4.2 Further Analysis

The analysis was limited to the rotation data of seven people within one run only. To draw a more general conclusion, rotation data of each participant are required. Furthermore, the studies should be repeated considering the suggested improvements and with a higher number of participants.

In prior Sections, basic relationships between twist angles, motivation, density and flow have been presented. Studies with broader bottleneck widths should be conducted to investigate the relation between bottleneck width and twist angles. Besides, the depth of the bottleneck might also be an interesting parameter effecting the rotation of the upper body. Furthermore, the investigation of the density in front of the bottleneck for larger crowds could provide more reliable information. The analysis of the flow may be advanced when rotational data for all participants are

available. Therefore, the relation between step widths (δt) and the occurred twist angles can be investigated.

Up to now, neither the shoulder width nor the neighborhoods and their interaction were investigated. Both have a crucial impact on the rotation in the bottleneck. People with wider shoulders need to rotate more to pass in a narrow space. Depending on the vicinity of neighbors, pedestrians are forced to rotate their bodies or can move unimpeded in the crowd or bottleneck.

Asymmetric shoulder movement has been observed in the studies. People retracted their shoulders in order to reduce their individual space requirements. Once the detection and measurement of asymmetric shoulder movements is possible, this information can be used to analyze the change of spatial requirements and improve corresponding models. The knowledge about how pedestrians rotate and change their individual space could help to improve simulations where pedestrians are represented as ellipses with a varying size as in [28].

Chapter 7

Closing Remarks

7.1 Conclusions

This work contributes to new data capturing techniques in laboratory pedestrian experiments and thus, provides new possibilities for an improved analysis of the movement of a person inside a crowd. A profound understanding of factors and their relations that are influencing this movement is fundamental for the safe design of pedestrians' environment.

Besides the development and testing of a novel hybrid tracking system, new movement data have been captured and a framework for processing these data sets is provided within the scope of this work. These main contributions are summarized below.

A **hybrid tracking system** for extended data capturing in pedestrian experiments was designed consisting of a given well-established overhead camera system as a basis and newly tested IMUs as extension worn by the pedestrians. The use of IMUs allows the reconstruction of movements that are difficult to capture by cameras due to the perspective view and occlusions in dense crowds. Due to the small size of the inertial sensors, they are comfortable to wear and do not restrict the movement of the participants which is important for capturing natural movement data. The IMUs are self-contained meaning no additional infrastructure other than the hub device for synchronization is required which keeps the extension of the camera system simple. Based on captured data with the developed hybrid system the analysis of microscopic movement data with high accuracy can be performed. Especially, the possibility to capture the individual rotation of the participants' upper body opens up new opportunities for the analysis of crowd dynamics. In addition, the tracking system also offers the possibility to examine alternative movement processes.

Several **tracking methods** have been applied, adapted, and extended to calculate information about rotation and traveled distance from the IMU data. While the algorithms for distance calculations were customized for wheelchair users, the methods for rotation calculation are generally applicable. IMUs capture relative movement data in the form of acceleration, gyroscope, and magnetometer data within the local frame of the device. The transformations of the IMU data from their local frame to the world and camera frame are fundamental steps before actual tracking approaches can be applied. For aligning the IMU data in the world frame and to keep track of the device's orientation, Madgwick's orientation filter has been applied. To calculate the position of a wheelchair from acceleration data the approach of double integration was tested. As this kind of IMU data processing is known to suffer from error accumulation the data of two IMUs mounted to the same wheelchair have been used to limit the drift in the data. The IMUs have been vertically aligned on the backrest of the wheelchair and therefore, tracked the same movement. This information was used for corrections when calculating the position of both sensors. For this purpose, a Measurement-Augmented Kalman Filter has been adopted.

Techniques for the fusion of IMU and camera data have been implemented to provide consistent data sets in the same coordinate system for each time step. For time synchronization an LED signal of the IMU system's hub device is used at the beginning and end of the experiments which creates corresponding signals in the IMU data and which are visible to the cameras. Additionally, time synchronization was realized with the help of specific movement patterns that are searched for in the IMU and camera data. To align the individual movement data of the IMUs in the camera frame of the trajectories, the IMU data are rotated so that the movement direction of the IMU aligns with the movement direction based on the trajectory of the participant wearing the IMU sensor.

In addition to the purpose of time synchronization and frame alignment, fusion techniques have been also used to improve the accuracy for distance tracking based on IMU data utilizing camera data. The basic idea is to use the movement properties of pedestrians surrounding the wheelchair user to correct the tracking data. In the case of occlusion of the wheelchair user, the distance tracking based on IMU data becomes important. If this happens it is assumed that camera data of the surrounding pedestrians that have lead to the temporary occlusion are available. These camera data can be used to calculate velocity and acceleration data of the pedestrians and to limit the drift of the calculated IMU trajectory. As a first approach data of the pedestrian

pushing the wheelchair user were used for this purpose and two correction strategies have been developed. First, the velocity of the wheelchair is set to the velocity of the pushing person if their difference exceeds a specific range. As the pushing person is moving close to the wheelchair user their velocity is expected to be similar and this information is used to correct the tracking data. Second, an adaptive approach was developed to remove noise and initialization errors. Again, the velocity of the pushing person and wheelchair user are supposed to be similar. If their difference reaches a specific threshold the IMU data are expected to be noisy. Therefore, the acceleration data are corrected based on the difference in acceleration that has lead to the difference in velocity and the position calculation is redone. If the threshold is reached again at a later point in time this process is repeated. Both approaches have been integrated into the basic double integration approach and also in the Measurement-Augmented Kalman Filter which is fusing the data of two IMUs. If the difference in velocity is becoming large for one of the sensor data, the tracking data are corrected accordingly.

Experimental data for validation have been captured in large-scale studies with heterogeneous crowds and small-scale studies with one single participant. The former studies were conducted with participants with and without disabilities moving through a bottleneck and corridor in various constellations. These studies have been recorded with the hybrid tracking system and participating wheelchair users were equipped with IMUs. The distance tracking quality of the above-mentioned methods has been validated leading to a mean spatial error of 0.13 m when fusing the data of two IMUs and applying adaptive corrections. The analysis showed that regular corrections are required to prevent drifting of the calculated trajectory.

In the small-scale studies the movement of one participant walking and using a wheelchair was recorded with IMUs and a 3D infrared camera tracking system to validate the rotation calculation based on IMU data. For the rotation calculation while walking a mean absolute error in heading of less than 5° was determined. For the rotation tracking of the wheelchair user a mean absolute error of less than 8° was achieved. IMU and camera data for both studies have been published in [133, 135], are freely accessible, and can be used for further analysis.

A **software framework** [147] has been developed to apply the tracking and fusion methods. In this work, the framework was used to process data of SABEL Lab sensors and camera data extracted with PeTrack and Motive (Optitrack). By providing several interfaces the framework is open for extension to process data of other

sensor systems as well. Besides, the framework offers the possibility to adapt existing algorithms or to develop new tracking and fusion methods. Therefore, the software framework provides a platform that future research can extend on.

The **application** of the hybrid tracking system for gathering rotation data of the upper body was demonstrated in small-scale experiments. Participants were equipped with inertial sensors on the upper body and moved through a bottleneck of different widths. The participants needed to stand still at the beginning of each run for initialization purposes and a straight walk was required for the alignment process. These are the only requirements that need to be considered when using the hybrid tracking system in the future. Based on the IMU data of the participants the rotation of their upper body was reconstructed which allowed to investigate its temporal and spatial course in the bottleneck and the relation to the width of the bottleneck, the motivation, density, and flow. As the rotation of the upper body changes the individual required space is an important factor to analyze. The conducted small-scale studies have shown that the hybrid tracking system is suitable to capture data of body rotations and can be used in the future for a deeper analysis of pedestrian dynamics. The captured IMU and camera data, and the calculated data of rotation have been published in [152] and are available for further analysis.

7.2 Outlook

To improve the **accuracy** of the distance tracking methods several approaches for limiting the drift have been applied in this work. Nevertheless, a maximum spatial error of 0.73 m was determined even when fusing the data of two IMUs and applying the adaptive correction approach. However, there are many possibilities to further improve the distance tracking accuracy which could be integrated into the framework and validated with the provided data sets. In this work, only the camera data of the pushing person have been used as an external source of information to limit the drift. Applying this approach to the data of several pedestrians that are surrounding the wheelchair user seems to be promising for further restrictions of the trajectory. This could be realized by considering distances between the participants, their individual space requirements, and velocities while tracking the position of the wheelchair user. Besides, the geometry of the experiment restricts the possible trajectories of the participants. For this purpose, the application of map matching filters and particle

filters as in [63–65] could be used to propagate the wheelchair user's trajectory with different noise parameters resulting in a set of possible trajectories. Based on this, the trajectories that are too close to walls could be discarded. Surrounding people could also be considered as 'moving obstacles' in this approach. Next to integrating additional camera data, the processing of the IMU data can be improved as well. Currently, the distance tracking is only calculated in a 2D plane without considering the course of the data along the z-axis (in camera frame). This z-component must remain the same while tracking the wheelchair user which is a further restriction for the derived movement data. In addition, more IMU sensors could be used to track one person which would create more restrictions for tracking by considering the relation of the sensors to each other and maximum values for velocity or acceleration.

To ensure the future use of the developed **software framework** by other research groups improved usability would be beneficial. Therefore, manual steps should be automated and data requirements should be attenuated. Especially, the detection of standstill phases for orientation initialization and the identification of straight movements for alignment of the data should be able to run automatically. Furthermore, the condition that the z-axis of the IMU must be aligned with the vector of the pedestrian's movement direction should be eliminated. Based on the provided IMU and camera data of a person the axis pointing in the movement direction could be extracted by the software. Also, backwards tracking methods should be implemented so that tracking data before actual standstill phases can be provided. For an easier assignment of camera and IMU data sets an integration of the software framework for IMU data processing in the PeTrack software which realizes the camera tracking would be very useful. Once these processes are automatized or adapted the tracking system and its software can be used for a high number of IMUs with less effort for data extraction.

Besides extensions and improvements of the framework, an **advanced analysis** of individual movements with **modified data capturing** is promising. As the studies on rotation of the upper body in bottlenecks have shown, the definition of rotation should be refined. In this work, the rotation of the upper body was interpreted as the rotation of the axis between participants' shoulders. As a result, asymmetric movements could not be analyzed in-depth but are important when it comes to the analysis of individual spatial requirements. For future experiments, the attachment of the sensors on both shoulder blades might solve this issue providing more precise

information about the movement of the upper body. Furthermore, capturing movement data of other body parts would allow an extended analysis e.g., rotation of the hips or detection of stumbling. The tracking system and its distance calculation methods can also be transferred to walking persons. For this purpose, corresponding limitations of the movement given by biomechanical models can be taken into account.

For future large-scale experiments, the use of inertial sensors integrated in the participants' smartphones could be considered for data capturing. Since many smartphones already contain IMUs those could be utilized to capture additional movement data without purchasing additional technical equipment. The smartphones could be attached with a chest belt to the upper body of the participants. The developed framework can be used to reconstruct the twist angles. For this purpose, high effort must be put into a system for collecting the IMU data of each person e.g., via a mobile application and to process several IMU data formats of the different smartphones.

Appendix A

List of Commerical IMU Systems

Due to the various application types of inertial sensors, many different companies are offering IMU systems. In the following, products that were found during the research are listed.

Manufacturers of **basic IMU sensors**:

- SABEL
  `https://sabellabs.com/sense/`
- Shimmer
  `http://www.shimmersensing.com/products/development-kits/`
- X-io
  `http://x-io.co.uk/ngimu/`
- EXEL
  `https://www.exel.tech/product/exl-s3-sensore-inerziale-bluetooth/`
- InertialElements
  `http://www.inertialelements.com/productpage.html`
- Inertia
  `http://inertia-technology.com/product/motion-capture-promove-mini`
- eliko
  `https://www.eliko.ee/products/inertial-motion-capture-system/`
- Vicon
  `https://www.vicon.com/hardware/blue-trident/`

- Noraxon
  https://www.noraxon.com/our-products/myomotion/

Manufacturers of **Full Motion Capturing IMU Systems** that also provide tracking software:

- Stt-Systems
  http://www.stt-systems.com/products/inertial-motion-capture/isen/
- Xsens
  https://www.xsens.com/products/xsens-mvn/
- Technaid
  https://www.technaid.com/products/motion-capture-system-tech-mcs-hub-imu/
- NexGen Ergonomics
  http://www.nexgenergo.com/ergonomics/I2M.html
- Perception Neuron
  https://www.neuronmocap.com
- Shadow
  https://www.motionshadow.com
- InertialLabs
  https://inertiallabs.com/3dsuit.html
- NANSENSE
  https://www.nansense.com/suits/
- AIQ-Synertial
  https://www.synertial.com
- APDM (without tracking software)
  http://www.apdm.com/wearable-sensors/

Please note that the URLs listed above were last checked for validity on the 3rd of May 2021.

Appendix B

Framework Usage and Extension

B.1 Preparatory Work and Requirements

For the fusion of camera and IMU data, the following manual steps need to be performed to prepare the run configuration files:

1. If synchronization is done via LED signal: Extract corresponding time codes from camera recordings
2. If synchronization is done via movement: Extract camera frames and IMU samples for synchronization by visual inspection of the data
3. Assign PeTrack ID(s) and IMU ID(s) by visual inspection of the video recordings
4. Search for start and end frame of a straight walking part by visual inspection of the camera trajectories
5. Verify the steady phase at the beginning for the initialization of heading calculation and choose an offset for IMU data if required

To ensure correct processing steps the IMU and camera data must be provided in right-handed coordinate systems. Besides, the local z-axis of the IMU is supposed to point to the movement direction when applying distance tracking approaches. In case of rotation tracking only, the IMU must be mounted to the pedestrian so that its local x-axis is vertically oriented.

B.2 Configuration Files

For executing the software, two configuration files must be provided. One file must contain IMU and camera-specific information for each run and the second file must provide algorithm parameters. The `configparser` module is used for reading in the configuration information which allows a simple definition and processing of these parameters. Listings B.1 and B.2 show the basic format of the files followed by a description of the parameters. The order of the parameters can be varied. If additional input parameters are needed they can be easily added using the presented format.

Listing B.1: Format of the initialization file containing the information about camera- and IMU-specific data for one data set to analyze (for one run). Information for several IMUs can be listed here.

```
[CameraData]
RunStart = HH:MM:SS:FF
RunEnd = HH:MM:SS:FF
File = Path/To/Trajectories.txt
Fps = XX

[IMUname 1]
File = Path/To/IMUdata.csv
StickerID = XX
CameraID = XX
PusherID = XX
SteadyStart = SampleXX
SteadyEnd = SampleXX
AlignmentStart = FrameXX
AlignmentEnd = FrameXX
Offset = SampleXX
Position = "Information about attachment"
Comment = "Sensor specific comment"

[IMUname 2]
...
```

For the camera data the following information is required:

Run Start/End Time codes that specify the start and end of the camera data set. These time codes are considered as ground truth and are used for scaling the IMU data samples.

File File of the camera trajectory data.

Fps Frame rate at which the camera data were recorded.

For several IMUs these parameters must be defined:

File File name containing the IMU data.

CameraID ID of the person wearing the IMU provided by the camera system.

PusherID ID of the pushing person provided by the camera system which is required for distance tracking with correction.

Alignment Start/End Frames defining the start and end of the alignment phase for which the pedestrian is moving straight without changing the movement direction.

Offset Number of IMU samples that are skipped before heading initialization is calculated.

These parameters are optional per IMU data set:

StickerID Parameter for documentation of the label on the shoulders to identify the person wearing the IMU (described in Sec. 2.2.1).

Steady Start/End Parameters for defining the sample range of a steady state that can be used for removing IMU bias noise.

Position Parameter for documentation of the attachment position of the sensor.

Comment Parameter for documentation of specific observations.

Listing B.2: Format of the initialization file containing the information about the parameters for the tracking algorithms.

```
[Algorithm]
Rotation = Madgwick
Distance = DoubleIntegration/DoubleIntegrationCorrection/
           DoubleIntegrationAdaptiveCorrection/
           MAUKF2D/MAUKF2DCorrection/MAUKF2DAdaptiveCorrection
VelocitySmoothRange = XX
VelocityDiffSurrounding = YY
ConvergenceTime = SampleXX
TrackingStart = SampleXX
TrackingEnd = SampleXX
OutputFileEnding = "_specific_file_ending"
```

Rotation Approach that is used for calculating the rotation of the IMU. Currently, only `Madgwick` is available.

Distance Approach that is used for calculating the distance. The different options are listed above.

Velocity SmoothRange Number of frames that are considered in the past and future to calculate a smoothed velocity. In this work, this value was set to 12 for recordings with a frame rate of 25. Thus, positions 12 frames before and after the current frame are chosen which corresponds to an averaging over one second.

Velocity DiffSurrounding Difference in velocity (in $\mathrm{m\,s^{-1}}$) that is acceptable when comparing the velocity of the tracked person and the surrounding person (see $\boldsymbol{v}_{\mathrm{range}}$ in Eq. 3.44). After analyzing the recorded data this value was set to $0.12\,\mathrm{m\,s^{-1}}$ as described in Sec. 3.3.2.2.

Convergence Time Number of IMU samples that are required for the initialization phase for the heading calculation. In this work, this value was set to 200 samples which is equal to a period of 2 s at a sample rate of 100.

Tracking Start/End Range of IMU samples for which tracking methods should be applied. This is useful when tracking should not be applied for a whole run or independent of camera time codes.

Output FileEnding Ending of file names generated by `Plotter` and `Analysis`.

B.3 Using the Classes

An example of the basic usage of the python classes is shown in Listing B.3. The `configparser` is used to read in the required parameters. Static functions of the `DataAccessManager` class are used to get a synchronized and scaled IMU sample range to read in the corresponding IMU data. After creating a `PeTrackDatabase` object an `ImuCameraTracker` is instantiated. Based on the algorithm configuration file the corresponding options are set in the tracker. As a fusion of camera and IMU data is desired in that example the required parameters are set. The orientation is

calculated for a specified range and the twist angles are determined with the help of the `Analysis` class.

Listing B.3: Pseudo code for calculating twist angles based on SABEL IMU data and camera data extracted with PeTrack.

```
# open inifiles with run and algorithm configurations
run_data_config = configparser.ConfigParser()
run_data_config.read('Path/To/run_inifile.ini')
algo_config = configparser.ConfigParser()
algo_config.read('Path/To/algo_inifile.ini')

# read in data from ini files
imu_file = run_data_config[sensor_name]['File']
...

# provide list of recorded camera sync times
camera_sync_times = ['time_code_1', 'time_code_2', ...]

# get corresponding range of imu samples
sample_range_imu = DataAccessManager.get_imu_run_range(
    imu_file, run_range, camera_sync_times)
# read in IMU data for that range
imu_data = SabelImuData(imu_file, sample_range_imu, ...)

# create PeTrack database
petrack_database = PeTrackDatabase(petrack_file, ...)

# create IMU Tracker
imu_tracker = ImuCameraTracker(algo_config, [imu_data],
    petrack_database)
# set PeTrackID and aligment data for fusion
imu_tracker.set_fusion_data([ground_truth_ID])
imu_tracker.set_alignment_frames([alignment_start,
    alignment_end])

# calc orientation from start to end of the ground truth
    trajectory
imu_tracker.calc_orientation([start, end], 0)

# calculate twist angles
[angle_diff, ...] = Analysis.calculate_rotation_diff(
    imu_tracker)
Analysis.write_angles_to_file("Path/To/Outputfile.txt",
    angle_diff, ...)
```

Appendix C

Supplementary Material for SiME Studies

C.1 Documentation of Analyzed Data Sets

IMU and camera data that have been used for validating the distance tracking methods are accessible via [133]. Trajectory information extracted from the central 4k camera has been used. Overall, data of 8 runs of the study "Bot_whe" were analyzed where the movement in front of a bottleneck with different widths was recorded. The analysis was limited to data of wheelchair users who were pushed by another person so that the correction methods could be applied. Therefore, the analysis was conducted for the data of four different wheelchair users each equipped with two sensors on the backrest. According to the documentation in [133] the PWD_IDs of the wheelchair users whose data have been analyzed for validation are listed in Table C.1.

Table C.1: Overview of validated SiME data sets. The different tracking approaches and the corresponding PWD_IDs of participants according to [133] whose data were used for validation are listed.

Distance tracking approach	PWD_IDs	Overall quantity
Integration Integration with correction Integration with adaptive correction	34, 35, 38, 39	54
MAUKF MAUKF with correction MAUKF with adaptive correction	34, 35, 39	23

The data of one sensor of the participant with PWD_ID = 38 needed to be excluded from analysis since the synchronization signal was not received. Besides a wheelchair user was moving on their own without a pusher for one run that was also excluded from the analysis (run0501, PWD_ID = 80). This results in 54 different data sets for validating tracking techniques with one sensor and 23 available data sets for testing tracking approaches with fusion of two sensors.

C.2 Raw IMU Data

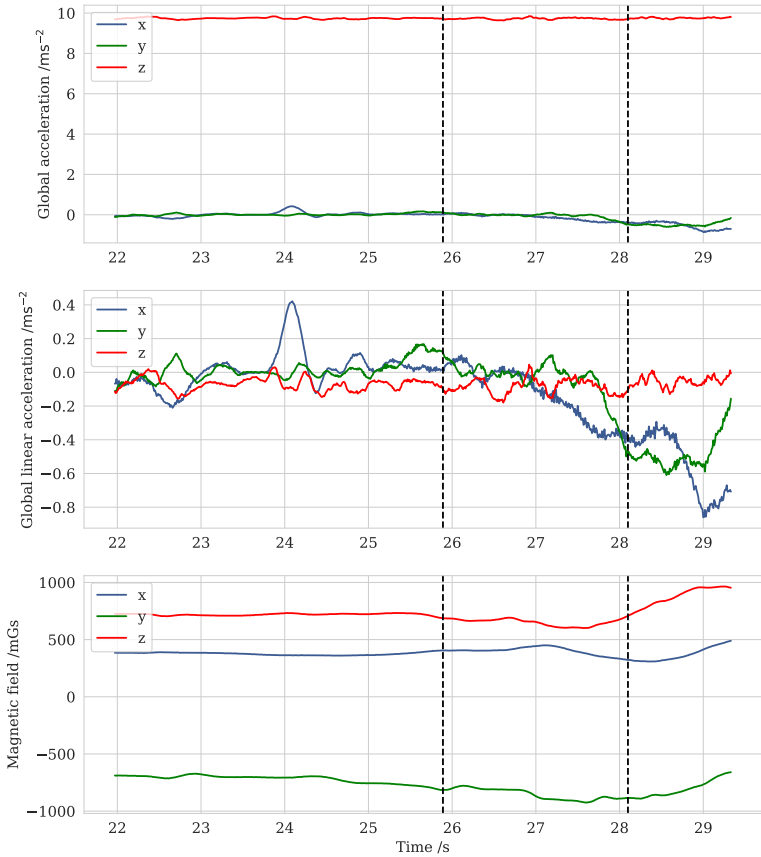

Figure C.1: Unprocessed measurements of the accelerometer (top), acceleration data without gravity (middle), and magnetometer measurements (bottom) in local reference frame I. Vertical lines represent timestamps according to the data shown in Fig. 5.1. Corresponding gyroscope data are part of Fig. 5.1b.

Appendix D

Supplementary Material for Optitrack Studies

D.1 Calculated Angles

For a better evaluation of the heading errors presented in Sec. 5.2, the actual angle values are provided in the following. Data for the wheelchair scenarios are shown in Fig. D.1 and D.2. Angles for the rotation of the upper body are presented in Fig. D.3 and D.4.

According to Fig. 5.9 the angle α represents the angle of the body or wheelchair axis (ground truth) while β represents the calculated axis based on IMU data. Both angles are calculated with reference to the positive x-axis in the camera reference frame. As the participant started to move in the direction of the negative x-axis, high angles occurred as start values. Please note that the course of angles is presented in a steady form to prevent fluctuations between the values 0° and 360° (and vice versa). Thus, the angles can reach values outside the range of [0°, 360°]. The start of the different runs according to Fig. 2.7 is marked with vertical lines.

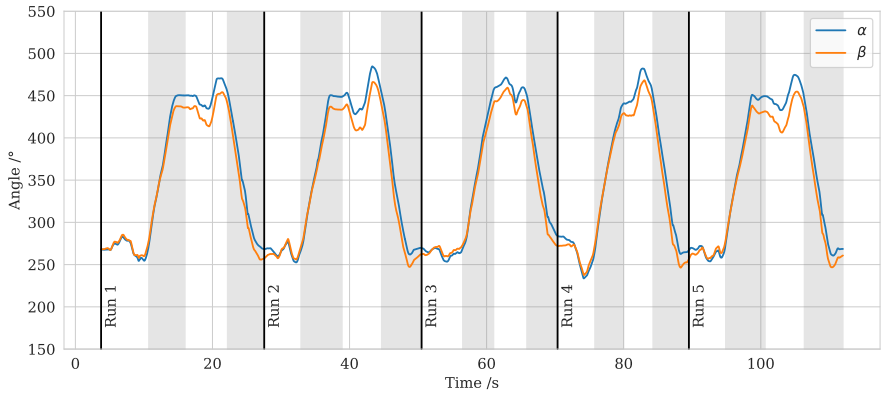

(a) Data for upper sensor

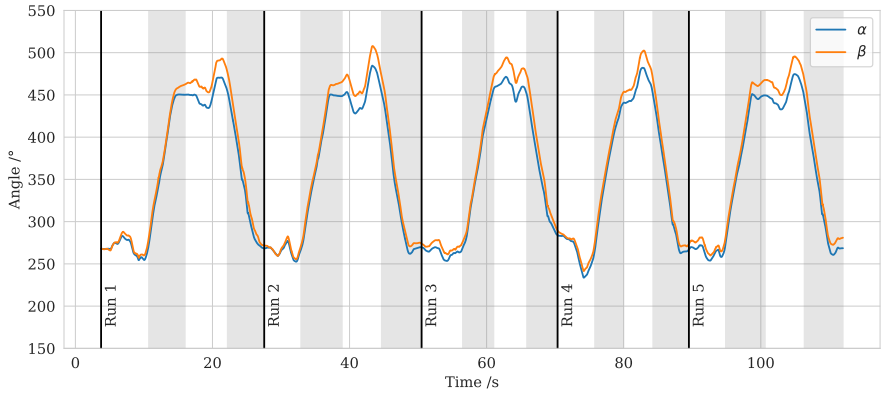

(b) Data for lower sensor

Figure D.1: Course of angles for the wheelchair moved with arms. Periods for 180° turns are marked in grey. Greater differences between the angles are visible when moving back to the start area. The corresponding difference between the angles is shown in Fig. 5.12.

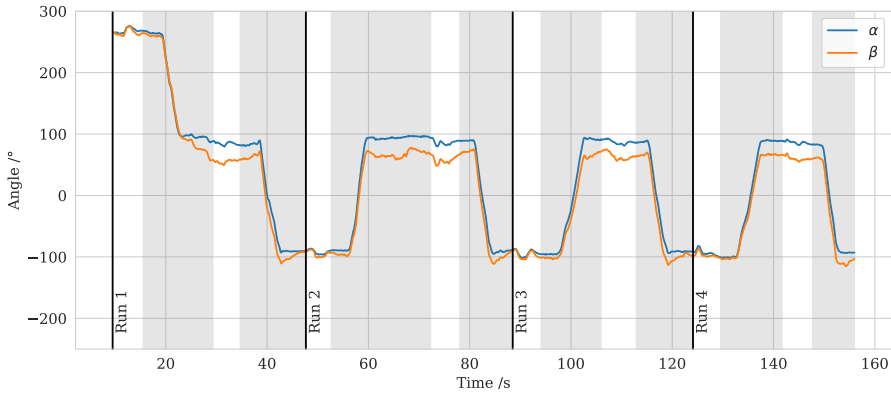

(a) Data for upper sensor

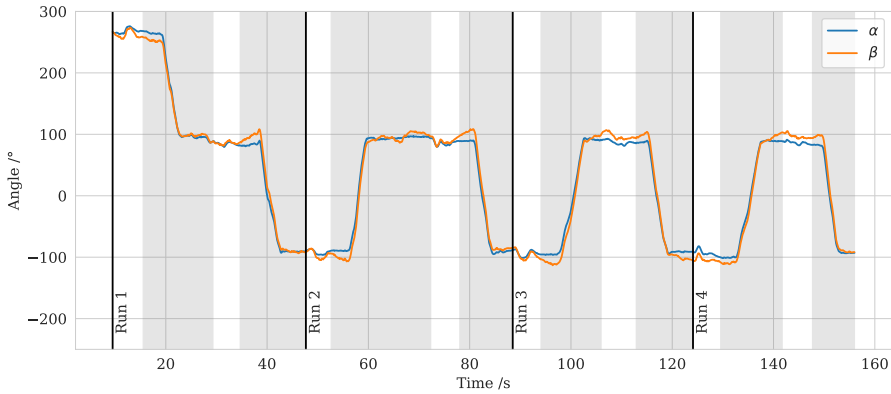

(b) Data for lower sensor

Figure D.2: Course of angles for the wheelchair moved with feet. Periods for 180° turns are marked in grey. Greater differences between the angles are visible when moving back to the start area. The corresponding difference between the angles is shown in Fig. D.5.

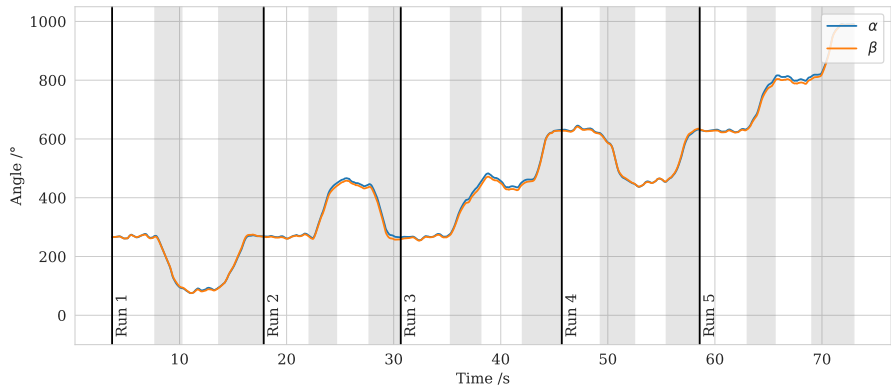

(a) Data for walking

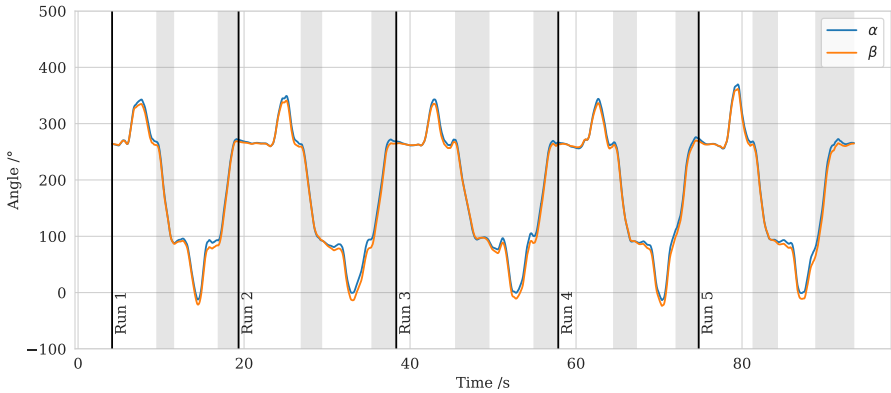

(b) Data for walking with strong rotation

Figure D.3: Course of angles for the rotation of the upper body for the walking scenarios. Periods for 180° turns are marked in grey. The corresponding difference between the angles is shown in Fig. 5.16 and D.6.

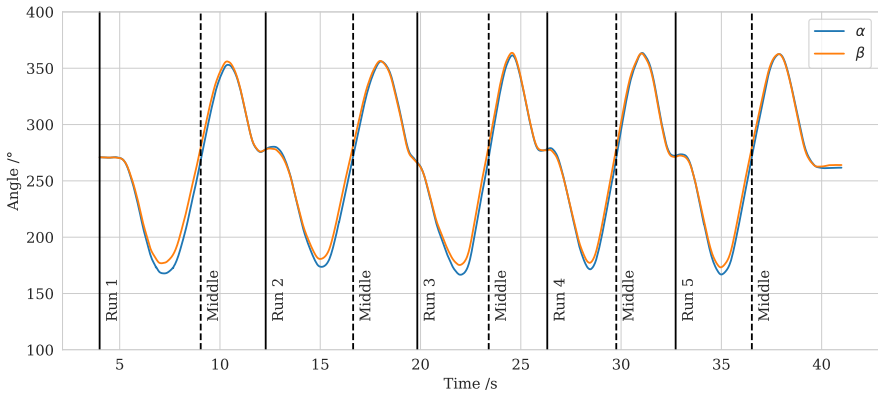

Figure D.4: Course of angles for the rotation of the upper body while standing on a fixed position. Time of passing the initial position when rotating from the right to the left side and at which the shoulder axis is parallel to initial shoulder axis are marked with the dashed lines. The corresponding difference between the angles is shown in Fig. 5.14.

D.2 Error in Heading

In the following, the course of the difference between angles of the ground truth axis and the local y-axis is shown. Data for the studies with a wheelchair user that moved with their feet are presented in Fig. D.5. As the person moving the wheelchair was not familiar with using it, turning the wheelchair required a lot of time and shows fluctuations of the error because the sensor was affected by local movements. The error for strong rotations while walking are presented in Fig. D.6.

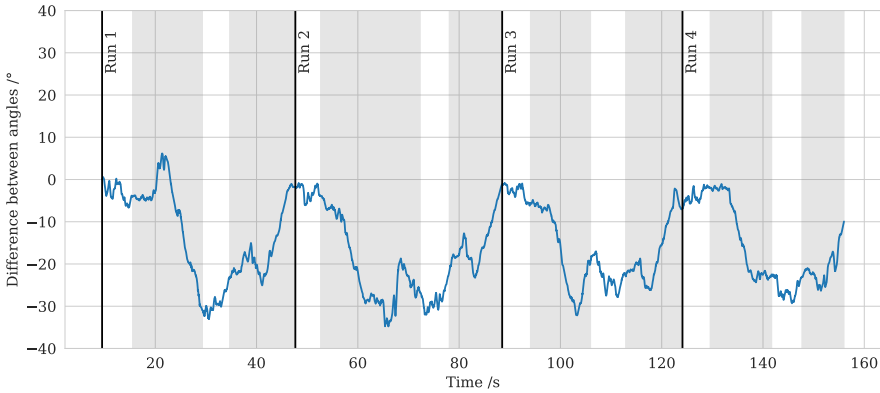

(a) Data for upper sensor

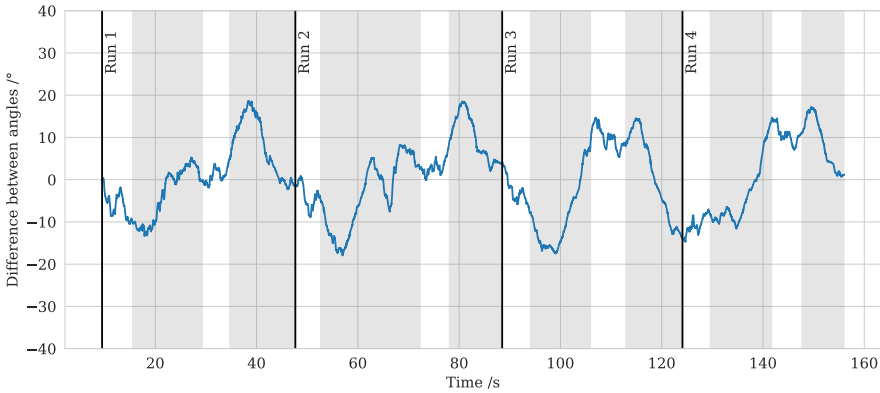

(b) Data for lower sensor

Figure D.5: Course of error in heading for the wheelchair user who moved with the feet.

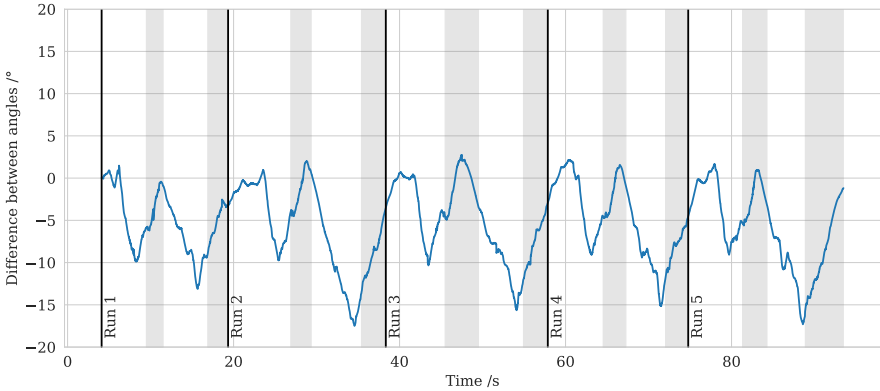

Figure D.6: Course of error in heading for the crowd walking scenario.

Appendix E

Supplementary Material for Studies on Twist Angle

E.1 Synchronization

Usually, the synchronization of IMU and camera data is done with the help of an LED signal emitted before the start and after finishing the experiments. Unfortunately, the synchronization signals were missing in the IMU data sets or could not be seen in the camera recordings. For this reason, the first and last heel drop was searched in the IMU and camera data. All used inertial sensors recorded the same amount of samples which means that the same scaling factor could be assumed for all data sets. Therefore, the heel drops were searched for one person only for whom the movement was clearly visible (in this case participant wearing device D7). In this way, the scaling factor $S = 323074/322412$ (see Eq. 3.35) was calculated and used to align frames and samples for each run for each pair of IMU and camera data.

E.2 Classification of IMU Data Sets

To ensure that only reasonable rotation data were considered for the analysis of the twist angle, the calculated acceleration data have been checked manually. For this purpose, the global acceleration (with gravity) and the global linear acceleration (without gravity) have been calculated for each person for each run.

Inspecting the global acceleration is a quick and easy approach to estimate how well the rotation could be calculated. Instead of a time-consuming visual comparison of the videos and corresponding calculated twist angles, the acceleration data of each person in standstill (before entering the bottleneck) were inspected. If the rotation calculation procedure worked well, the global acceleration while standing still should

measure the global gravity $\boldsymbol{g}$ only. When rotating the local acceleration data (with the calculated quaternions) to the camera frame, the global acceleration data ${}^{C}\boldsymbol{a}$ should be equal to $\boldsymbol{g}$ while the person is standing still. Therefore, the angle ϵ between ${}^{C}\boldsymbol{a}$ and $\boldsymbol{g}$ as defined in Eq. E.1 is used as a measure for the quality of the rotation calculation. If the orientation of the sensor could not be determined well, the gravitational force was spread over the global x-, y- and z-axis leading to a bigger ϵ.

$$\epsilon = \angle({}^{C}\boldsymbol{a}, \boldsymbol{g}) = \angle({}^{C}\begin{pmatrix} a_x \\ a_y \\ a_z \end{pmatrix}, \begin{pmatrix} 0 \\ 0 \\ 9.81 \end{pmatrix}) \tag{E.1}$$

The time for the standstill phases (before the entrance phase started) were searched manually for each run. Besides, the global linear acceleration has been looked at to verify the actual acceleration (due to movement) on a better scale. While standing still all components (x, y, and z) should be steady without any rotation. If the rotated acceleration data were changing it is indicated that there were problems with calculating the rotation. Hereby, a faulty rotation could be the result of a too short initialization phase (no convergence) or faulty sensor data e.g., gyroscope offset.

The occurred error was traced back to the following possible reasons:

- Too loose attachment of the sensors caused local movements of the sensors.
- No clear standstill of the upper body led to an insufficient initialization phase.
- Technical issues of the sensors caused a gyroscope offset.
- Heat development (especially for sensors worn beneath clothes) could have caused higher noise in data.

Due to these sources of errors the data sets of both sensors for each person for each run were checked manually and divided into the following classes:

- Good: $\epsilon \leq 2°$ and steady global acceleration while standing still
- Acceptable: $\epsilon \leq 18°$ and steady right before the movement through the bottleneck begins
- Unusable: $\epsilon > 18°$ or not steady before movement through bottleneck

In the following, examples of good (see Fig. E.1), acceptable (see Fig. E.2), and unusable IMU data (see Fig. E.3 and E.4) are listed. A data set can be unusable even when a small ϵ was calculated since gravity can be measured perfectly for one time step but with a rotation before or after as shown in Fig. E.3.

The classification for each data set is given in Table E.1 and E.2 according to the data documentation in [152]. The actually selected data sets that were used for the analysis in Chapter 6 are listed in Table E.3 and E.4.

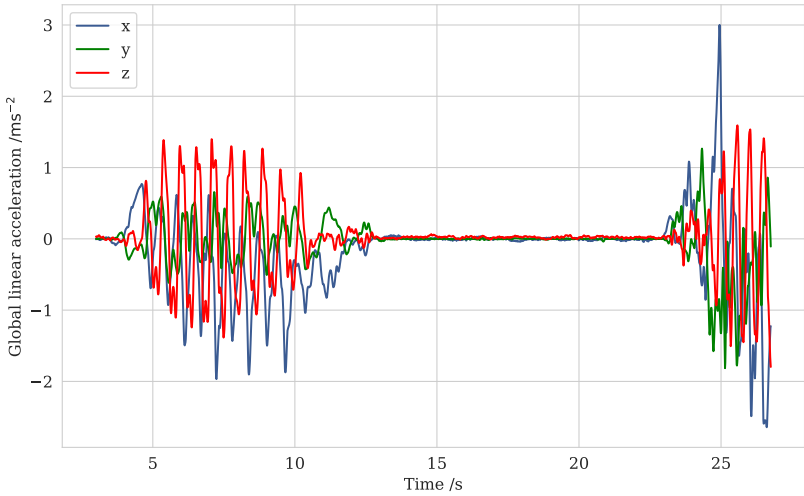

Figure E.1: Example of IMU data classified as good. The first part from t = 5 s to 10 s was recorded during the preparation phase which is followed by a standstill and the start of the entrance phase around t = 23 s.

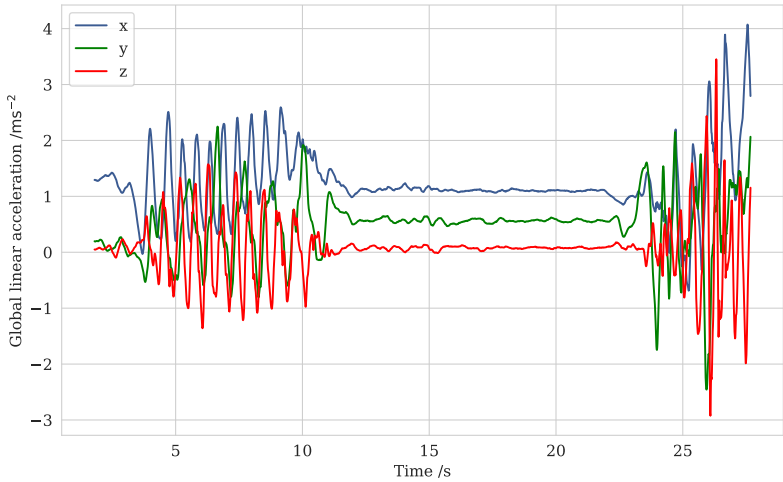

(a) Data remain the same while standstill but with an offset which is caused by a slight (calculated) misalignment of the orientation

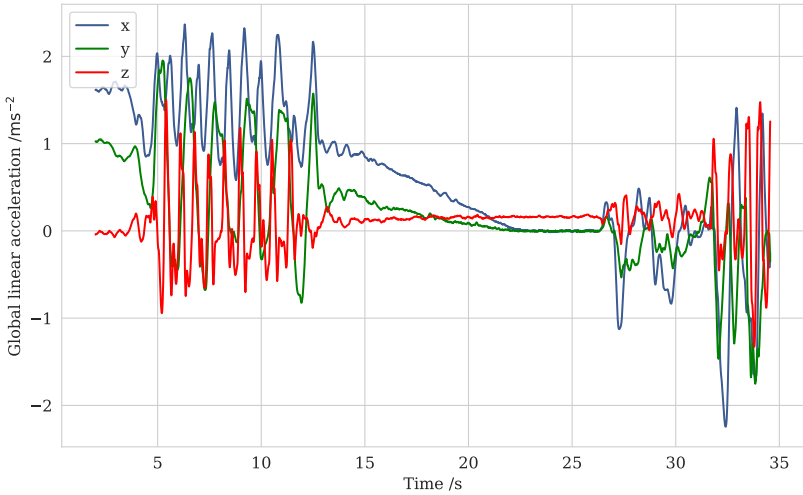

(b) Convergence was not reached after the first standstill but before the entrance phase started

Figure E.2: Examples of acceptable IMU data.

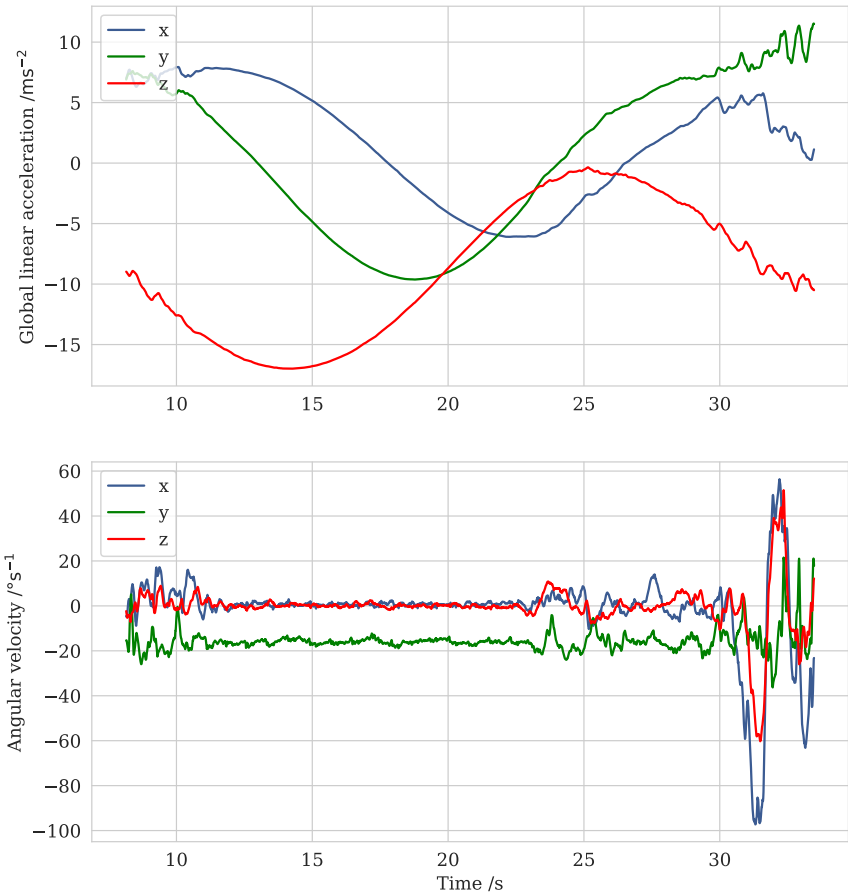

Figure E.3: Example of unusable IMU data. There is an offset in the gyroscope data (y-axis) which leads to a permanent rotation of the acceleration data.

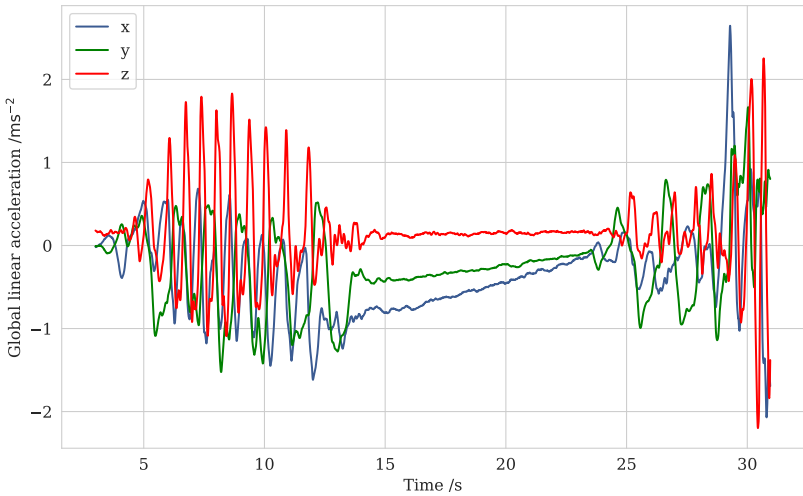

(a) Convergence not finished before the entrance phase started

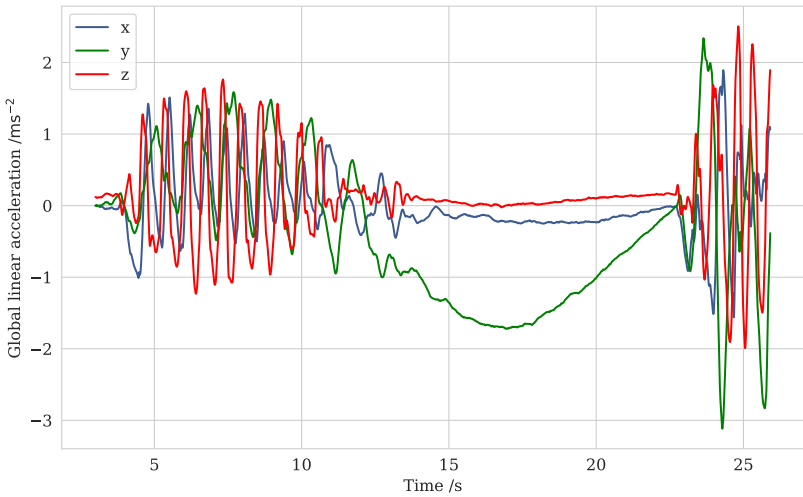

(b) Rotation while standstill

Figure E.4: Examples of unusable IMU data due to insufficient convergence of the orientation filter.

Table E.1: Classification of sensor data based on the achieved rotation tracking quality. Data for runs with $N = 25$ are shown.

Run	Good	Acceptable	Unusable
100_N25_h-_R1	D1, D4, D9, D11, D12, D14, D16, D18	D7, D13, D17, D19	D8, D10
100_N25_h-_R2	D1, D4, D9, D11, D12, D16, D17, D18	D7, D10, D13, D14, D19	D8
100_N25_h0_R1	D1, D4, D9, D12, D17, D18, D16	D7, D10, D11, D14	D8, D13, D19
100_N25_h0_R2	D1, D4, D9, D14, D16, D17, D18	D7, D10, D12, D13, D19	D8, D11
090_N25_h-_R1	D1, D4, D9, D11, D12, D14, D17, D18, D19	D7, D10, D13, D16	D8
090_N25_h-_R2	D4, D9, D11, D12, D14, D18, D19	D1, D13, D17	D7, D8, D10, D16
090_N25_h0_R1	D1, D4, D9, D12, D17, D18, D19	D10, D11, D13	D7, D8, D16
090_N25_h0_R2	D1, D4, D9, D11, D12, D14, D17, D18	D7, D10, D13, D19	D8, D16
080_N25_h-_R1	D1, D4, D9, D12, D17, D18	D10, D11, D13, D14, D19	D7, D8, D16
080_N25_h-_R2	D1, D4, D9, D11, D12, D14, D18	D7, D10, D13, D19	D8, D16, D17
080_N25_h0_R1	D1, D4, D9, D12, D14, D17, D18	D10, D11, D13, D19	D7, D8, D16
080_N25_h0_R2	D1, D4, D9, D14, D17, D18	D7, D10, D11, D12, D13, D16, D19	D8
070_N25_h-_R1	D1, D4, D9, D12, D14, D17, D18	D13, D16, D19	D7, D8, D10, D11
070_N25_h-_R2	D9, D12, D14, D17, D18	D1, D4, D13, D19	D7, D8, D10, D11, D16
070_N25_h0_R1	D1, D4, D9, D12, D14, D16, D17, D18	D7, D10, D11, D13, D19	D8
070_N25_h0_R2	D1, D4, D9, D11, D12, D16, D17, D18, D19	D7, D10, D13, D14	D8

Table E.2: Classification of sensor data based on the achieved rotation tracking quality. Data for runs with $N = 8$ are shown.

Run	Good	Acceptable	Unusable
070_N08_h-_R1	D4, D9, D12, D18	D1, D7, D10, D11, D13, D19	D8, D14, D16, D17
070_N08_h-_R2	D1, D4, D9, D12, D18	D10, D11, D13, D16, D17	D7, D8, D14, D19
070_N08_h0_R1	D1, D9, D12, D14, D17, D18	D4, D7, D11, D13, D16	D8, D10, D19
070_N08_h0_R2	D1, D4, D9, D12, D17, D18	D10, D14	D7, D8, D11, D13, D16, D19
060_N08_h-_R1	D1, D4, D9, D12, D17, D18, D19	D7, D10, D11, D13, D14	D8, D16
060_N08_h-_R2	D4, D9, D12, D17, D18	D1, D10, D11, D13, D14, D16	D7, D8, D19
060_N08_h0_R1	D4, D9, D12, D17, D18	D1, D7 D10, D11, D13, D16,	D8, D14, D19
060_N08_h0_R2	D9, D1, D4, D12, D14, D17, D18	D7, D10, D13, D16	D8, D11, D19
050_N08_h-_R1	D4, D9, D11, D12, D17, D18	D1, D7, D10, D13, D14, D16	D8, D19
050_N08_h-_R2	D4, D9, D10, D12, D18	D7, D14, D16, D17	D1, D8, D11, D13, D19
050_N08_h0_R1	D4, D9, D12, D17, D18	D7, D10, D13, D14	D1, D8, D11, D16, D19
050_N08_h0_R2	D1, D4, D9, D12, D19	D7, D10, D13, D16, D17, D18	D8, D11, D14
040_N08_h-_R1	D4, D9, D11, D12, D17, D18	D1, D7, D10, D13, D14, D16	D8, D19
040_N08_h-_R2	D4, D9, D12, D18	D7, D10, D14, D16, D19	D8, D11, D13, D17
040_N08_h0_R1	D4, D9, D12, D18, D19	D7, D13	D1, D8, D10, D11, D14, D16
040_N08_h0_R2	D4, D9, D12, D14, D17, D18	D7, D10, D13, D16	D1, D8, D11, D19

Table E.3: List of devices per run whose data have been used for twist angle calculation. Information for runs with $N = 25$ is shown.

Run	Considered devices
100_N25_h-_R1	D1, D7, D9, D11, D12, D14, D18
100_N25_h-_R2	D1, D7, D11, D12, D14, D16, D18
100_N25_h0_R1	D1, D7, D9, D11, D12, D14, D18
100_N25_h0_R2	D1, D7, D9, D10, D12, D14, D17
090_N25_h-_R1	D1, D9, D11, D12, D17, D19
090_N25_h-_R2	D4, D9, D11, D12, D18, D19
090_N25_h0_R1	D1, D9, D11, D12, D17, D19
090_N25_h0_R2	D4, D7, D9, D11, D12, D14, D17
080_N25_h-_R1	D4, D9, D11, D12, D18, D19
080_N25_h-_R2	D1, D7, D9, D11, D12, D18, D19
080_N25_h0_R1	D1, D9, D11, D12, D14, D18
080_N25_h0_R2	D1, D7, D9, D11, D12, D14, D17
070_N25_h-_R1	D4, D9, D13, D14, D17
070_N25_h-_R2	D1, D9, D13, D14, D17
070_N25_h0_R1	D1, D7, D11, D12, D14, D16, D18
070_N25_h0_R2	D4, D7, D11, D12, D16, D17, D19

Table E.4: List of devices per run whose data have been used for twist angle calculation. Information for runs with $N = 8$ is shown.

Run	Considered devices
070_N08_h-_R1	D4, D7, D9, D11, D12, D18, D19
070_N08_h-_R2	D1, D9, D11, D12, D18
070_N08_h0_R1	D1, D7, D9, D11, D12, D14, D18
070_N08_h0_R2	D4, D9, D10, D12, D14, D17
060_N08_h-_R1	D1, D7, D9, D11, D12, D17, D19
060_N08_h-_R2	D4, D9, D11, D12, D14, D17
060_N08_h0_R1	D4, D7, D9, D11, D12, D17
060_N08_h0_R2	D1, D7, D9, D10, D12, D14, D17
050_N08_h-_R1	D4, D7, D9, D11, D12, D14, D17
050_N08_h-_R2	D4, D7, D9, D10, D12, D14, D18
050_N08_h0_R1	D4, D7, D9, D10, D12, D14, D17
050_N08_h0_R2	D1, D7, D9, D10, D12, D17, D19
040_N08_h-_R1	D1, D7, D9, D11, D12, D14, D18
040_N08_h-_R2	D7, D9, D10, D12, D14, D18, D19
040_N08_h0_R1	D4, D7, D9, D12, D18, D19
040_N08_h0_R2	D4, D7, D9, D10, D12, D14, D17

Appendix F

Publications

The benefits of IMUs and the **hybrid tracking system** are introduced in:

- Maik Boltes, Jette Schumann and Daniel Salden. "Gathering of data under laboratory conditions for the deep analysis of pedestrian dynamics in crowds". In: *2017 14th IEEE International Conference on Advanced Video and Signal Based Surveillance (AVSS)*. 2017. DOI: 10.1109/AVSS.2017.8078471
- Jette Schumann and Maik Boltes. "Tracking of wheelchair users in dense crowds". In: *2017 International Conference on Indoor Positioning and Indoor Navigation (IPIN)*. 2017
- Jette Schumann, Maik Boltes and Armin Seyfried. "Hybrid Tracking System for Pedestrians in Dense Crowds". In: *Traffic and Granular Flow '17*. Ed. by Hamdar S. H. 2019. DOI: 10.1007/978-3-030-11440-4_23

The following **data publications** provide trajectory and IMU data captured in the studies presented in this thesis:

- Forschungszentrum Jülich and Federal Institute for Materials Research and Testing. *Influence of individual characteristics*. 2017. DOI: 10.34735/PED.2017.1
- Jette Schumann, Maik Boltes and James Lee. *Studies for validating tracking algorithms based on IMU data with 3D camera data*. 2018. DOI: 10.34735/PED.2018.3
- Jette Schumann, Maik Boltes, Juliane Adrian et al. *Studies on rotation of the upper body in bottlenecks using a hybrid tracking system*. 2018. DOI: 10.34735/PED.2018.4

Besides, work on the **analysis of pedestrian streams** was published. The need for considering aspects of **social psychology** is demonstrated based on the analysis of an experiment with a crowd entering a concert with two different spatial barrier structures in:

- Anna Sieben, Jette Schumann and Armin Seyfried. "Collective phenomena in crowds—Where pedestrian dynamics need social psychology". In: *PLOS ONE* 12.6 (June 2017). Ed. by Dante R. Chialvo, e0177328. DOI: 10.1371/journal.pone.0177328

Within the scope of the SiME project properties of the movement of crowds considering **people with disabilities** are determined and analyzed in:

- Paul Geoerg, Robert Malte Polzin, Jette Schumann et al. "Small-scale Studies on Evacuation Characteristics of Pedestrians with physical, mental or age-related Disabilities". In: *Journal of Physics: Conference Series* 1107 (Nov. 2018), p. 072006. DOI: 10.1088/1742-6596/1107/7/072006
- Paul Geoerg, Jette Schumann, Stefan Holl et al. "The Influence of Wheelchair Users on Movement in a Bottleneck and a Corridor". In: *Journal of Advanced Transportation* 2019 (June 2019), pp. 1–17. DOI: 10.1155/2019/9717208
- Paul Geoerg, Jette Schumann, Maik Boltes et al. "The Influence of Individual Impairments on Crowd Dynamics". In: *INTERFLAM 2019*. Ed. by Stephen Grayson. London: Interscience Communications, 2019, pp. 775–791
- Paul Geoerg, Jette Schumann, Stefan Holl et al. "The influence of individual impairments in crowd dynamics". In: *Fire and Materials* (Feb. 2020). DOI: 10.1002/fam.2789
- Paul Geoerg, Jette Schumann, Maik Boltes et al. "The influence of physical and mental constraints to a stream of people through a bottleneck". In: *Proceedings of Pedestrian and Evacuation Dynamics 2018, PED18, Lund, Sweden, Collective dynamics* 5 (2020). DOI: 10.17815/cd.2020.57

References

[1] Maik Boltes, Jun Zhang, Antoine Tordeux et al. "Empirical Results of Pedestrian and Evacuation Dynamics". In: *Encyclopedia of Complexity and Systems Science*. Ed. by Robert A. Meyers. Berlin, Heidelberg: Springer Berlin Heidelberg, 2018, pp. 1–29. ISBN: 978-3-642-27737-5. DOI: 10.1007/978-3-642-27737-5_706-1 (cit. on p. 1).

[2] Maik Boltes and Armin Seyfried. "Collecting Pedestrian Trajectories". In: *Neurocomputing, Special Issue on Behaviours in Video* 100 (2013), pp. 127–133. ISSN: 0925-2312. DOI: 10.1016/j.neucom.2012.01.036 (cit. on pp. 1, 4, 16).

[3] Xiaomeng Shi, Zhirui Ye, Nirajan Shiwakoti et al. "A State-of-the-Art Review on Empirical Data Collection for External Governed Pedestrians Complex Movement". In: *Journal of Advanced Transportation* 2018 (2018), p. 1063043. DOI: 10.1155/2018/1063043 (cit. on p. 1).

[4] Milad Haghani. "Empirical methods in pedestrian, crowd and evacuation dynamics: Part I. Experimental methods and emerging topics". In: *Safety Science* 129 (Sept. 2020), p. 104743. DOI: 10.1016/j.ssci.2020.104743 (cit. on pp. 1, 2).

[5] Milad Haghani. "Empirical methods in pedestrian, crowd and evacuation dynamics: Part II. Field methods and controversial topics". In: *Safety Science* 129 (Sept. 2020), p. 104760. DOI: 10.1016/j.ssci.2020.104760 (cit. on p. 1).

[6] Armin Seyfried, Maik Boltes, Jens Kähler et al. "Enhanced empirical data for the fundamental diagram and the flow through bottlenecks". In: *Pedestrian and Evacuation Dynamics 2008*. Ed. by Wolfram W. F. Klingsch, Christian Rogsch, Andreas Schadschneider et al. Springer Berlin Heidelberg, 2010, pp. 145–156. DOI: 10.1007/978-3-642-04504-2_11 (cit. on p. 1).

[7] Andreas Schadschneider and Armin Seyfried. "Empirical results for pedestrian dynamics and their implications for modeling". In: *Networks and Heterogeneous Media* 6.3 (Sept. 2011), pp. 545–560. DOI: 10.3934/nhm.2011.6.545 (cit. on p. 1).

[8] Juliane Adrian, Nikolai Bode, Martyn Amos et al. "A Glossary for Research on Human Crowd Dynamics". In: *Collective Dynamics* 4 (Mar. 2019). DOI: 10.17815/cd.2019.19 (cit. on p. 2).

[9] Thiago Teixeira, Gershon Dublon and Andreas Savvides. "A survey of human-sensing: Methods for detecting presence, count, location, track, and identity". In: *ACM Computing Surveys* 5.1 (2010) (cit. on p. 3).

[10] Saad Ali and Mubarak Shah. "A Lagrangian Particle Dynamics Approach for Crowd Flow Segmentation and Stability Analysis". In: *Conference on Computer Vision and Pattern Recognition*. ,Minneapolis, Minnesota, USA: IEEE Computer Society, 2007, pp. 1–6. DOI: 10.1109/CVPR.2007.382977 (cit. on p. 3).

[11] Barbara Krausz and Christian Bauckhage. "Loveparade 2010: Automatic video analysis of a crowd disaster". In: *Computer Vision and Image Understanding, Special issue on Semantic Understanding of Human Behaviors in Image Sequences* 116.3 (2012), pp. 307–319. ISSN: 1077-3142. DOI: 10.1016/j.cviu.2011.08.006 (cit. on p. 3).

[12] Saira Saleem Pathan and Klaus Richter. "Pedestrian Behavior Analysis with Image-Based Method in Crowds". In: *Traffic and Granular Flow 2013*. Forschungszentrum Jülich. Springer, 2015, pp. 187–194. DOI: 10.1007/978-3-319-10629-8_22 (cit. on p. 3).

[13] Alessandro Corbetta, Jasper Meeusen, Chung-min Lee et al. "Continuous measurements of real-life bidirectional pedestrian flows on a wide walkway". In: *Proceedings of Pedestrian and Evacuation Dynamics 2016*. 2016, pp. 18–24 (cit. on p. 3).

[14] Pietro Morerio, Lucio Marcenaro and Carlo S Regazzoni. "People count estimation in small crowds". In: *2012 IEEE Ninth International Conference on Advanced video and signal-based surveillance (AVSS)*. 2012, pp. 476–480 (cit. on p. 3).

[15] David Ryan, Simon Denman, Sridha Sridharan et al. "An Evaluation of Crowd Counting Methods, Features and Regression Models". In: *Computer Vision and Image Understanding* 130 (2014), pp. 1–17. DOI: 10.1016/j.cviu.2014.07.008 (cit. on p. 3).

[16] Alexander Gmiterko and Tomas Liptak. "Motion Capture of Human for Interaction with Service Robot". In: *American Journal of Mechanical Engineering* 1.7 (2013), pp. 212–216. DOI: 10.12691/ajme-1-7-12 (cit. on p. 4).

[17] Serge P. Hoogendoorn, Winnie Daamen and Piet H.L. Bovy. "Extracting microscopic pedestrian characteristics from video data". In: *TRB2003 Annual Meeting*. 2003 (cit. on p. 4).

[18] Winnie Daamen and Serge Hoogendoorn. "Capacity of doors during evacuation conditions". In: *Procedia Engineering, 1st Conference on Evacuation Modeling and Management* 3.0 (2010), pp. 53–66. ISSN: 1877-7058. DOI: 10.1016/j.proeng.2010.07.007 (cit. on p. 4).

[19] Xuan Liu, Weiguo Song and Jun Zhang. "Extraction and quantitative analysis of microscopic evacuation characteristics based on digital image processing". In: *Physica A: Statistical Mechanics and its Applications* 388.13 (July 2009), pp. 2717–2726. ISSN: 0378-4371. DOI: 10.1016/j.physa.2009.03.017 (cit. on p. 4).

[20] Xiaodong Liu, Weiguo Song, Libi Fu et al. "Experimental study of pedestrian inflow in a room with a separate entrance and exit". In: *Physica A: Statistical Mechanics and its Applications* 442 (2016), pp. 224–238. ISSN: 0378-4371. DOI: 10.1016/j.physa.2015.09.026 (cit. on p. 4).

[21] Liping Lian, Xu Mai, Weiguo Song et al. "An experimental study on four-directional intersecting pedestrian flows". In: *J. Stat. Mech* (2015), P08024 (cit. on p. 4).

[22] Wei Tian, Weiguo Song, Jian Ma et al. "Experimental study of pedestrian behaviors in a corridor based on digital image processing". In: *Fire Safety Journal* 47.0 (2012), pp. 8–15. ISSN: 0379-7112. DOI: 10.1016/j.firesaf.2011.09.005 (cit. on p. 4).

[23] S. C. Wong, W. L. Leung, S. H. Chan et al. "Bidirectional Pedestrian Stream Model with Oblique Intersecting Angle". In: *Journal of Transportation Engineering* 136.3 (2010), pp. 234–242 (cit. on p. 4).

[24] Nirajan Shiwakoti, Yanshan Gong, Xiaomeng Shi et al. "Examining influence of merging architectural features on pedestrian crowd movement". In: *Safety Science* 75 (2015), pp. 15–22. ISSN: 0925-7535. DOI: http://dx.doi.org/10.1016/j.ssci.2015.01.009 (cit. on p. 4).

[25] Nirajan Shiwakoti, Xiaomeng Shi, Ye Zhirui et al. "Empirical study on pedestrian crowd behaviour in right angled junction". In: *37th Australasian Transport Research Forum (ATRF)*. 2015 (cit. on p. 4).

[26] Akiyasu Tomoeda, Daichi Yanagisawa and Katsuhiro Nishinari. "Escape Velocity of the Leader in a Queue of Pedestrians". In: *Traffic and Granular Flow 2013*. Forschungszentrum Jülich. Springer, 2015, pp. 213–218. DOI: 10.1007/978-3-319-10629-8_25 (cit. on pp. 4, 16).

[27] Bernhard Steffen and Armin Seyfried. "Methods for measuring pedestrian density, flow, speed and direction with minimal scatter". In: *Physica A* 389.9 (May 2010), pp. 1902–1910. DOI: 10.1016/j.physa.2009.12.015 (cit. on pp. 4, 99).

[28] Mohcine Chraibi, Armin Seyfried and Andreas Schadschneider. "Generalized centrifugal force model for pedestrian dynamics". In: *Physical Review E* 82 (2010), p. 046111. DOI: 10.1103/PhysRevE.82.046111 (cit. on pp. 4, 104).

[29] Maik Boltes, Jette Schumann and Daniel Salden. "Gathering of data under laboratory conditions for the deep analysis of pedestrian dynamics in crowds". In: *2017 14th IEEE International Conference on Advanced Video and Signal Based Surveillance (AVSS)*. 2017. DOI: 10.1109/AVSS.2017.8078471 (cit. on pp. 4, 16, 139).

[30] Samuel Lemercier, Mathieu Moreau, Mehdi Moussaïd et al. "Reconstructing Motion Capture Data for Human Crowd Study". In: *Motion in Games*. Ed. by Jan M. Allbeck and Petros Faloutsos. Vol. 7060. Lecture Notes in Computer Science. Springer Berlin Heidelberg, 2011, pp. 365–376. ISBN: 978-3-642-25089-7. DOI: 10.1007/978-3-642-25090-3_31 (cit. on p. 4).

[31] Mineko Imanishi and Tomonori Sano. "Level of Avoidance in Crossing Pedestrian Flow". In: *Transportation Research Procedia* 2 (2014), pp. 367–375. DOI: 10.1016/j.trpro.2014.09.034 (cit. on p. 4).

[32] Mineko Imanishi, Akihide Jo and Tomonori Sano. "Effects of pedestrian motivation and opening shape on pedestrian flow rate at an opening". In: *Fire Safety Journal* (May 2020), p. 103056. DOI: 10.1016/j.firesaf.2020.103056 (cit. on pp. 4, 89).

[33] Dragan Stojanović and Natalija Stojanović. "Indoor localization and tracking: Methods, technologies and research challenges". In: *Facta Universitatis, Series: Automatic Control and Robotics* 13.1 (2014), pp. 57–72 (cit. on pp. 4, 5).

[34] Hui Liu, Houshang Darabi, Pat Banerjee et al. "Survey of Wireless Indoor Positioning Techniques and Systems". In: *IEEE Trans. Syst., Man, Cybern. C* 37.6 (Nov. 2007), pp. 1067–1080. DOI: 10.1109/tsmcc.2007.905750 (cit. on p. 5).

[35] Pavel Davidson and Robert Piche. "A Survey of Selected Indoor Positioning Methods for Smartphones". In: *IEEE Communications Surveys Tutorials* PP.99 (2016), pp. 1–1. ISSN: 1553-877X. DOI: 10.1109/COMST.2016.2637663 (cit. on p. 5).

[36] Alejandro Correa, Marc Barcelo, Antoni Morell et al. "A Review of Pedestrian Indoor Positioning Systems for Mass Market Applications". In: *Sensors* 17.8 (2017). ISSN: 1424-8220. DOI: 10.3390/s17081927 (cit. on p. 5).

[37] Norhafizan Ahmad, Raja Ariffin Raja Ghazilla, Nazirah M. Khairi et al. "Reviews on Various Inertial Measurement Unit (IMU) Sensor Applications". In: *International Journal of Signal Processing Systems* (2013), pp. 256–262. DOI: 10.12720/ijsps.1.2.256-262 (cit. on p. 6).

[38] Robert Harle. "A Survey of Indoor Inertial Positioning Systems for Pedestrians". In: *IEEE Communications Surveys & Tutorials* 15.3 (2013), pp. 1281–1293. DOI: 10.1109/surv.2012.121912.00075 (cit. on pp. 6, 7).

[39] Oliver J Woodman. "An introduction to inertial navigation". In: *University of Cambridge, Computer Laboratory, Tech. Rep. UCAMCL-TR-696* 14 (2007), p. 15 (cit. on p. 6).

[40] Raúl Feliz, Eduardo Zalama and Jaime Gómez García-Bermejo. "Pedestrian tracking using inertial sensors". In: *Journal of Physical Agents (JoPha)* 3.1 (2009), pp. 35–43. DOI: 10.14198/jopha.2009.3.1.05 (cit. on p. 7).

[41] Rui Zhang and Leonhard M. Reindl. "Pedestrian motion based inertial sensor fusion by a modified complementary separate-bias Kalman filter". In: *2011 IEEE Sensors Applications Symposium*. Institute of Electrical & Electronics Engineers (IEEE), Feb. 2011. DOI: 10.1109/sas.2011.5739766 (cit. on p. 7).

[42] Xiaoping Yun, James Calusdian, Eric R. Bachmann et al. "Estimation of Human Foot Motion During Normal Walking Using Inertial and Magnetic Sensor Measurements". In: *IEEE Trans. Instrum. Meas.* 61.7 (July 2012), pp. 2059–2072. DOI: 10.1109/tim.2011.2179830 (cit. on pp. 7, 32).

[43] Hassen Fourati. "Heterogeneous Data Fusion Algorithm for Pedestrian Navigation via Foot-Mounted Inertial Measurement Unit and Complementary Filter". In: *IEEE Trans. Instrum. Meas.* 64.1 (Jan. 2015), pp. 221–229. DOI: 10.1109/tim.2014.2335912 (cit. on pp. 7, 32).

[44] Zeashan Khan, Muhammad Arif, A Kattan et al. "Pedestrian tracking using MEMS based wireless inertial measurement unit". In: *4th International Conference on Computer Engineering & Mathematical Sciences (ICCEMS 2015)*. 2015 (cit. on p. 7).

[45] Feyissa Woyano, Soyeon Lee and Sangjoon Park. "Evaluation and comparison of performance analysis of indoor inertial navigation system based on foot mounted IMU". In: *2016 18th International Conference on Advanced Communication Technology (ICACT)*. Institute of Electrical & Electronics Engineers (IEEE), Jan. 2016. DOI: 10.1109/icact.2016.7423562 (cit. on p. 7).

[46] Haoyu Li, Stephane Derrode, Lamia Benyoussef et al. "Free-Walking 3D Pedestrian Large Trajectory Reconstruction from IMU Sensors". In: *2018 26th European Signal Processing Conference (EUSIPCO)*. IEEE, Sept. 2018. DOI: 10.23919/eusipco.2018.8553462 (cit. on pp. 7, 32).

[47] Wenchao Zhang, Dongyan Wei and Hong Yuan. "The Improved Constraint Methods for Foot-Mounted PDR System". In: *IEEE Access* 8 (2020), pp. 31764–31779. DOI: 10.1109/access.2020.2973184 (cit. on p. 7).

[48] Juan Carlos Alvarez, Diego Alvarez, Antonio López et al. "Pedestrian Navigation Based on a Waist-Worn Inertial Sensor". In: *Sensors* 12.8 (Aug. 2012), pp. 10536–10549. DOI: 10.3390/s120810536 (cit. on p. 7).

[49] Estefania Munoz Diaz, Ana Luz Mendiguchia Gonzalez and Fabian de Ponte Muller. "Standalone inertial pocket navigation system". In: *2014 IEEE/ION Position, Location and Navigation Symposium - PLANS 2014*. Institute of Electrical & Electronics Engineers (IEEE), May 2014. DOI: 10.1109/plans.2014.6851382 (cit. on p. 7).

[50] Alexandre Patarot, Mehdi Boukallel and Sylvie Lamy-Perbal. "A case study on sensors and techniques for pedestrian inertial navigation". In: *2014 International Symposium on Inertial Sensors and Systems (ISISS)*. Feb. 2014, pp. 1–4. DOI: 10.1109/ISISS.2014.6782527 (cit. on p. 7).

[51] Wonho Kang, Seongho Nam, Youngnam Han et al. "Improved heading estimation for smartphone-based indoor positioning systems". In: *2012 IEEE 23rd International Symposium on Personal, Indoor and Mobile Radio Communications - (PIMRC)*. Institute of Electrical & Electronics Engineers (IEEE), Sept. 2012. DOI: 10.1109/pimrc.2012.6362768 (cit. on p. 7).

[52] Valérie Renaudin and Christophe Combettes. "Magnetic, Acceleration Fields and Gyroscope Quaternion (MAGYQ)-Based Attitude Estimation with Smartphone Sensors for Indoor Pedestrian Navigation". In: *Sensors* 14.12 (Dec. 2014), pp. 22864–22890. DOI: 10.3390/s141222864 (cit. on pp. 7, 32).

[53] Qinglin Tian, Zoran Salcic, Kevin I-Kai Wang et al. "An enhanced pedestrian dead reckoning approach for pedestrian tracking using smartphones". In: *2015 IEEE Tenth International Conference on Intelligent Sensors, Sensor Networks and Information Processing (ISSNIP)*. Institute of Electrical & Electronics Engineers (IEEE), Apr. 2015. DOI: 10.1109/issnip.2015.7106923 (cit. on p. 7).

[54] Thibaud Michel, Hassen Fourati, Pierre Geneves et al. "A comparative analysis of attitude estimation for pedestrian navigation with smartphones". In: *2015 International Conference on Indoor Positioning and Indoor Navigation (IPIN)*. IEEE, Oct. 2015. DOI: 10.1109/ipin.2015.7346767 (cit. on p. 7).

[55] Michael Angermann, Patrick Robertson, Thomas Kemptner et al. "A high precision reference data set for pedestrian navigation using foot-mounted inertial sensors". In: *2010 International Conference on Indoor Positioning and Indoor Navigation*. Institute of Electrical & Electronics Engineers (IEEE), Sept. 2010. DOI: 10.1109/ipin.2010.5646839 (cit. on p. 7).

[56] Dina Bousdar Ahmed, Luis Enrique Diez Blanco and Estefania Munoz Diaz. "Performance comparison of wearable-based pedestrian navigation systems in large areas". In: *2017 International Conference on Indoor Positioning and Indoor Navigation (IPIN)*. IEEE, Sept. 2017. DOI: 10.1109/ipin.2017.8115942 (cit. on p. 7).

[57] Parinaz Kasebzadeh, Gustaf Hendeby, Carsten Fritsche et al. "IMU dataset for motion and device mode classification". In: *2017 International Conference on Indoor Positioning and Indoor Navigation (IPIN)*. IEEE, Sept. 2017. DOI: 10.1109/ipin.2017.8115956 (cit. on p. 7).

[58] Eric Foxlin. "Pedestrian tracking with shoe-mounted inertial sensors". In: *Computer Graphics and Applications, IEEE* 25.6 (2005), pp. 38–46 (cit. on pp. 7, 8).

[59] Bernhard Krach and Patrick Robertson. "Integration of foot-mounted inertial sensors into a Bayesian location estimation framework". In: *5th Workshop on Positioning, Navigation and Communication (WPNC 2008)*. IEEE. 2008, pp. 55–61 (cit. on p. 7).

[60] Oliver Woodman and Robert Harle. "Pedestrian localisation for indoor environments". In: *Proceedings of the 10th international conference on Ubiquitous computing - UbiComp '08*. ACM Press, 2008. DOI: 10.1145/1409635.1409651 (cit. on p. 7).

[61] Oliver Woodman and Robert Harle. "RF-Based Initialisation for Inertial Pedestrian Tracking". In: *Pervasive Computing*. Ed. by Hideyukiand Tokuda, Michaeland Beigl, Adrianand Friday et al. Springer Berlin Heidelberg, 2009, pp. 238–255. DOI: 10.1007/978-3-642-01516-8_17 (cit. on p. 7).

[62] Michael Angermann and Patrick Robertson. "FootSLAM: Pedestrian Simultaneous Localization and Mapping Without Exteroceptive Sensors – Hitchhiking on Human Perception and Cognition". In: *Proceedings of the IEEE* 100.Special Centennial Issue (May 2012), pp. 1840–1848. ISSN: 0018-9219. DOI: 10.1109/JPROC.2012.2189785 (cit. on p. 7).

[63] Kun-Chan Lan and Wen-Yuah Shih. "On Calibrating the Sensor Errors of a PDR-Based Indoor Localization System". In: *Sensors* 13.4 (Apr. 2013), pp. 4781–4810. DOI: 10.3390/s130404781 (cit. on pp. 7, 109).

[64] Qinglin Tian, Zoran Salcic, Kevin I-Kai Wang et al. "A Hybrid Indoor Localization and Navigation System with Map Matching for Pedestrians Using Smartphones". In: *Sensors* 15.12 (2015), p. 29827. ISSN: 1424-8220. DOI: 10.3390/s151229827 (cit. on pp. 7, 109).

[65] Yang Gu, Qian Song, Yanghuan Li et al. "An Anchor-Based Pedestrian Navigation Approach Using Only Inertial Sensors". In: *Sensors* 16.3 (Mar. 2016), p. 334. DOI: 10.3390/s16030334 (cit. on pp. 7, 109).

[66] Nagesh Yadav and Chris Bleakley. "Two stage Kalman filtering for position estimation using dual Inertial Measurement Units". In: *SENSORS, 2011 IEEE*. Oct. 2011, pp. 1433–1436. DOI: 10.1109/ICSENS.2011.6127064 (cit. on pp. 7, 11, 37).

[67] Haiyu Lan, Chunyang Yu, You Li et al. "An efficient method for evaluating the performance of integrated multiple pedestrian navigation systems". In: *2015 International Conference on Indoor Positioning and Indoor Navigation (IPIN)*. IEEE, Oct. 2015. DOI: 10.1109/ipin.2015.7346775 (cit. on p. 7).

[68] Yuhao Zhang, Chenghao Lyu, Haotian Xu et al. "Improved position estimation by fusing multiple inaccurate inertial measurement unit sensors". In: *2016 IEEE MTT-S International Wireless Symposium (IWS)*. Mar. 2016, pp. 1–4. DOI: 10.1109/IEEE-IWS.2016.7585483 (cit. on pp. 7, 11, 37, 38).

[69] S. Godha and G. Lachapelle. "Foot mounted inertial system for pedestrian navigation". In: *Measurement Science and Technology* 19.7 (2008), p. 075202 (cit. on p. 8).

[70] Jin-Feng Li, Qing-Hui Wang, Xiao-Mei Liu et al. "A Pedestrian Dead Reckoning System Integrating Low-Cost MEMS Inertial Sensors and GPS Receiver". In: *Journal of Engineering Science and Technology Review* 7.2 (2014), pp. 197–203 (cit. on p. 8).

[71] Antonio Ramón Jimenez Ruiz, Fernando Seco Granja, José Carlos Prieto Honorato et al. "Accurate Pedestrian Indoor Navigation by Tightly Coupling Foot-Mounted IMU and RFID Measurements". In: *Instrumentation and Measurement, IEEE Transactions on* 61.1 (Jan. 2012), pp. 178–189. ISSN: 0018-9456. DOI: 10.1109/TIM.2011.2159317 (cit. on p. 8).

[72] Duy Duong Pham and Young Soo Suh. "Pedestrian Navigation Using Foot-Mounted Inertial Sensor and LIDAR". In: *Sensors* 16.1 (2016), p. 120. ISSN: 1424-8220. DOI: 10.3390/s16010120 (cit. on p. 8).

[73] Beakcheol Jang, Hyunjung Kim and Jong Wook Kim. "IPSCL: An Accurate Indoor Positioning Algorithm Using Sensors and Crowdsourced Landmarks". In: *Sensors* 19.13 (June 2019), p. 2891. DOI: 10.3390/s19132891 (cit. on p. 8).

[74] Korbinian Frank, Bernhard Krach, Noel Catterall et al. "Development and evaluation of a combined wlan & inertial indoor pedestrian positioning system". In: *ION GNSS*. 2009 (cit. on p. 8).

[75] Helena Leppäkoski, Jussi Collin and Jarmo Takala. "Pedestrian Navigation Based on Inertial Sensors, Indoor Map, and WLAN Signals". In: *Journal of Signal Processing Systems* 71.3 (Nov. 2012), pp. 287–296. DOI: 10.1007/s11265-012-0711-5 (cit. on p. 8).

[76] Mi Luna, Guo Meifeng, Zhang Xinxi et al. "An indoor pedestrian positioning system based on inertial measurement unit and wireless local area network". In: *Control Conference (CCC), 2015 34th Chinese*. July 2015, pp. 5419–5424. DOI: 10.1109/ChiCC.2015.7260487 (cit. on p. 8).

[77] Eric Foxlin and Leonid Naimark. "VIS-Tracker: A Wearable Vision-Inertial Self-Tracker". In: *Proceedings of the IEEE Virtual Reality 2003*. VR '03. Washington, DC, USA: IEEE Computer Society, 2003, pp. 199–. ISBN: 0-7695-1882-6 (cit. on p. 8).

[78] Hongsheng He, Yan Li, Yong Guan et al. "Wearable Ego-Motion Tracking for Blind Navigation in Indoor Environments". In: *Automation Science and Engineering, IEEE Transactions on* 12.4 (Oct. 2015), pp. 1181–1190. ISSN: 1545-5955. DOI: 10.1109/TASE.2015.2471175 (cit. on p. 8).

[79] Jorge Lobo and Jorge Miranda Dias. "Vision and inertial sensor cooperation using gravity as a vertical reference". In: *IEEE Transactions on Pattern Analysis and Machine Intelligence* 25.12 (Dec. 2003), pp. 1597–1608. DOI: 10.1109/tpami.2003.1251152 (cit. on p. 8).

[80] Gerard Pons-Moll, Andreas Baak, Thomas Helten et al. "Multisensor-fusion for 3D full-body human motion capture." In: *CVPR*. 2010, pp. 663–670 (cit. on p. 8).

[81] Thomas Helten, Meinard Muller, Hans-Peter Seidel et al. "Real-Time Body Tracking with One Depth Camera and Inertial Sensors". In: *2013 IEEE International Conference on Computer Vision*. Institute of Electrical & Electronics Engineers (IEEE), Dec. 2013. DOI: 10.1109/iccv.2013.141 (cit. on p. 8).

[82] Jouni Rantakokko, Joakim Rydell, Peter Strömbäck et al. "Accurate and reliable soldier and first responder indoor positioning: multisensor systems and cooperative localization". In: *IEEE Wireless Commun.* 18.2 (Apr. 2011), pp. 10–18. DOI: 10.1109/mwc.2011.5751291 (cit. on p. 8).

[83] Sz-Pin Huang, Jun-Wei Qiu, Chi-Chung Lo et al. "Wearable Localization by Particle Filter with the Assistance of Inertial and Visual Sensors". In: *2014 11th International Conference on Wearable and Implantable Body Sensor Networks*. Institute of Electrical & Electronics Engineers (IEEE), June 2014. DOI: 10.1109/bsn.2014.15 (cit. on p. 8).

[84] Jeroen Hol. "Sensor Fusion and Calibration of Inertial Sensors, Vision, Ultra-Wideband and GPS". Linköping Studies in Science and Technology. Dissertations. No. 1368. Department of Electrical Engineering, Automatic Control, June 2011 (cit. on p. 8).

[85] Ghazaleh Panahandeh, Nasser Mohammadiha, Arne Leijon et al. "Chest-mounted inertial measurement unit for pedestrian motion classification using continuous hidden Markov model". In: *2012 IEEE International Instrumentation and Measurement Technology Conference Proceedings*. IEEE, May 2012. DOI: 10.1109/i2mtc.2012.6229380 (cit. on p. 8).

[86] Ferhat Attal, Samer Mohammed, Mariam Dedabrishvili et al. "Physical human activity recognition using wearable sensors". In: *Sensors* 15.12 (2015), pp. 31314–31338 (cit. on p. 8).

[87] Sebastijan Sprager and Matjaz Juric. "Inertial Sensor-Based Gait Recognition: A Review". In: *Sensors* 15.9 (Sept. 2015), pp. 22089–22127. DOI: 10.3390/s150922089 (cit. on p. 8).

[88] James B. Lee, Rebecca B. Mellifont and Brendan J. Burkett. "The use of a single inertial sensor to identify stride, step, and stance durations of running gait". In: *Journal of Science and Medicine in Sport* 13.2 (Mar. 2010), pp. 270–273. DOI: 10.1016/j.jsams.2009.01.005 (cit. on pp. 8, 40).

[89] Hung Manh La, Luan V. Nguyen and Trung H. Duong. "Dynamic Human Gait Phase Detection Algorithm". In: *Proceedings - ISSAT International Conference on Modeling of Complex Systems and Environments 2015*. 2015. DOI: 10.13140/RG.2.1.1831.2165 (cit. on p. 8).

[90] H. J. Luinge and P. H. Veltink. "Measuring orientation of human body segments using miniature gyroscopes and accelerometers". In: *Medical & Biological Engineering & Computing* 43.2 (Apr. 2005), pp. 273–282. DOI: 10.1007/bf02345966 (cit. on p. 8).

[91] Xiaoping Yun and Eric R. Bachmann. "Design, Implementation, and Experimental Results of a Quaternion-Based Kalman Filter for Human Body Motion Tracking". In: *IEEE Transactions on Robotics* 22.6 (Dec. 2006), pp. 1216–1227. ISSN: 1552-3098. DOI: 10.1109/TRO.2006.886270 (cit. on pp. 8, 32).

[92] Daniel Roetenberg, Per J. Slycke and Peter H. Veltink. "Ambulatory Position and Orientation Tracking Fusing Magnetic and Inertial Sensing". In: *IEEE Transactions on Biomedical Engineering* 54.5 (May 2007), pp. 883–890. DOI: 10.1109/tbme.2006.889184 (cit. on p. 8).

[93] Rick A. Hyde, Laurence P. Ketteringham, Simon A. Neild et al. "Estimation of Upper-Limb Orientation Based on Accelerometer and Gyroscope Measurements". In: *IEEE Transactions on Biomedical Engineering* 55.2 (Feb. 2008), pp. 746–754. DOI: 10.1109/tbme.2007.912647 (cit. on p. 8).

[94] Thomas Seel, Jörg Raisch and Thomas Schauer. "IMU-Based Joint Angle Measurement for Gait Analysis". In: *Sensors* 14.4 (Apr. 2014), pp. 6891–6909. DOI: 10.3390/s140406891 (cit. on p. 8).

[95] Alessandro Filippeschi, Norbert Schmitz, Markus Miezal et al. "Survey of Motion Tracking Methods Based on Inertial Sensors: A Focus on Upper Limb Human Motion". In: *Sensors* 17.6 (June 2017), p. 1257. DOI: 10.3390/s17061257 (cit. on p. 8).

[96] Sheng Shen, Mahanth Gowda and Romit Roy Choudhury. "Closing the Gaps in Inertial Motion Tracking". In: *Proceedings of the 24th Annual International Conference on Mobile Computing and Networking - MobiCom '18*. ACM Press, 2018. DOI: 10.1145/3241539.3241582 (cit. on p. 8).

[97] Pengzhan Chen, Ye Kuang and Jie Li. "Human Motion Capture Algorithm Based on Inertial Sensors". In: *Journal of Sensors* 2016 (2016), pp. 1–15. DOI: 10.1155/2016/4343797 (cit. on p. 8).

[98] Daniel Roetenberg, Henk Luinge and Per Slycke. *Xsens MVN: full 6DOF human motion tracking using miniature inertial sensors*. Tech. rep. Xsens Technologies B.V., 2009 (cit. on p. 8).

[99] Martin Schepers, Matteo Giuberti and Giovanni Bellusci. *Xsens MVN: Consistent Tracking of Human Motion Using Inertial Sensing*. Tech. rep. Xsens Technologies B.V., 2018. DOI: 10.13140/RG.2.2.22099.07205 (cit. on p. 8).

[100] Claudio Feliciani and Katsuhiro Nishinari. "Pedestrians rotation measurement in bidirectional streams". In: *Proceedings of Pedestrian and Evacuation Dynamics 2016*. Ed. by Weiguo Song, Jian Ma and Libi Fu. Oct. 2016 (cit. on pp. 8, 81).

[101] Hiroki Yamamoto, Daichi Yanagisawa, Claudio Feliciani et al. "Body-rotation behavior of pedestrians for collision avoidance in passing and cross flow". In: *Transportation Research Part B: Methodological* 122 (Apr. 2019), pp. 486–510. DOI: 10.1016/j.trb.2019.03.008 (cit. on pp. 8, 81, 100).

[102] Koki Nagao, Daichi Yanagisawa and Katsuhiro Nishinari. "Estimation of crowd density applying wavelet transform and machine learning". In: *Physica A: Statistical Mechanics and its Applications* 510 (Nov. 2018), pp. 145–163. DOI: 10.1016/j.physa.2018.06.078 (cit. on p. 8).

[103] Claudio Feliciani and Katsuhiro Nishinari. "Estimation of pedestrian crowds' properties using commercial tablets and smartphones". In: *Transportmetrica B: Transport Dynamics* 7.1 (2019), pp. 865–896. DOI: 10.1080/21680566.2018.1517061 (cit. on pp. 8, 10).

[104] J. Pansiot, Z. Zhang, B. Lo et al. "WISDOM: wheelchair inertial sensors for displacement and orientation monitoring". In: *Measurement Science and Technology* 22.10 (Aug. 2011), p. 105801. DOI: 10.1088/0957-0233/22/10/105801 (cit. on pp. 8, 10).

[105] Jonathan Shepherd, Tomohito Wada, David Rowlands et al. "A Novel AHRS Inertial Sensor-Based Algorithm for Wheelchair Propulsion Performance Analysis". In: *Algorithms* 9.3 (Aug. 2016), p. 55. DOI: 10.3390/a9030055 (cit. on pp. 8, 10, 19, 33).

[106] Olarn Wongwirat and Chutchai Chaiyarat. "A position tracking experiment of mobile robot with Inertial Measurement Unit (IMU)". In: *ICCAS 2010*. 2010, pp. 304–308 (cit. on p. 9).

[107] Jan Koch, C. Hillenbrand and K. Berns. "Inertial navigation for wheeled robots in outdoor terrain". In: *Proceedings of the Fifth International Workshop on Robot Motion and Control, 2005. RoMoCo '05*. Institute of Electrical & Electronics Engineers (IEEE), 2005. DOI: 10.1109/romoco.2005.201419 (cit. on p. 9).

[108] Bong-Su Cho, Woo-sung Moon, Woo-Jin Seo et al. "A dead reckoning localization system for mobile robots using inertial sensors and wheel revolution encoding". In: *Journal of Mechanical Science and Technology* 25.11 (Nov. 2011), pp. 2907–2917. DOI: 10.1007/s12206-011-0805-1 (cit. on p. 9).

[109] Maik Boltes and Stefan Holl. "SiME - Improved safety for disabled people". In: *inSiDE* 14.1 (2016), p. 75 (cit. on pp. 9, 20).

[110] Oliver J. Woodman. "Pedestrian localisation for indoor environments". dissertation. University of Cambridge, 2010 (cit. on p. 10).

[111] Fabian Hoflinger, Rui Zhang and Leonard M. Reindl. "Indoor-localization system using a Micro-Inertial Measurement Unit (IMU)". In: *European Frequency and Time Forum (EFTF), 2012*. Apr. 2012, pp. 443–447. DOI: 10.1109/EFTF.2012.6502421 (cit. on p. 10).

[112] Anna Sieben, Jette Schumann and Armin Seyfried. "Collective phenomena in crowds—Where pedestrian dynamics need social psychology". In: *PLOS ONE* 12.6 (June 2017). Ed. by Dante R. Chialvo, e0177328. DOI: 10.1371/journal.pone.0177328 (cit. on pp. 11, 140).

[113] Maik Boltes and Daniel Salden. *Software PeTrack*. http://ped.fz-juelich.de/petrack (Retrieved: 2020-04-15) (cit. on p. 16).

[114] Mohammed Khaled Gdoura, Rainald Löhner, Eberhard Haug et al. "On the influence of columns in densely populated corridors". In: *Pedestrian and Evacuation Dynamics 2014*. 2014. DOI: 10.1016/j.trpro.2014.09.002 (cit. on p. 16).

[115] Ilias Sakellariou, Omar Kurdi, Marian Gheorghe et al. "Crowd formal modelling and simulation: The Sa'yee ritual". In: *Computational Intelligence (UKCI), 2014 14th UK Workshop on*. Sept. 2014, pp. 1–8. DOI: 10.1109/UKCI.2014.6930176 (cit. on p. 16).

[116] Takahiro Ezaki, Kazumichi Ohtsuka, Mohcine Chraibi et al. "Inflow Process of Pedestrians to a Confined Space". In: *Collective Dynamics* 1 (2016), pp. 1–18. ISSN: 2366-8539. DOI: 10.17815/CD.2016.4 (cit. on p. 16).

[117] Yiwen Liu, Xiaomeng Shi, Zhirui Ye et al. "Controlled Experiments to Examine Different Exit Designs on Crowd Evacuation Dynamics". In: *16th COTA International Conference of Transportation Professionals*. 2016, pp. 779–790. DOI: 10.1061/9780784479896.072 (cit. on p. 16).

[118] Milad Haghani and Majid Sarvi. "Stated and revealed exit choices of pedestrian crowd evacuees". In: *Transportation Research Part B: Methodological* 95 (2017), pp. 238–259. ISSN: 0191-2615. DOI: 10.1016/j.trb.2016.10.019 (cit. on p. 16).

[119] Maik Boltes, Armin Seyfried, Bernhard Steffen et al. "Automatic Extraction of Pedestrian Trajectories from Video Recordings". In: *Pedestrian and Evacuation Dynamics 2008*. Ed. by Wolfram W. F. Klingsch, Christian Rogsch, Andreas Schadschneider et al. Springer Berlin Heidelberg, 2010, pp. 43–54. DOI: 10.1007/978-3-642-04504-2_3 (cit. on p. 16).

[120] Maik Boltes, Stefan Holl, Antoine Tordeux et al. "Influences of Extraction Techniques on the Quality of Measured Quantities of Pedestrian Characteristics". In: *Proceedings of Pedestrian and Evacuation Dynamics 2016*. 2016, pp. 500–547 (cit. on pp. 16, 17).

[121] SABEL Labs. *Sports technology, biomedical engineering and wearable technologies, Australia*. https://sabellabs.com (Retrieved: 2020-04-23) (cit. on pp. 17, 22).

[122] Daniel A. James and Andrew Wixted. "ADAT: A Matlab toolbox for handling time series athlete performance data". In: *Procedia Engineering* 13 (2011), pp. 451–456. DOI: 10.1016/j.proeng.2011.05.113 (cit. on p. 18).

[123] Alan Lai, Daniel A. James, Jason P. Hayes et al. "Semi-automatic calibration technique using six inertial frames of reference". In: *Microelectronics: Design, Technology, and Packaging*. Vol. 5274. International Society for Optics and Photonics. 2004, pp. 531–543 (cit. on pp. 19, 31).

[124] Tomohito Wada, Mirai Mizutani, James Lee et al. "3D Visualisation of Wearable Inertial/Magnetic Sensors". In: *Proceedings* 2.6 (Feb. 2018), p. 292. DOI: 10.3390/proceedings2060292 (cit. on p. 19).

[125] James Lee, Hugo Espinosa and Daniel James. "The inertial sensor: A base platform for wider adoption in sports science applications". In: *Journal of Fitness Research* 4 (Jan. 2015) (cit. on p. 19).

[126] James Lee, Keane Wheeler and Daniel A James. *Wearable Sensors in Sport: A Practical Guide to Usage and Implementation*. Springer, 2019 (cit. on p. 19).

[127] Paul Geoerg, Florian Berchtold, Steven Gwynne et al. "Engineering egress data considering pedestrians with reduced mobility". In: *Fire and Materials* 43.7 (Aug. 2019), pp. 759–781. DOI: 10.1002/fam.2736 (cit. on p. 20).

[128] Paul Geoerg, Rainer Block, Werner Heister et al. "A score regarding the need for assistance: Considering pedestrians with disabilities in evacuation planning". In: *Proceedings of the 5th Magdeburg Fire and Explosion Prevention Day*. Ed. by Ulrich Krause and Michael Rost. Magdeburg and Germany, 2017. ISBN: 978-3-00-056201-3 (cit. on p. 20).

[129] Paul Geoerg, Jette Schumann, Maik Boltes et al. "The influence of physical and mental constraints to a stream of people through a bottleneck". In: *Proceedings of Pedestrian and Evacuation Dynamics 2018, PED18, Lund, Sweden, Collective dynamics* 5 (2020). DOI: 10.17815/cd.2020.57 (cit. on pp. 21, 140).

[130] Paul Geoerg, Jette Schumann, Stefan Holl et al. "The Influence of Wheelchair Users on Movement in a Bottleneck and a Corridor". In: *Journal of Advanced Transportation* 2019 (June 2019), pp. 1–17. DOI: 10.1155/2019/9717208 (cit. on pp. 21, 31, 140).

[131] Paul Geoerg, Jette Schumann, Maik Boltes et al. "The Influence of Individual Impairments on Crowd Dynamics". In: *INTERFLAM 2019*. Ed. by Stephen Grayson. London: Interscience Communications, 2019, pp. 775–791 (cit. on pp. 21, 140).

[132] Paul Geoerg, Jette Schumann, Stefan Holl et al. "The influence of individual impairments in crowd dynamics". In: *Fire and Materials* (Feb. 2020). DOI: 10.1002/fam.2789 (cit. on pp. 21, 140).

[133] Forschungszentrum Jülich and Federal Institute for Materials Research and Testing. *Influence of individual characteristics*. 2017. DOI: 10.34735/PED.2017.1 (cit. on pp. 21, 107, 119, 139).

[134] NaturalPoint. *OptiTrack - Motion Capture Sytems*. https://optitrack.com (Retrieved: 2021-01-03) (cit. on p. 22).

[135] Jette Schumann, Maik Boltes and James Lee. *Studies for validating tracking algorithms based on IMU data with 3D camera data*. 2018. DOI: 10.34735/PED.2018.3 (cit. on pp. 25, 107, 139).

[136] Sebastian O. H. Madgwick. "An efficient orientation filter for inertial and inertial/magnetic sensor arrays". In: *Report x-io and University of Bristol (UK)* (2010) (cit. on pp. 28, 33, 35, 68, 69).

[137] Bruno O. S. Teixeira, Jaganath Chandrasekar, Leonardo A. B. Torres et al. "State estimation for linear and non-linear equality-constrained systems". In: *International Journal of Control* 82.5 (2009), pp. 918–936. DOI: 10.1080/00207170802370033 (cit. on pp. 28, 38).

[138] Eric R. Bachmann, I. Duman, U.Y. Usta et al. "Orientation tracking for humans and robots using inertial sensors". In: *Proceedings 1999 IEEE International Symposium on Computational Intelligence in Robotics and Automation. CIRA'99 (Cat. No.99EX375)*. IEEE, 1999. DOI: 10.1109/cira.1999.810047 (cit. on p. 32).

[139] Demoz Gebre-Egziabher, Roger C. Hayward and J. David Powell. "Design Of Multi-sensor Attitude Determination Systems". In: *IEEE Transactions on Aerospace and Electronic Systems* 40.2 (Apr. 2004), pp. 627–649. DOI: 10.1109/taes.2004.1310010 (cit. on p. 32).

[140] Xiaoying Kong. "INS algorithm using quaternion model for low cost IMU". In: *Robotics and Autonomous Systems* 46.4 (Apr. 2004), pp. 221–246. DOI: 10.1016/j.robot.2004.02.001 (cit. on p. 32).

[141] Roberto Valenti, Ivan Dryanovski and Jizhong Xiao. "Keeping a Good Attitude: A Quaternion-Based Orientation Filter for IMUs and MARGs". In: *Sensors* 15.8 (Aug. 2015), pp. 19302–19330. DOI: 10.3390/s150819302 (cit. on p. 32).

[142] Kaiqiang Feng, Jie Li, Xiaoming Zhang et al. "A New Quaternion-Based Kalman Filter for Real-Time Attitude Estimation Using the Two-Step Geometrically-Intuitive Correction Algorithm". In: *Sensors* 17.9 (Sept. 2017), p. 2146. DOI: 10.3390/s17092146 (cit. on p. 32).

[143] Jack B. Kuipers. "Quaternions and Rotation Sequences". In: *Proceedings of the International Conference on Geometry, Integrability and Quantization*. Ed. by Ivaïlo M. Mladenov and Gregory L. Nabe. Coral Press Scientific Coral Press Scientific Publishing, 2000, pp. 127–143. ISBN: 954-90618-1-7 (cit. on pp. 32, 33).

[144] Sebastian O. H. Madgwick, Andrew J. L. Harrison and Ravi Vaidyanathan. "Estimation of IMU and MARG orientation using a gradient descent algorithm". In: *2011 IEEE International Conference on Rehabilitation Robotics*. Institute of Electrical and Electronics Engineers (IEEE), June 2011. DOI: 10.1109/icorr.2011.5975346 (cit. on p. 33).

[145] Rudolph Emil Kalman. "A New Approach to Linear Filtering and Prediction Problems". In: *Transactions of the ASME–Journal of Basic Engineering* 82.Series D (1960), pp. 35–45 (cit. on p. 37).

[146] A. H. Mohamed and K. P. Schwarz. "Adaptive Kalman Filtering for INS/GPS". In: *Journal of Geodesy* 73.4 (May 1999), pp. 193–203. ISSN: 1432-1394. DOI: 10.1007/s001900050236 (cit. on p. 39).

[147] Jette Schumann. *Software Repository ImuTracker*. https://github.com/JetteSchumann/ImuTracker.git (Retrieved: 2021-05-18) (cit. on pp. 47, 107).

[148] Wes McKinney. *Python for Data Analysis*. Sebastopol: O'Reilly Media, Inc., 2013. ISBN: 978-1-449-31979-3 (cit. on p. 47).

[149] Dusty Phillips. *Python 3 Object-Oriented Programming - Build robust and maintainable software with object-oriented design patterns in Python 3.8, 3rd Edition*. Birmingham: Packt Publishing Ltd, 2018. ISBN: 978-1-789-61707-8 (cit. on p. 47).

[150] Robert Cecil Martin. *Agile Software Development: Principles, Patterns, and Practices*. USA: Prentice Hall PTR, 2003. ISBN: 0135974445 (cit. on p. 47).

[151] Maik Boltes, Jana Pick and Janine Klein. "Smoothing Trajectories of People's Heads". In: *Traffic and Granular Flow 2019*. Springer International Publishing, 2020, pp. 21–29. DOI: 10.1007/978-3-030-55973-1_3 (cit. on p. 65).

[152] Jette Schumann, Maik Boltes, Juliane Adrian et al. *Studies on rotation of the upper body in bottlenecks using a hybrid tracking system*. 2018. DOI: 10.34735/PED.2018.4 (cit. on pp. 84, 108, 131, 139).

[153] Helen C. Muir, David M. Bottomley and Claire Marrison. "Effects of Motivation and Cabin Configuration on Emergency Aircraft Evacuation Behavior and Rates of Egress". In: *The International Journal of Aviation Psychology* 6 (1996), pp. 57–77. DOI: 10.1207/s15327108ijap0601_4 (cit. on p. 97).

[154] Armin Seyfried, Oliver Passon, Bernhard Steffen et al. "New insights into pedestrian flow through bottlenecks". In: *Transportation Science* 43.3 (Aug. 2009), pp. 395–406. DOI: 10.1287/trsc.1090.0263 (cit. on p. 101).

[155] Jette Schumann and Maik Boltes. "Tracking of wheelchair users in dense crowds". In: *2017 International Conference on Indoor Positioning and Indoor Navigation (IPIN)*. 2017 (cit. on p. 139).

[156] Jette Schumann, Maik Boltes and Armin Seyfried. "Hybrid Tracking System for Pedestrians in Dense Crowds". In: *Traffic and Granular Flow '17*. Ed. by Hamdar S. H. 2019. DOI: 10.1007/978-3-030-11440-4_23 (cit. on p. 139).

[157] Paul Geoerg, Robert Malte Polzin, Jette Schumann et al. "Small-scale Studies on Evacuation Characteristics of Pedestrians with physical, mental or age-related Disabilities". In: *Journal of Physics: Conference Series* 1107 (Nov. 2018), p. 072006. DOI: 10.1088/1742-6596/1107/7/072006 (cit. on p. 140).

Band / Volume 37
Analysis of I/O Requirements of Scientific Applications
S. El Sayed Mohamed (2018), XV, 199 pp
ISBN: 978-3-95806-344-0
URN: urn:nbn:de:0001-2018071801

Band / Volume 38
Wayfinding and Perception Abilities for Pedestrian Simulations
E. Andresen (2018), 4, x, 162 pp
ISBN: 978-3-95806-375-4
URN: urn:nbn:de:0001-2018121810

Band / Volume 39
Real-Time Simulation and Prognosis of Smoke Propagation in Compartments Using a GPU
A. Küsters (2018), xvii, 162, LIX pp
ISBN: 978-3-95806-379-2
URN: urn:nbn:de:0001-2018121902

Band / Volume 40
Extreme Data Workshop 2018
Forschungszentrum Jülich, 18 – 19 September 2018
Proceedings
M. Schultz, D. Pleiter, P. Bauer (Eds.) (2019), 64 pp
ISBN: 978-3-95806-392-1
URN: urn:nbn:de:0001-2019032102

Band / Volume 41
A lattice QCD study of nucleon structure with physical quark masses
N. Hasan (2020), xiii, 157 pp
ISBN: 978-3-95806-456-0
URN: urn:nbn:de:0001-2020012307

Band / Volume 42
Mikroskopische Fundamentaldiagramme der Fußgängerdynamik – Empirische Untersuchung von Experimenten eindimensionaler Bewegung sowie quantitative Beschreibung von Stau-Charakteristika
V. Ziemer (2020), XVIII, 155 pp
ISBN: 978-3-95806-470-6
URN: urn:nbn:de:0001-2020051000

Band / Volume 43
Algorithms for massively parallel generic *hp*-adaptive finite element methods
M. Fehling (2020), vii, 78 pp
ISBN: 978-3-95806-486-7
URN: urn:nbn:de:0001-2020071402

Band / Volume 44
The method of fundamental solutions for computing interior transmission eigenvalues
L. Pieronek (2020), 115 pp
ISBN: 978-3-95806-504-8

Band / Volume 45
Supercomputer simulations of transmon quantum computers
D. Willsch (2020), IX, 237 pp
ISBN: 978-3-95806-505-5

Band / Volume 46
The Influence of Individual Characteristics on Crowd Dynamics
P. Geoerg (2021), xiv, 212 pp
ISBN: 978-3-95806-561-1

Band / Volume 47
Structural plasticity as a connectivity generation and optimization algorithm in neural networks
S. Diaz Pier (2021), 167 pp
ISBN: 978-3-95806-577-2

Band / Volume 48
Porting applications to a Modular Supercomputer
Experiences from the DEEP-EST project
A. Kreuzer, E. Suarez, N. Eicker, Th. Lippert (Eds.) (2021), 209 pp
ISBN: 978-3-95806-590-1

Band / Volume 49
Operational Navigation of Agents and Self-organization Phenomena in Velocity-based Models for Pedestrian Dynamics
Q. Xu (2022), xii, 112 pp
ISBN: 978-3-95806-620-5

Band / Volume 50
Utilizing Inertial Sensors as an Extension of a Camera Tracking System for Gathering Movement Data in Dense Crowds
J. Schumann (2022), xii, 155 pp
ISBN: 978-3-95806-624-3

Weitere ***Schriften des Verlags im Forschungszentrum Jülich*** unter
http://wwwzb1.fz-juelich.de/verlagextern1/index.asp

IAS Series
Band / Volume 50
ISBN 978-3-95806-624-3

Mitglied der Helmholtz-Gemeinschaft

JÜLICH
Forschungszentrum